Spring 2008

Development of a high-resolution target movement monitoring system for convergence monitoring in mines

Tristan H. Jones

Department: Mining and Nuclear Engineering

DEVELOPMENT OF A HIGH-RESOLUTION TARGET MOVEMENT MONITORING SYSTEM FOR CONVERGENCE MONITORING IN MINES

by

TRISTAN H. JONES

A DISSERTATION

Presented to the Faculty of the Graduate School of the

MISSOURI UNIVERSITY OF SCIENCE AND TECHNOLOGY

In Partial Fulfillment of the Requirements for the Degree

DOCTOR OF PHILOSOPHY

In

MINING ENGINEERING

2008

Approved by

Derek B. Apel, Advisor
Jerry C. Tien
Lee W. Saperstein
Steve E Watkins
Randy H. Moss

ABSTRACT

The research performed for this dissertation has been conducted with the goal of developing a ground convergence monitor that may better meet the needs of some mines, leading to increased use of ground monitoring programs and reduced fatality rates from falling and sliding rock. The developed monitor is a convergence monitor capable of achieving sensitivities similar to those of currently available convergence meters such as tape extensometers. The monitor is inexpensive and is capable of totally remote operation in some circumstances.

The monitor is a triangulation-based laser distance meter similar to those used in manufacturing and quality-control situations, though it is capable of ranges greatly exceeding those sensors currently available. It integrates a consumer digital camera, an inexpensive laser diode, a target, and custom-written computer software to track the convergence-driven movement of a laser spot across the target from image to image. The monitor was developed and components selected based on extensive experimentation and experiences in the laboratory and in the field.

A physical model of the meter was developed based on experimental results and compared to a derived theoretical model to show that the monitor was capable of accurately reproducing the predicted sensitivity values. The sensitivity was found to be dependent upon the width of the sensor imaging chip, the distance between the target and the camera, the focal length of the camera lens, the angle of incidence of the laser, and the width of the produced image (expressed in pixels). These five variables were evaluated along with error-inducing variables to make recommendations concerning the construction, deployment, use, sensitivity, error and potential of the monitor.

PREFACE

Upon beginning my Ph.D. studies at the Missouri University of Science and Technology mining department I had no particular research ideas of my own. It took only a very short time for me to narrow my interests and begin this current research, suggested by my advisor, Dr. Derek Apel. I thank Dr. Apel for providing me with this initial direction, for the many extended conversations sharing ideas, and for providing just the right number of pokes and prods of guidance and encouragement throughout the project to keep my motivation high and my interest focused. This is a talent and a sure sign of an excellent advisor.

Special thanks are given to the Doe Run Company whose generosity has funded this research, and to the university, whose additional generosity has funded my education. Tom Yanske and Robby Vetter of the Technical Services Department at Doe Run also deserve my gratitude for their assistance with the field experiments in the Fletcher Mine.

I would also like to thank the members of my committee: Dr. Larry Grayson, who initially convinced me to attend this fine university, Dr. Jerry Tien, whose conversations concerning this project and mining-at-large have been memorable; Dr. Lee Saperstein, whose help during the preparation of this document has been irreplaceable; Dr. Steve Watkins, whose guidance through my initial leap into Electromagnetic Optics helped me to come out with my head held high; and Dr. Randy Moss, whose insight and thoughts concerning the project have proven extremely useful.

Special thanks to the mining engineering and Electrical and Computer Engineering Departments, for providing me with such wonderful facilities and opportunities, and especially to Shirley Hall, secretary of the mining department, whose

assistance has allowed for relatively painless navigation through the many purchases, forms, and budget-business necessary for this project.

Additional gratitude is given to a few people that have helped me along the way through assistance or support: David Nutakor, James Fonda, Matt Kimbel, Nassib Aouad, Yi Zheng and Oyku Selimoglu; as well as Jimmie Taylor Sr., Dr. Paul Worsey, Jack Jones, Jimmie Taylor Jr., and Paula Cochran. Each person has played a part in this project even if they did not know it.

I would like to thank the members of my family. Especially my mother and father, who have both been extremely supportive of this entire process and have been watching out for me for longer than I can remember. Aaron, Katie, Grandma and Aunt Pat, I'm very glad to know that you are always there to listen and provide input and support if it is needed.

Finally, I would like to thank my wonderful wife, Anu. I met you during this project while you were visiting as a foreign scholar. Perhaps I should thank Dr. Tien for that. Regardless, I never would have imagined that a single person could be such a completing influence on my life. I'm grateful that you have been here to love and support me, and to occasionally provide me with guidance through this Ph.D. process. Minä rakastan sinua, viamoni.

Tristan H. Jones

April, 2008

TABLE OF CONTENTS

LIST OF FIGURES

LIST OF TABLES

NOMENCLATURE

Symbol	Description
λ	Wavelength
ψ	Frequency
ω	Phase angle
Δt_d	Change in target distance
ρ	Density
σ_w	Wire tensile stress
μm	Micrometer
θ	Laser incidence angle relative to normal
AC	Alternating current
c	Speed of light
C	Centroid movement distance (mm)
CCD	Charge-coupled devise
DC	Direct current
DGPS	Differential global positioning system
DSLR	Digital single lens reflex
EDM	Electronic Distance Measurement
F	Effective focal length (mm)
f	Focal length (mm)
FOV	Field of view
fps	Frames per second
ft	Feet
GB	Gigabyte
GHz	Gigahertz
GPS	Global positioning system
H	Humidity (millibars)
HRTMM	High Resolution Target Movement Monitor
I	Reduced irradiance
I_o	Initial irradiance

k	Atmospheric extinction coefficient
LED	Light emitting diode
LVDT	Linearly variable differential transformer
l_w	Wire length
m	Meter
M_c	Modifying coefficient
mm	Millimeter
MSHA	Mine Safety and Health Administration
MST	Missouri University of Science and Technology
mW	Milliwatt
n	Refractive index
nm	Nanometer
P	Pressure (millibars)
ppm	Part per million
PSD	Position-sensitive devise
p_w	Cross-sectional width of the image in pixels – "pixel-width" (pixels)
r	Range
R_c	Resolution coefficient
s	Sensitivity (mm)
t	Time
T	Temperature (Kelvin)
t_d	Target distance
TOF	Time of flight
USB	Universal serial bus
V	Velocity
VTSB	Vincent Thomas Suspension Bridge
w	Width of the imaging sensor (mm)
ω_o	Laser beam radius at the aperture
w_p	Width of one pixel in the far-field (mm)
ω_z	Laser beam radius at a distance, z
x	Distance

X	X centroid location (pixels)
Y	Y centroid location (pixels)
z	Laser propagation distance

1. INTRODUCTION

1.1. BACKGROUND

Mining is an industry of constant change and varied environments. Due to the special characteristics inherent to each individual mine site, procedures, processes and equipment that prove successful in one mine may not be best suited to the needs of another. These special circumstances require the use of robust technology capable of adapting to fill the broadest need at the lowest cost, thus contributing to the overall mine efficiency. This requisite must extend beyond the machinery and equipment used during production to include every aspect of the site, including the safety equipment installed to prevent injury, destruction of property, and disruption of production.

One characteristic that is associated with any industrial activity and found in all mine sites is danger to personnel and equipment. Among the many hazards that pose this danger is that of falling or sliding material. According to the US Mine Safety and Health Administration (MSHA), 287 fatalities were reported by the mining industry in the U.S. during the period between 2003 and 2007 [1]. Falling or sliding material was the most frequent cause of these fatalities in coal mining and the fourth most frequent in metal and nonmetal mines. During this time period, underground coal mining had the unfortunate position of leading the way in fatalities due to ground movement (Figure 1.1). For 2007 alone, the fatality rate for falling material was higher than for any time in the last 5 years.

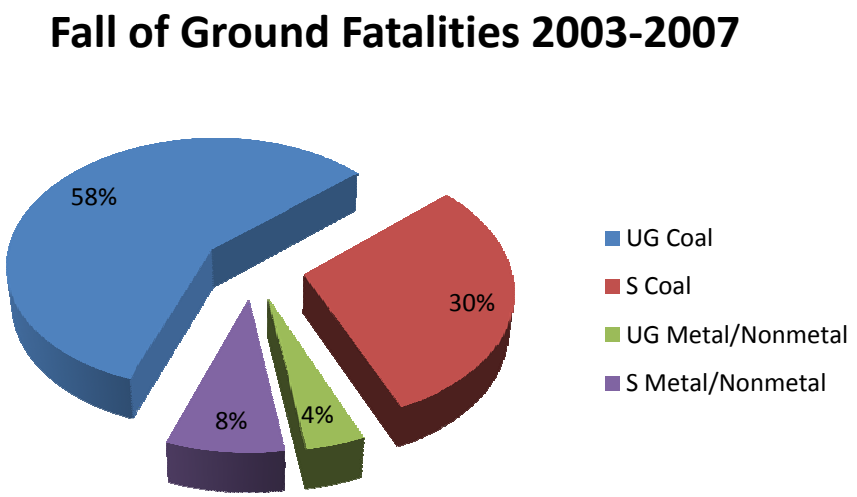

Figure 1.1: Fall of ground fatalities between years 2003 and 2007. Underground coal had more fall of ground fatalities than all other industry segments combined.

Roof beam failures or sliding rock also accounted for the overall majority of injuries experienced by employees in U.S. underground mines. In addition, the injuries caused by falling or sliding material are generally severe, as determined by the MSHA severity rankings (1-fatality, 2-permanent disability, 3-lost time accident, etc.). Approximately three fifths of all roof, face and rib fall injuries are designated by MSHA as some kind of lost-time accident (Figure 1.2).

Even with the great advancements in safe mining techniques made over the past few decades, the threats involved still require additional mitigation. Loss of life, equipment and production can be reduced through the use of a ground movement monitoring system [2-5]. Removal of material immediately alters the forces found in the remaining rock, potentially causing instability. These changes are seen through the

deformation of underground openings. Monitoring deformation in an area provides essential information for assessing

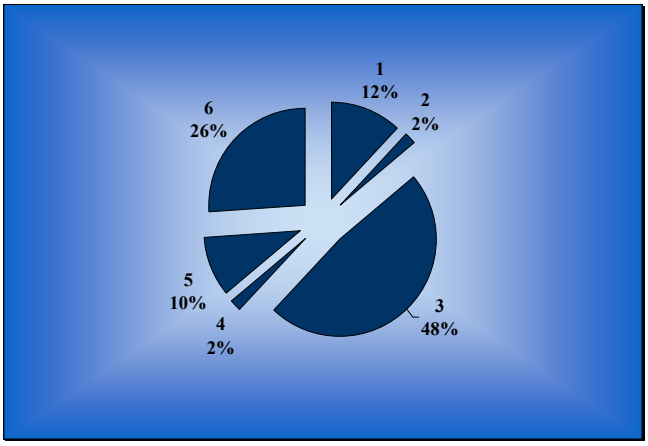

Figure 1.2: Severity of roof, face and rib-fall accidents from 1990 - 1996 [3].

overall ground stability. In the event of instability, movement monitors can act as warning devices as well. Devices of this sort are already used by many mines.

Ground movement monitors are not used only as warning devices. Mining results in continuous stress changes in the remaining rock, which immediately translates to deformations of the underground openings or surface wall. Monitoring of convergence of these openings and outcrops, particularly when driven through rock showing a time-dependent behavior, provides essential information to assess the overall ground stability. The data obtained from these monitors not only warn the mine personnel about the potential hazards of rock failures but also allow for better understanding of the rock failure mechanism. Based on the gathered data from ground movement monitors,

personnel can calculate the mine-induced stresses around the excavations, make recommendations about the required rock support and the geometry of future excavations, and make decisions about the mining techniques which must be used to safely and most economically advance underground development.

1.2. OBJECTIVES

In the broadest terms, the aim of this project is to develop and evaluate a prototype High-Resolution Target Movement Monitor (HRTMM) that can remotely measure the relative change in position of a target with sub-millimeter accuracy. More specifically, the developed monitor should be capable of measuring the change in position of a target or object with a sensitivity less than or equal to 0.1 mm.

Development of the monitor is a conclusion of the work originally begun as part of the master's thesis by Gray [6]. In this thesis, the HRTMM software was written and the most basic form of the monitor was constructed for laboratory use only. The current project will begin from this point and develop the monitor into a potentially usable instrument for geotechnical convergence monitoring in an actual field environment.

Refinement will be necessary for the camera platform designed by Gray. Development of a secure method of mounting and protecting monitor components in a mine environment will be necessary. Calibration procedures will be designed and incorporated into the design. A method of aiming the camera without using the viewport will also be included.

Development must also necessarily include a survey of available technology and selection of components that best suit the needs of the monitor. The primary user of this

monitor is seen as small mines with limited resources, thus the components chosen must help to minimize the cost of the monitor and should ideally be available in an off-the-shelf form. The total capital cost of the monitor is seen as being less than $1500 so as to easily compete with preexisting monitoring technology.

The monitor must be capable of remote operation, meaning that no installed target is required, though it is understood that monitor performance will be better with a standard target. Also, under no circumstances should a physical connection between the target and sensor be necessary for monitor operation, though physical approach to the target is considered acceptable for target preparation, characterization, measurement, or for calibration purposes, but not for routine measurements.

It is also necessary to develop an understanding of how different parameters and environmental variables will affect the monitor. Error characterization must be completed and methods of dealing with nuisance variables should be considered.

1.3. RESEARCH METHODS

The research methods involved with this project have been varied. A thorough literature review was conducted and continued throughout the entirety of the project. This was required due to the sheer number of allied fields that encompass the topic. The largest contribution of this review was in the development of the ideal model equation governing the sensitivity of the monitor.

The literature review also aids in understanding the needs of the mining industry in order to best design the monitor. As part of the literature survey, a significant review of currently available technology was completed. This was essential given the main overall

objective of the project: designing a new type of ground movement monitor. Part of the vision of this project was that the developed monitor might someday supplement or replace the existing technology in operating mines. For this reason a thorough understanding of the principles used in other technologies and the capabilities of those same technologies was required.

The project itself deals with a large number of variables and parameters requiring characterization. In order to accomplish this, a great deal of laboratory evaluation was completed so as to approach the characterization in a controlled manner. As the monitor itself is optically-based, an optical vibration-elimination table was utilized as the general platform for the experiments. This worked well for short-range testing but larger target distances required an alternative method. For these tests an open space inside of a building was used during quiet hours in order to eliminate vibration and air currents. The components of the monitor were supported by high quality tripods that could be positioned to meet the requirements of the test.

Laboratory testing was completed by using a micrometer movement stage and a fabricated target in order to simulate small target movements away from or towards the camera. These movements produced a measurable change that could be detected by the monitor. This change was compared to the manually produced target movement in order to determine the actual monitor sensitivity under a specific set of experimental conditions. The measured sensitivity of the monitor could then be compared with that predicted by the developed equation for ideal sensitivity in order to help determine monitor performance and error. All laboratory testing was completed on the campus of

the Missouri University of Science and Technology (MST), formerly the University of Missouri-Rolla.

Field evaluations were completed in addition to laboratory testing. These were necessary in order to assess the performance of the monitor under actual mine conditions and to conduct experiments for nuisance variables that could not be easily reproduced in the laboratory. These variables include mine fog and dust conditions and vibrations due to blasting. Field evaluations were completed at the Fletcher Mine, an underground lead mine owned and operated by the Doe Run Company in the Viburnum trend of Southeast Missouri. This was located approximately 60 miles from MST.

Finally, a sensitivity study was conducted on the developed ideal equation in order to determine the monitor sensitivity due to small changes in the experimental variables. As there is an infinite number of combinations of variables this was useful for determining which would have the largest impact on the sensitivity of the monitor for any condition. This is especially useful since the sensitivity of the monitor changes differently depending on which parameter is being varied.

1.4. SCOPE

The development of the HRTMM involves a myriad of variables. Laser theory, optics, digital photography, electromagnetic transmission, ground control, geomechanical behavior, health and safety, astrophotography, and blast engineering are only some of the fields influencing this research. As such it has been difficult to limit the extent of this study. Limits were set, though, based the on the objectives defined for the project and the boundaries of practicality.

Considering the very wide range of influences on this research an attempt has been made to provide a good base for understanding of the monitor operation. Many different technologies are referenced within this project but the claims made only extend to their use in the field of geotechnical monitoring.

It has been the goal to develop the HRTMM as a ground movement monitor. It has not, however, been attempted to fully perfect the system. Many experiments conducted during this research have pointed in the direction of a theoretical solution to a problem yet it has not always been feasible to pursue said solution for verification. Based on the recommendations provided in this document and information within the literature review, construction and use of a fully-functional HRTMM should be possible given sound engineering judgment.

It has been attempted to take most variables affecting the performance of the HRTMM into consideration to some extent. Those that have been judged to have the greatest impact on the operation of the monitor have been explored in detail both theoretically and experimentally. Variables such as air velocity, thermal gradients in the air, air density, humidity or particulate matter that cause light refraction have no adequate method for completely eliminating or compensating for error. This type of variable has been considered from the point of view of recommendations made in order to minimize error. These recommendations are based on the literature search and more detailed information can be found from those sources.

1.5. CONTRIBUTIONS

The development of the HRTMM represents the addition of a new ground movement monitoring technology to the suite of resources available to mine personnel. Due to the extreme variety of environments and situations found in a mine no single technology can ideally suit every circumstance. Thus any development of this type can likely find a niche.

Additionally, it has been a goal of the project to create the monitor from off-the-shelf components. This has been accomplished and has primarily been an attempt to keep the cost of the monitor at a minimum in order to make it accessible to every mine, regardless of the financial situation. In the current economic environment where profit margins and mine capital expenditures are up it is perhaps not as important as otherwise, but there are likely mines that cannot afford other, more highly-priced monitoring technologies.

Along with the development of the monitor came the derivation of an equation that governs the sensitivity of this type of optically-based movement monitoring system. Review shows that this has not been accomplished before. Theoretically, the equation allows the HRTMM system to be used with any combination of digital camera or image recording device, a lens of any focal length, and any laser incidence angle at any target distance. This greatly increases the flexibility of the system as it can be modified through substitution of components to fit the needs of a very broad range of circumstances. While the individual tests and values obtained from evaluation during this project may not apply directly to every conceivable combination of equipment, the principles remain the same.

2. LITERATURE REVIEW

2.1. PREDICTING FAILURE

The ability of a mining engineer to predict the failure of an area of interest within either surface or underground excavations has very obvious advantages. In today's society the injury or fatality of employees is no longer acceptable as it was during the early days of mining. Research and experience have increased the body of knowledge surrounding the topic of rock stability. This has enhanced understanding of the behavior of rock and improvements in monitoring technology have greatly increased the ability of a mining engineer to design a safe working environment, identify and reinforce an unsafe working environment, and provide advance warning of an impending failure. This helps to limit production downtime and allows for the evacuation of expensive equipment and irreplaceable human lives.

Initially a mine is designed in order to offer a level of safety and stability. Finite element or boundary element design software is often used to speed design of safe work areas while optimization algorithms such as Lerch-Grossman help to make a project economical. However, while initial design may help to ensure a safe beginning, the time-dependent nature of rock and slope failures can degrade a safety factor until hazards result.

Identification of potential hazardous areas of a mine begins with routine inspection and an understanding of the geological and structural nature of an area. Visual and other methods of inspection such as soundings or identification of voids between rock layers during drilling, bolting, or scaling activities plays an important role in this process and is completed by every member of a mine workforce. Hollow soundings,

spalling, tension crack formation and convergence are all signs of increasing likelihood of failure [5, 7].

Existence of a tension crack or spalling does not signal that immediate evacuation is necessary or even prudent. However, in areas known to be unstable or that become unstable it may be necessary to take precautionary measures that can identify the need for mediation, additional support, or evacuation. Mine monitoring has been shown to be a viable method of measuring and tracking ground deformation and movement in both surface and underground environments [8-10].

Much rock has been shown to react over time depending on its support conditions and the stresses being exerted on it. Surface excavations focus on sliding of material based on its shear strength while underground mines are more concerned with the closure of a space due to the exerted horizontal and vertical stresses. In each case stress and strain can be measured in order to help predict when failure may occur, however, strain-rate plays just as important a part.

The goal of a mine monitoring program for determining rock failure is to routinely measure the strain at a particular location in order to determine its strain rate and strain acceleration. In both surface and underground situations strain acceleration is a precursor to slope failure or collapse. Displacement-versus-time plots are very helpful in this regard. In most cases a warning is given before a major failure, allowing engineers time to plan for the event. Ground movement monitoring devices with high resolution allow for prediction of slope or excavation failure much sooner than monitors with low resolution.

As stated previously, surface slides and failures depend upon the shear strength of the rock and typically take place along a discontinuity or soft layer of material. A previously stable slope can be damaged by local blasting causing instability. Heavy rains have the ability to increase pore pressures helping to induce a slide. One excellent example of this sort of rock slide was located at the Chuquicamata Mine, Chile, in 1969 [8, 11-13].

The Chuquicamata Mine experienced a massive rock slide in 1969. This danger was identified well in advance and the slope was fully monitored using a number of methods. The mine engineers were able to use previous experience with the geology of the area and displacement measurements in order to predict the date of failure five weeks before its occurrence. The primary tool utilized for this accomplishment was a graph tracking the cumulative movement of the slope. It was observed that initial displacements grew in magnitude until they reached an asymptotic form near the failure date.

Underground mining also utilizes measurement of strain for calculation of strain rate with the goal of determining stability. The magnitude of the displacement necessary to cause failure underground is generally smaller than that required in surface mining conditions. Soft rocks such as salt, potash, shale, trona, and some limestone experience creep in much the same way as surface mines, also requiring strain measurements. Some hard-rock formations have also been known to exhibit creep. Underground, these strain measurements are generally taken in the form of a convergence measurement, a relative measurement of the amount of closure between two points [10, 14].

In addition to normal creep-like behavior, underground excavations are also under the stress of the overlaying rock layers. As excavation progresses, stress is redistributed

to the surrounding rock or to intermittent pillars causing convergence. These stress-induced convergences exhibit the same sort of response with strain-rate playing a critical role in prediction of failure. In each of these situations it is a convergence measurement that is made in order to monitor strain-rate, making development of convergence monitoring technology a fundamental part of improving understanding of the process and warning capabilities for underground failure.

2.2. MONITORING THEORY

2.2.1. Phase Change Measurement Technique. Electronic Distance Measurement (EDM) technology is based on the rate of propagation of light through the atmosphere [15]. The rate of propagation of light is determined by Equation 1 where V is the velocity expressed in meters per second, f is the frequency of the emitted energy in hertz and λ is the wavelength of the light expressed in meters.

$$\boldsymbol{V = f\lambda} \tag{1}$$

A typical EDM emits a series of electromagnetic waves that travel towards the intended target and uses the reflected energy to determine the distance to the target. Usually this is an infrared or laser light source and each of the emitted waves is modulated to have a given wavelength. Figure 2.1 illustrates the process of the departure and arrival of the generated electromagnetic wave at point E. It can be observed that the double distance between the EDM and the reflector (point R) is equal to a whole number

of wavelengths, plus a partial wavelength occurring at the EDM. The phase angle of the partial wavelength (ϕ) is determined in the instrument by noting the phase delay required to precisely match up the transmitted and reflected or retransmitted waves [16]. The phase shift corresponds to a change in target distance according to Equation 2.

$$\boldsymbol{\Delta D = \frac{\lambda}{4\pi}\Phi} \qquad 2$$

Since a phase shift of 2π corresponds to a distance of one half the wavelength, distances measured using this technique must be limited to [0, λ/2]. Generally the series of emitted waves is modulated to have respectively shorter wavelengths (higher frequencies), i.e. 10000 m, 1000.0 m, 100.00 m, and 10.000 m. Since each separate modulated wave is only capable of giving information about its own partial wavelengths, the high resolution is delivered by the 10.000-m wave, while the other three waves verify the initial readings and provide information about the larger distance values [16].

Manufacturers of EDM-based surveying equipment claim that the accuracy of these instruments ranges from approximately +/- (1 mm + 1 ppm) to +/- (10 mm + 5 ppm) [16]. Such sensitivity is sufficient for many slope monitoring applications in the surface mining industry, but it is unacceptable for underground convergence monitoring where much more precise measurements are required.

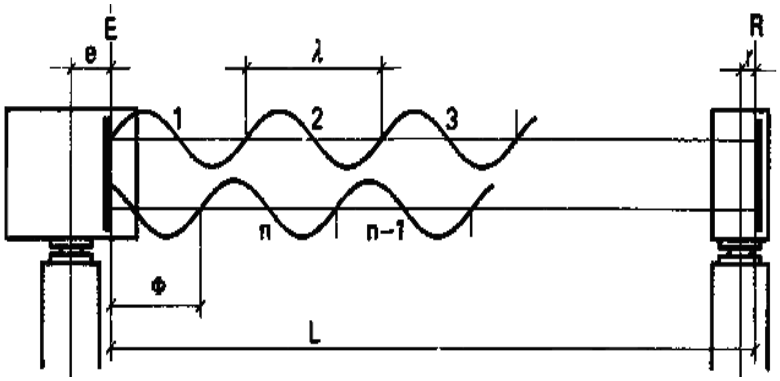

Figure 2.1: Principles of EDM Measurement from [15].

2.2.2. Time-Of-Flight Measurement Technique. Examples of time-of-flight (TOF) devices are the Acuity Rangefinders[1], which are products of Schmitt Measurement Systems, Inc. Acuity Rangefinders employ a modified TOF measurement principle [17, 18]. Figure 2.2 reveals the functionality of a common TOF mechanism. A laser pulse emitted by the laser pulser is routed through a beam splitter with one part traveling to the target and another part reflected into a receiver channel. Upon reflection from the target a second receiver collects the energy. Both signals are fed into a time-to-digital converter (TDC) which outputs a distance measurement based on the delay between the first signal and the reflected signal [19].

[1] Brand names are used throughout this document as examples or to specify the equipment used during this research. Use of a brand name does not constitute an endorsement for the mentioned brand.

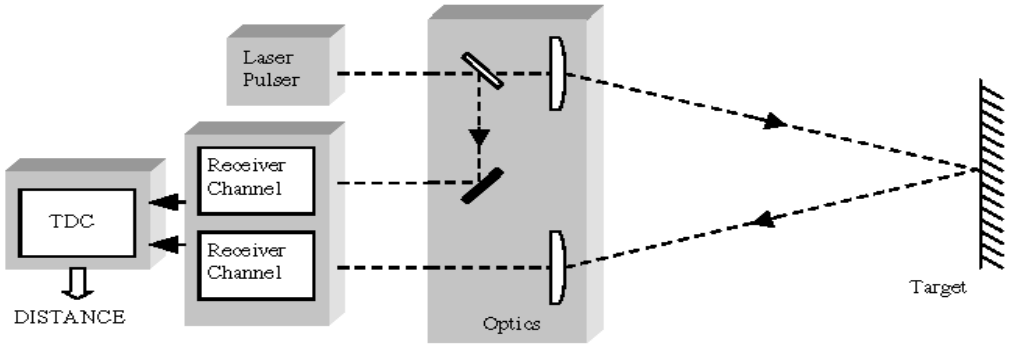

Figure 2.2: Schematic of a pulsed laser rangefinding system [19].

TOF measuring devices have two main advantages. A TOF device has both the emitting-energy source and the receiver in coaxial alignment. This has the benefit of reducing the chance of having the system be inoperable because one of the line-of-sight paths between the target and sensor or emitter is blocked. The other advantage is that the accuracy does not depend on distance. Error in a TOF system is caused by noise, changes in emitted pulse shape and amplitude, and changes in the delay of optical and electrical signals [20].

The manufacturer of the Acuity rangefinders gives the following specifications for the AR4000 rangefinder: range of 54 ft and an accuracy of 0.1 in (16.45 m and 2.54 mm respectively) [17]. This particular instrument requires the use of reflective tape and is primarily used for measuring linear displacement of a target.

2.2.3. Triangulation Based Laser Distance Meters. The triangulation-based laser distance meter is based on measurement of the internal angle of a right triangle and is frequently used in manufacturing and quality control situations. A single unit integrates both the emitting laser and the sensor. The integrated laser emits a beam that strikes the

object being measured and reflects back to the unit. The meter then senses the location of the laser spot on the object and determines the distance between the distance meter and the target [21, 22].

Meters that function on this principle incorporate a position-sensitive device (PSD) or a charge-coupled device (CCD) as their sensor that measures the amount of light that is reflected off the object being measured. Each individual diode collects light and the distribution of light collected along the array is used to calculate the angle of the internal angle, α. This type of system is shown in Figure 2.3 below. The distance between the integrated sensor and laser is precisely known, allowing for accurate distance measurements to be developed with the measured internal angle [22-24].

One drawback to this type of laser distance meter is that the sensitivity of the meter is not constant. From the figure it can be seen that when the target is moving away from the receiver the angle (α) decreases. However, the same change in the distance ΔD, that causes a large angular change, α_1, close to the sensor, causes a much smaller angular change, α_2, further away. An example of this type of laser system is the Laser Distance Sensor produced by the Waycon Corporation based in Munich, Germany. Another is the ODS Laser Triangulation Measurement Meter developed by Moduloc Control Systems.

Other drawbacks to this type of system are that the maximum range is limited to less than 800 mm in the case of the Waycon model [23], and 4000 mm for one of the Moduloc models [25]. These systems have resolutions ranging from 0.0008 ± 0.0008 mm to 0.5 ± 0.5 mm depending on the model. While the resolution is attractive, the short usable range makes this type of distance meter impractical for almost all convergence

monitoring applications in the mining industry. Prices of the triangulation-based systems start at about $1500 and go up from there.

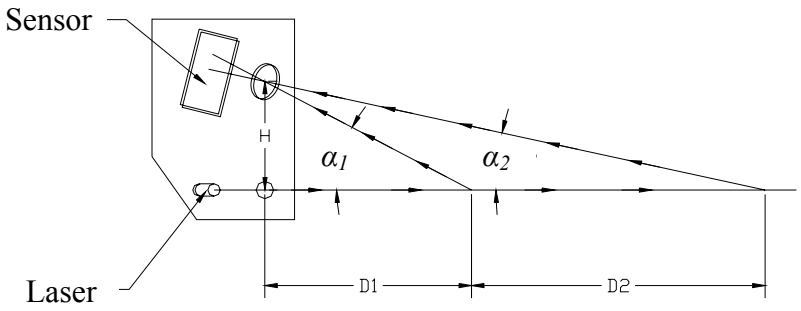

Figure 2.3: Principles of operation of triangulation-based laser distance meters [23].

2.2.4. Vibrating Wire Gages. Vibrating wire gauges are a type of strain gage used for remotely measuring stress and strain. They are widely used in the fields of mining, tunneling, civil engineering, and for monitoring many types of structures. They are used in piezometers, soil pressure cells, stressmeters and load cells as well as for monitoring stress changes in rock, concrete and in metallic structures.

Operation of a vibrating wire gage is based on the principle that a tensioned wire has a natural frequency of vibration that varies due to the tensile stress of that wire. This relationship is expressed by Equation 3 where ψ is the frequency off the vibration, l_w is the length of the wire, ρ is the density of the wire, and σ_w is the tensile stress of the wire [26].

$$\psi = \left(\frac{l}{2l_w}\right)\left(\frac{\sigma_w}{\rho}\right)^{1/2}$$

3

Operation of the gages consists of artificially vibrating, or "plucking", the tensioned wire with an electromagnetic impulse. A nearby electromagnetic sensor picks up the vibrations and transmits them over some distance to a frequency counting device that determines the frequency of the vibration and allows the tension of the wire to be determined [27].

Vibrating wire gages have benefits over electrical resistance strain gages in that their mechanical nature is unaffected by changes in electrical current, voltage, resistance or capacitance. Frequency counts are also able to be transmitted over long distances without losing fidelity among high background noise. They do however, respond to changes in temperature as the wire expands or contracts, though these temperature changes can be measured and corrected for to some extent [26, 27].

2.2.5. Linear Variable Differential Transformers. The linear variable differential transformer (LVDT) is another type of electrical displacement measurement device. It relies upon a mutual inductance principle and consists of a primary coil and two secondary coils symmetrically placed around a magnetic core and wound in opposite directions [26, 28].

In an LVDT an alternating current is supplied to the primary coil, which causes the formation of a varying magnetic field around the core. Through inductance, the magnetic field around the core causes a voltage to flow through the secondary coils that are closest in proximity to the core. Displacement of the core causes the number of

windings in each secondary coil to change in a linear fashion changing the amplitude of the output voltage linearly as well [28].

The opposite windings of the two secondary coils allow the LVDT to indicate direction of the displacement by causing induced voltages to differ in sign for each coil. The induced voltages from each coil are summed together, producing a single output which indicates both displacement magnitude and direction.

The LVDT is used to measure displacements for many types of sensors including borehole extensometers and convergence meters. It is a very reliable sensor with failures being caused primarily by rare electrical shorts. Displacement measurements of ± 1 μm are possible.

2.3. CURRENT CONVERGENCE MONITORING TECHNOLOGY

2.3.1. Tape Extensometer. The Tape Extensometer consists of a steel survey tape with punched holes loaded on a reel and fixed to the body of the instrument. It incorporates a tensioning mechanism for the tape as well as a dial indicator based distance measuring system. Two hooks are provided, one at the movable extremity of the tape and the other on the reel frame. Tensioning of the tape to a predetermined load is easily done by rotating a large knurled collar until two reference lines are precisely aligned. For an actual measurement, the tape extensometer is stretched between two reference points consisting of two steel eyebolts fixed on their respective anchors. A calibration frame can be used to check the instrument regularly and to determine, when applicable, a temperature-related correction. The highest resolution of a tape extensometer is +/- 0.01 mm [29].

One of the main advantages of the tape extensometer is the low initial price of the instrument, generally starting at between $1000 and $1500. This price is even more reasonable when it is taken into consideration that the same instrument can be used to make measurements at multiple measurement locations. On the other hand, the use of a tape extensometer is a manual exercise requiring at least one person. This manual element increases the true cost of a tape extensometer when factoring in the related labor costs.

Tape extensometers suffer, as do any manually operated monitoring system, from error introduced by the user. Depending on the skill and care of the user this has the potential of introducing unacceptable levels of error into the measurements. Another disadvantage of the tape extensometers is that they are not suitable for continuous monitoring of ground closures. Due to the manual nature of the monitor, convergence measurements are conducted only on a monthly or weekly basis in most mines where tape extensometers are used.

The tape extensometer's lack of continuous monitoring capabilities results in information being provided only about general trends in the stresses and strains in a mine but does not allow for detection of sudden changes in strain rate caused by mining of neighboring excavations. This, along with the necessity for an operator to enter a potentially dangerous area, eliminates the extensometer as a practical warning tool.

2.3.2. Rod Extensometer. The Rod Extensometer (also known as a tube extensometer or convergence meter) typically has precisions of 0.01 to 0.025 mm [30, 31]. It consists of a central section of pipe graduated with a Vernier scale and connected to a telescopic section. This telescopic section can be adjusted to provide a series of steps

inside which small rock movements between permanently mounted studs can be measured.

Rod extensometers are inexpensive and simple to use, reducing initial cost and training time. A single instrument can be used for monitoring many different measurement locations, increasing their cost efficiency. The disadvantages of these devices include their limited range (generally less than 4.0 meters) and their dependence on permanently mounted measurement anchors within a tunnel, passageway, or opening. Classical extensometers obstruct travel ways and prevent efficient movement through the areas in which they are in use. It has also been shown that the quality of the results depend greatly on the technique and experience of the operator [32]. And, of course, they are neither continuous nor inherently safe.

2.3.3. Borehole Extensometer. A borehole extensometer consists of an instrument head anchored in the collar of a borehole and a number of other anchors deeper within the borehole. The various anchors are connected with the collar anchor by a mechanical link, generally a tensioned wire or rod. Deformation components parallel with the borehole are measured by sensing the change in distance between the collar and rockmass anchors. The anchors on the far end of the wires or rods can be aligned to coincide with discontinuities in the rock mass such as cracks or bedding planes. They are best used to monitor known structural features and are relatively expensive compared to other monitoring technologies Resulting data can assist in understanding rock stability and behavior [33, 34].

Using multiple-point borehole extensometers, the distribution of displacements in a relatively large volume of rock can be recorded. This can be very helpful in determining

bed sag and separation in strata above coal mining road ways [35]. This data can be more useful than simple convergence measurements as these may be influenced by rock surface conditions. One drawback, though, is that typical borehole extensometers are only capable of measuring deformation parallel to the borehole. This does not prevent bore hole extensometers from being used for convergence measurements as well [26].

Suggested methods for monitoring rock movements with borehole extensometers are presented in the International Society for Rock Mechanics commission on Standardization of Laboratory and Field Tests [36]. Precision and accuracy with these devices is quite good, though is dependent on the length of the extensometer. Common error sources include mechanical damage to the instrument head, dial indicator, signal cable or cable connectors and accelerated wear due to dirt, dust or ice accumulations. These error sources can be minimized through proper protection and maintenance. Friction within the borehole due to dirt or ice buildup can also cause error. Extensometers are installed within the rockmass which makes temperature a very small component of error. This is fortunate because the corrections are complex and imprecisely defined [34].

2.3.4. Total Stations. Total stations consist of an electronic theodolite, an EDM, and an on-board computer all linked to allow for simultaneous measurement of distance, and vertical and horizontal angles. They are currently the accepted workhorse of most surveying operations. Some do not require a reflector or refractor target for short-range measurements, but longer distances and higher accuracies are acquired when using these targets. Total stations can be automated by incorporating small servomotors which direct the instrument according to a user-specified program. Total stations range in price

from $2500-$15,000 based on required accuracy, range and other features such as data-processing capabilities.

Precisions of better than 2 mm for range measurements and better than 1 second for horizontal or vertical angle measurements can be attained [37, 38]. It is also important to remember that measurements made with total stations are calculated measurements, relying upon the accuracy of distance measurements and calculated angle measurements taken from a control point. These inherently impart error into collected data [39].

Due to the relatively high error, total stations are not a practical solution for a comprehensive convergence monitoring program in an underground mine, though they are used frequently for surface slope monitoring programs.

2.3.5. Automated Slope Monitoring Systems. Automated Slope Monitoring Systems are primarily used at surface mine sites to monitor the stability of pit walls and tailings impoundments. They generally consist of a system of robotic total stations that can be programmed to allow for automatic monitoring of many different targets across the pit, though a Laser Scanning System is occasionally used. The EDM's in these systems generally have acceptable accuracy and precision for their purposes when used at ranges up to 10,000 feet. The benefits of these systems are from the drastically reduced labor costs, increased rates of sampling, and the early warning capabilities that come with that increased sampling rate. The biggest obstacle to mass installation of these systems is their high initial cost, which can range from $100,000 - $300,000 or higher depending on the size of the installation [40].

2.3.6. Global Positioning System. The global positioning system (GPS) is comprised of a group of orbiting satellites, each of which sends out a coded timing signal. The signal is a repeating binary pattern that is encoded to allow for receivers to determine the distance to a particular satellite based on this code. The code acts as a method of determining the length of time it takes the signal to pass from the satellite to the receiver. In combination with the position of the satellite within its orbit, which is precisely known, this allows the receiver to calculate the distance between the satellite and itself based on Equation 4, where *r* is the range, *c* is the speed of light, and *t* is the determined time. At least four satellites must be within line-of-sight of the receiver in order to determine both horizontal position and elevation accurately. The more satellites within sight, the more precise the calculated position will be [16].

$$\boldsymbol{r = ct} \tag{4}$$

GPS receivers range in precision from many meters to sub-millimeter depending on the type of receiver and receiver technology being used. The ability to track multiple satellites at once, to use the United States Coast Guard's Differential Global Positioning System (DGPS), and techniques such as Relative Positioning all help to improve the accuracy of a GPS receiver.

Relative positioning is a technique that uses two receivers tracking the same satellites. The combined observations allow determination of a baseline vector (ΔX, ΔY, ΔZ) between the two receivers. Using relative positioning accuracies can be in the millimeter range for carrier phase measurements after post-processing [41].

As a monitoring technology in the field of mining, the GPS system has many potential uses even though it is restricted to the surface portion of an operation. It can be used to map an operation, calculate the volume of a stockpile, assist in planning and reclamation and to locate drill holes. These are only a few examples of the uses of the GPS within a mine operation. Within the scope of this research, though, the GPS can be used for monitoring the movements of unstable slopes, pit walls, tailings impoundments and reservoir dams.

GPS receivers with accuracies within the millimeter range are suitable for monitoring creep and strain rates on slopes, walls, impoundments and dams. The system has also been used successfully to monitor structural deformation with baselines shorter than 500 m [42, 43]. The system is especially suited for large surface monitoring applications where use of a total station would be impossible due to lack of line of site between the reference points.

The GPS system does have some drawbacks. Error within the system must be carefully controlled. Post-processing is frequently necessary, though automated systems have been designed and installed to minimize the manual labor costs involved in using the system. Receiver placement must be carefully chosen to maximize visual access to the horizon to provide for ideal satellite constellation geometry. Additionally, the cost of survey-grade receivers can be up to $20,000 each, making an extensive, permanently installed network of automated monitoring stations quite expensive to implement.

2.4. REVIEW OF SIMILAR MONITORING DEVICES

Section 2.2.3 provides an outline of the monitoring devices currently available that can be used to monitor convergence. They use a photodiode array similar to those found in digital cameras to gather the scattered and reflected light from a target in order to determine the incident angle upon the target. The technology uses similar components to the HRTMM and the software processing is focused on determining the incident angle of the laser. While some laser triangulation sensors have been in use for 25 years, they have never been put to use for ground movement monitoring purposes in the mining industry due to their relatively short measurement ranges.

One other monitoring system has been found that uses a technology similar to that utilized by the HRTMM. This is a vision-based approach for monitoring displacements in vibrating systems [44]. In this article, researchers from the University of Southern California Department of Civil and Environmental Engineering utilized a video camera with a sample rate of 30 fps and a mounted target consisting of 2 red light-emitting diodes (LEDs) affixed to a 32 x 28 inch black steel sheet. The targets were placed under the Vincent Thomas Suspension Bridge (VTSB) in San Pedro, California, while the camera was mounted at a different location under the bridge. The two LED lights were mounted a known distance apart. A computer program tracked the movement of the LEDs in each frame and, after determining the average number of pixels between the two LEDs, was able to successfully measure the sensed motion of the LEDs in order to determine the vibration of the bridge.

Some of the problems with this study that were identified in the original article include use of a video camera with insufficient resolution, unstable mounting platforms

for the camera, and the fact that environmental conditions were not taken into consideration. Even with these deficiencies, the technique did give vibration results consistent with those other researchers have estimated through alternate measurement methods on the VTSB.

It is important to note that the VTSB system is incapable of monitoring convergence or divergence. If the target in that study were to move towards or away from the camera the LED lights would appear to move closer or further together due to the nature of visual perspective, i.e., as an object moves closer or further from the sensor the angular dimension changes. It is, however, capable of detecting side to side movement in the target.

2.5. LIMITATIONS OF THE TECHNOLOGY

While there are many monitoring technologies currently available for measuring ground movement in both surface and underground mines, their use is inconsistent [45]. Many of the challenges of monitoring in a mining environment preclude one or more monitoring technologies from being applicable to a given situation. General trends towards streamlining business and minimizing labor and equipment costs also play a role in limiting monitoring technology use.

Of the technologies reviewed above, none is universally suited to all mining situations. GPS, total stations and automatic slope monitoring systems are limited in their use as ground-movement monitoring systems to surface applications. This is either due to their basic operational principles or due to their precision, which generally does not need to be as fine for slope monitoring as for underground convergence monitoring. While

some mines have significant enough convergence to make monitoring with a total station feasible, generally other methods are chosen.

Assuming that a remote nature is frequently desirable for ground movement monitoring, each of the technologies available presents different constraints. Total stations, automatic slope monitoring systems, GPS and the HRTMM are all completely remote, meaning that no physical connection is required between the target and the sensor. It is also noteworthy that the only remote monitoring system that is free of connection between the target and the sensor and also does not require line-of-sight between the two stations is the GPS. Borehole extensometers can be considered remote if there is no problem running data cables between the monitor and the data collection and storage system. Tape and rod extensometers are not remote. Their use causes stoppage of traffic on any roadways in which they are implemented, and they require an operator to be directly exposed at their measurement location. This makes their use in areas which are currently unstable or unsafe impossible.

Each of the technologies also requires installation at the target itself. GPS receivers, reflectors, anchor points, and boreholes are all necessary and impossible to install in a location that may be potentially unstable. To some extent it will be shown that this is not the case with the HRTMM. While accuracy and precision certainly improve with installation of a fabricated metal target, depending on the rock being measured and the incident laser being used it may not be necessary. Many total stations are also designed for use without a reflector within a given distance. The accuracy and precision of these measurements will be compared with that of the HRTMM when used without a target.

Monitoring systems also vary in the number of personnel required to make use of them. Most of the remote technologies used today for monitoring are automated. The HRTMM also has great potential for automation as will be discussed later. For these systems, operational staff are limited to reviewing the collected data and/or responding when a critical amount of movement is exceeded and a warning signal is given. Other systems such as the tape or rod extensometers have a definite niche, but require one or more operators to collect each and every data point. This increases the responsibilities of the mine personnel. Their accurate use is also largely dependent on the skill and experience of the operator.

Systems vary greatly in their initial installation cost and time. Mine-wide systems are the most expensive with costs up to hundreds of thousands of dollars. This large cost is due to the large number of monitoring stations that must be individually purchased and installed, installation of the networking required to link the data gathering devices with the control devices generally located in another part of the mine, and the time required to test, troubleshoot, and calibrate the entire system. Systems such as a single borehole extensometer are less expensive when drilling of the hole, installation, wiring, and data collection is taken into account. Systems such as a rod or tape extensometer are the least expensive, though they have higher operational costs and are very limited in their ability to measure long distances and operate remotely.

In summary, each type of ground movement monitoring system has unique limitations and abilities, the most basic of which are discussed here. Other sources should be referenced for complete details concerning the use of these systems as it is outside the scope of this presentation. There is no single monitoring system that will wholly resolve

all mine monitoring needs. Given the number of monitoring systems currently available and the number of mines that do not use monitoring systems as a warning device, it seems that there is still a need to develop additional technologies that may entice some non-participating mines to take advantage of a proven method of protecting personnel and equipment.

3. SYSTEM DESCRIPTION

3.1. HRTMM COMPONENTS

The HRTMM is a remote convergence monitor that relies on the recording and tracking of a laser spot across a target to determine target convergence. This lateral movement is induced by target convergence due to the positioning of the projecting laser relative to the sensor recording the image data (Figure 3.1).

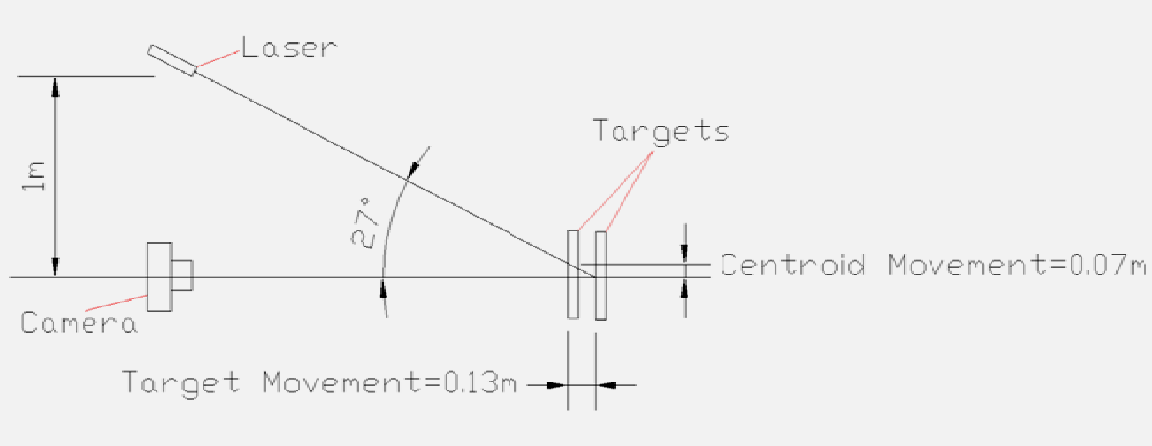

Figure 3.1: Illustration of the HRTMM operational principles.

The HRTMM consists of four main sections; the sensor, the target, the incidence laser(s), and a computer. Each of these sections is responsible for a particular aspect of the monitor's function. The sensor is responsible for capturing the light in the monitor's field of view, converting it to an image, and storing the data or routing it directly to the

computer. The target is the focus at which the sensor and incidence laser(s) are aimed in order to monitor movement. The incidence laser(s) provide(s) the coherent light that moves across the target in response to target movement. The computer is responsible for setting and carrying out a data capturing program, operating the sensor, recording data, and running the HRTMM software that tracks the movement of the incidence laser across the target, ultimately allowing for measurement of movement sensed by the monitor.

One of the goals of this project has been to keep the construction of the monitor both inexpensive and simple. Smaller mines with smaller budgets are more likely to use an inexpensive monitoring solution than an expensive one, thus making the permeation of this technology through the industry more likely. One of the easiest methods of keeping the price down is to utilize parts and equipment that are easily purchased "off-the-shelf" and to refrain from having too many specialized components produced exclusively for the monitor. This has been a large factor in the decision to use many of the components of the monitor.

3.1.1. The Sensor. The HRTMM is designed to primarily utilize a digital camera as a sensor, though other methods of recording digital image data are available. A mounting platform has been designed to firmly hold the digital camera and a targeting laser. The platform consists of a ½ inch thick piece of aluminum approximately 9 inches square. An upright sheet of the same aluminum is bolted perpendicularly to the platform and is drilled to accept the mounting threads of a high-quality video tripod head. In this configuration the camera is oriented in a horizontal position. The video tripod head allows the entire sensor to be rotated along three axes, giving complete control over the aim of the sensor.

The mounting platform has been drilled to accept the standard quarter-twenty bolts used in the camera industry for mounting cameras to tripods. A locking pin has also been installed to match the locking hole provided on the base of many cameras. The location of this hole will need to be altered depending on what model of camera is used, but locating and drilling the hole is a simple matter. When attached to the platform, the imaging plane of the camera is parallel to the upright sheet of aluminum. The camera is aligned with the locking pin and mounting bolt and a ¾-inch long bolt attaches the camera firmly to the mount.

Next to the camera, a targeting laser is attached to facilitate faster alignment of the sensor portion of the monitor with the target, thus helping to assure quick and simple installation. The targeting laser is a simple pen laser that operates on two AAA batteries. The targeting laser is a 635 ±10 nm class IIIA red laser with not more than 5 mW of output power. The range of the targeting laser is significantly longer than the current practical range of the monitor with the setup used in this research. A more powerful laser could easily be substituted if necessary. Substitution of a more powerful laser would require that precautionary measures be taken by the user to ensure that no eye damage could occur.

The targeting laser is aligned so that it is parallel to the line-of-sight of the digital camera. This was accomplished by first measuring the offset of the targeting laser aperture from the center of the digital camera lens. Next the complete sensor mount was placed on a tripod at one end of a hallway and aimed at a marked target point the other end of the hallway approximately 75 m away. The center crosshairs viewed through the camera were placed directly on a target point. Next the previously measured laser offset

was measured from the target point on the opposing wall and marked, showing where the targeting laser should intersect the opposite end of the hallway if it were aligned parallel to the camera line-of-sight. Finally the targeting laser attached to the camera mount was aligned to intersect the point. This method is sufficiently accurate for the purpose of aiming the sensor at the HRTMM target due to the long distance between the mount on the tripod and the point of measurement on the opposing wall. Also, the distance at which the alignment was made is further than what is currently considered practical for the monitor. While one purpose of the targeting laser is aiming the sensor at the target, the primary use of the laser is for helping to align the camera and the target. This will be covered in more detail later.

The digital camera used in the HRTMM is not limited to a particular brand, make or model. The decision concerning which type of camera to employ with the monitor depends on the required accuracy and desired cost, as well as the maximum range at which the monitor will be used. The environment in which the sensor will be placed, the frequency of image capture, and the method of transferring data to the computer need also be considered.

During testing on this project two different types of digital cameras were tested. Initially and for a short period a Konica Minolta DiMAGE A2 digital camera was used. This camera is an 8.0 megapixel camera with a fixed lens capable of 8x zoom. The lens has a 35 mm. equivalent focal length of 28 - 200 mm. and is capable of apertures from F/2.8 – 3.5 [46]. Unfortunately, as of March 31st, 2006 Konica Minolta has ceased production of all consumer cameras. This camera was used for initial testing and validation of the system as well as for all testing during software development [6].

When replacing the Konica Minolta DiMAGE A2 certain criteria were set forth for the digital camera. It was decided that the camera should be of the digital single lens reflex (DSLR) variety and should have a maximum resolution of at least 10 megapixels. This type of camera would provide greater flexibility in camera usage for research and would also allow for a higher sensor sensitivity due to the enhanced resolution. The camera also needed to be capable of taking delayed images so that it could be set to allow for vibrations to be eliminated. The camera was also required to use interchangeable lenses in order to allow for greater flexibility and the use of a telephoto lens.

The search for a more suitable camera led to the Nikon D200. The D200 is already incorporated into a number of other geotechnical monitors [47-49]. It met every criteria set forth in the search and had dozens of additional features that made it an ideal choice for this research.

The Nikon D200 is easily available off-the-shelf to anyone. It is a 10.2 megapixel DSLR with interchangeable lenses and a crop factor of 1.5. It has great flexibility in its usage options with respect to sensitivity, shutter control, focus options and image control. It is capable of outputting data in both compressed .jpg format and in a proprietary and lossless .nef format as well.

The D200 is very easy to interface with a computer system. It provides a regular USB interface as well as an option for interfacing over the wireless 802.11b/g standard. Every option on the camera can be completely controlled via computer when it is used in conjunction with the computer program Nikon Capture Control 4.4.0.

The camera control program allows a user to make a predefined program to remotely activate and use the camera. It has very flexible time-lapse photography

routines allowing for images to be taken repeatedly for as long or as short a time as necessary and it is capable of directing the camera to take images in bursts of any desired number of images at a given time. The data is automatically transferred and named according to user definition and can be stored on any computer hard drive. Batch routines can also be used to automatically perform certain modifications to the images such as file type conversions and automatic white balance corrections. The camera is also capable of operating independently of this computer control program and stores its data on a compact flash memory card.

The Nikon D200 is a consumer-grade camera that has many features making it more suitable for use in harsh environments such as mine sites. It has oversize controls that would make use with a gloved hand easier. Also, while most digital cameras are built with a plastic camera body, the D200 actually uses a magnesium alloy body covered in plastic and soft rubber coating and grips. The magnesium alloy increases the durability of the camera while the plastic and rubber help to deal with light bumps that the camera might take during use. It also helps to ensure a secure grip should the camera be damp from high humidity. As a consumer camera it is designed to be handled frequently, to travel via automobile and also to withstand trips on an airplane. This does give some stability to the camera with respect to its build, though like any consumer grade camera it is not designed to withstand being severely dropped or being struck by falling rock.

The camera does, however, provide an attractive option with respect to its use in mines. Most of the body seams, compartment doors and controls have either rubber seals or gaskets surrounding them in order to keep out moisture and dust. This is an essential feature in underground mines where there can be very high levels of both humidity and

airborne particulates. The camera itself is not waterproof, but it is much more sealed than a normal DSLR camera. If the camera might come into direct contact with water a waterproof housing would be recommended of the sort used by underwater divers. None of these housings were actually used during the course of research, but the adaptation of the monitor to their use would be elementary.

Another positive attribute for the camera is that the screens are very large and bright, but have power-saving options that significantly reduce their drain on the battery. The camera operates on a 1500 mAh Nikon EN-EL3 lithium ion battery at 7.4 V. and is capable of up to 1800 shots per charge. During testing the camera was left turned on in a mine for approximately 12 hours with very little noticeable battery drain. From experience it is expected that the camera could easily be left on and used for a week without needing a battery recharge, though a DC power port is available if direct powering is desired from a standard 110 V AC power source. A supplemental battery pack is available that allows the use of either two EN-EL3 batteries or can be fitted with a cartridge holding six AA batteries [50]. Complete camera specifications can be found in Appendix A.

Since the beginning of this project Nikon has introduced the D300 DSLR camera. It has many improvements over the D200 and should be considered as a potential camera for this monitor. The price is similar to that of the price of the D200 when it was originally introduced, about $1,800.00. The introduction has decreased the price of the D200, making it more economical. This can now be found online for prices as low as $700.00.

During the project two interchangeable lenses were used. One was a Sigma 28-70 mm F2.8-4 DG standard lens while the other was a Sigma 70-300 mm F4-5.6 DG Macro telephoto lens. These lenses had 35 mm equivalent focal lengths of 42–105 and 105–450 mm respectively when the camera's crop factor of 1.5 is taken into account. The increased performance of the camera and lenses over the DiMAGE A2 made them all very suitable for the project.

Even though Sigma lenses are not OEM lenses for Nikon, they are designed to work with the Nikon D-Mount. Nikon lenses are generally known to be superior in construction to Sigma lenses, though the question of optical quality is largely a function of owner opinion. Sigma lenses are, however, less expensive than comparable Nikon lenses. This was the impetus behind the choice to use the Sigma lenses. In order to meet the $1,500 monitor cost the price had to be reduced. As all data collected for this project was completed with the Sigma lenses, improvements in optical quality made by purchasing a Nikon lens instead would only tend to improve the quality of the image, most likely in the form of improving the clarity. It is considered unlikely that this would result in a change in the precision of the monitor.

The full specifications of all monitor components are located in Appendix A, while a breakdown of the complete monitor cost and components is included in Appendix B. The Nikon D200 and entire sensor section of the HRTMM can be seen in Figure 3.2

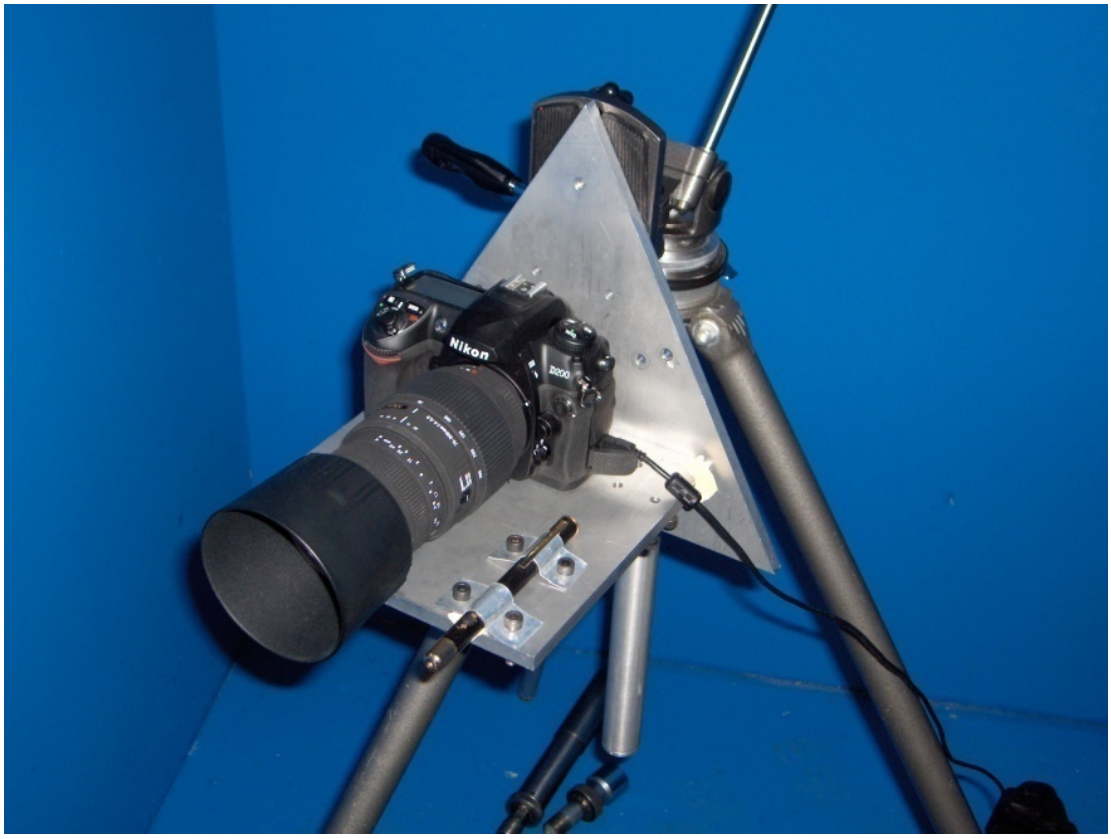

Figure 3.2: Sensor section of the HRTMM including the Nikon D200, Sigma lens, targeting laser, sensor platform, and video tripod head all mounted on a tripod.

3.1.2. Alternative Sensors. Digital cameras are not the only sensors that function with the HRTMM. In theory any method of capturing digital image data that utilized a raster data collection method and was capable of sensing the wavelengths being utilized in the incidence laser would be compatible with the HRTMM program. While this may be the case, certain sensors are certainly more suitable than others.

Another sensor used during this project was a Philips ToUCam Pro II webcam. The ToUCam is a very popular camera used by amateurs in the field of astrophotography [51]. Noting the similarity of photographing stars through a telescope to photographing

laser spots in a dark mine, a telescope was used in conjunction with this webcam in an attempt to increase monitor sensitivity. The webcam comes with an adapter designed to fit in the eyepiece of the telescope and screw into the webcam. This allows the camera to use the telescope as a large lens.

While the webcam only had a maximum resolution of 1.2 megapixels, this reduction was offset by the increased focal length of the telescope and the decreased size of the imaging chip (3.69 mm across the chip compared with 23.6 mm for the D200). A Meade EXT-80AT telescope was used and had focal length of 400 mm, a 9.7 mm eyepiece, and a 2x Barlow lens. Unfortunately, when the webcam was installed on the telescope the 9.7 mm eyepiece had to be removed eliminating a large part of the benefit of using the telescope.

The telescope that was used was chosen to meet the needs of finding a longer focal length lens and still keeping the overall cost of the monitor as low as possible. When tested it was found that the telescope and webcam combination were not stable enough to create a sensor equivalent to the D200 with the 300 mm lens. The large size of the telescope made it especially sensitive to any movement around it and greatly enhanced any vibrations imparted to the telescope. The small resolution of the web cam also reduced the sensitivity of the monitor to the point that it was not suitable. A telescope might still be used as a lens for a webcam for use with the HRTMM, but the price of the scope would necessarily go up dramatically in order to achieve the quality of construction and stability of image that would be necessary for use as a monitor measuring relative movements like convergences.

Another possible sensor would be many of the digital camcorders currently available. While none of these camcorders were tested during this project their usage would be very similar to the experiment conducted beneath the VTSB [44]. This same experiment provides verification that the use of a digital camcorder is not only feasible, but that it has the potential to work quite well. It would provide measurements with relatively high temporal frequency and could be very useful for monitoring during other research experiments where quick displacement or convergence measurements would be of interest over a short time span. Unfortunately while the HRTMM program would be capable of analyzing the image data produced by the camcorder, real time measurements would not be possible as the processing time for a single image is much too time consuming with the program in its current form.

3.1.3. The Target. The target for the HRTMM was designed for use in a mining situation where the natural rock wall being measured would be too rough reflect sufficient light for accurate measurement. The target consisted of a stainless steel plate that attached to a quick release mount for a heavy duty camera tripod head. The tripod head was free to move along three axes, thus allowing for complete control over the orientation of the target. On top of the metal plate a micrometer movement stage was secured. This movement stage was used during testing as a way to control the convergence or divergence of the target with the sensor. It also served as a method of calibration for the monitor. A Newport M-360-90 right angle bracket was secured to the micrometer, and an approximately ¼ inch thick stainless steel plate was bolted to the upright side of the bracket. The plate was 190 mm (7.5 in) wide by 300 mm (11.8 in) tall in order to provide plenty of targeting room. The pieces were aligned so that the direction

of movement of the micrometer was perpendicular to the plane of the stainless steel plate. When properly mounted on a rock wall the plane of the stainless steel plate should be perpendicular to the line-of-sight of the sensor. In actual mine use the target would be secured directly to the tripod head and the micrometer movement stage would be removed. The target section of the monitor can be seen in Figure 3.3.

One of the stated goals of this research was to develop a relative movement monitor capable of measuring convergence as small as 0.1 mm. The target therefore was required to be especially flat. Measurements made utilizing the stainless steel plate as a target have the laser spot moving over a very small area of the target itself. Generally spot movements were no longer than 28.4 mm (1.12 in) in length across the width of the target, which constitutes only about 15 percent of the target width. While no attempt was made to completely characterize the "flatness" of the stainless steel plate used in the target, the metal thickness was measured in order to gain some understanding of whether or not it had serious flaws.

In thirty evenly spaced locations around the perimeter of the target the thickness of the stainless steel plate was measured. All readings were taken within 5 cm of the edge of the target. Measurements were made using a digital micrometer capable of measuring thickness to a precision of 0.01 mm. The value recorded for each location was an average of three readings. The target ended up having very little variability in the thickness. Working under this knowledge, experimentation proceeded under the assumption that within the small distances that the laser spot would be moving across the target the target could be assumed to be flat. The descriptive statistics of the target thickness are presented in Table 3.1.

Table 3.1: Descriptive statistics of the target thickness.

Number of Observations	Mean (mm)	Median (mm)	Mode (mm)	Standard Deviation (mm)
30	6.15	6.15	6.15	0.00845

Figure 3.3: The target section of the HRTMM mounted on a rock anchor. The heavy-duty tripod head, aluminum plate, micrometer, right-angle bracket and stainless steel plate are visible from the bottom up.

Throughout this document the term “target” will be used when referring to the stainless steel plate and platform. Since the monitor can be focused on any surface within range that will diffusely reflect laser light, if the text of this document concerns using the monitor to record data without the “target” other terminology will be introduced at that juncture in order to refer to the focus of measurement.

3.1.4. The Incidence Lasers. Two types of lasers were used for the incidence Lasers; at the beginning of the project some Roithner-Lasertechnik lasers were used. These had an output of about 1 mW and emitted at a wavelength of 650 nm. For later use in the mining environment, the lasers chosen to serve were the 201-5-650 laser diodes available from BEA Lasers in Chicago. These were chosen because of their durable metal housing and plastic lens. They project a 2-mm by 4-mm laser spot with a divergence of less than 2 mRads. The beam is also emitted at a 650-nm wavelength, but the BEA lasers have an output power of approximately 5 mW. The lasers are operated on 3 volts DC, making powering them simple. None of these lasers were waterproof so future use in a very high humidity environment would require adaptation of a waterproof housing or substitution of a different laser.

The original lasers were considered a class II laser while the later BEA lasers qualified as class IIIA laser product according to the American National Standards Institute [52]. A class IIIA laser is generally considered safe within the United States and will not cause eye damage within the time period for a person's natural aversion response to take effect. In some foreign countries, only lower rated lasers are easily available to the public. The higher output powers of the lasers do allow for longer range applications to be attempted and helps to increase contrast between the background and the laser spot due to its increased intensity.

Power limits have also been determined for safe operation of lasers within an explosive atmosphere of either methane or coal dust. It has been found that ignition of these explosive atmospheres is dependent upon the output power of the laser and the beam diameter. In one methane-air mixture scenario a laser with 600 mW of output

power and a diameter of 200 μm was capable of ignition; though lower output powers are also capable of ignition with smaller beam diameters. Coal dust ignition is also possible under similar circumstances. While laser power limits are not part of an established mining related regulation, eventually this could be the case. Fortunately, for the beam diameter used with the HRTMM the laser power threshold would be much too high for the chosen lasers to ignite a flammable atmosphere [53-56].

Since red lasers are the most common lasers available they are lowest in cost and go well with the goal of having a low-cost monitor. Substituting a laser with a shorter wavelength (i.e. green) would likely increase the performance of the monitor with respect to the ability of the HRTMM program to successfully identify and locate the laser spot on the target. The shorter wavelengths of light, especially green, would contrast more against the background when the images were converted to grayscale. Additionally, since the majority of off-the-shelf digital cameras are produced with consumer photography as their primary function, they are designed to be more sensitive to green light. This is due to the fact that the human vision response is more sensitive to green light. Most camera sensors are twice as sensitive to green light as they are to red or blue light [57].

Two negative factors influenced the selection of the incidence laser wavelength in favor of the 650 nm laser over the green 532 nm laser. Firstly, green lasers are more expensive. In comparison to the approximately $50/laser for the red laser, the green laser diodes are approximately $200 per laser. Secondly, the green lasers are actually more hazardous to eyes than the red lasers due to the eye's increased sensitivity to that wavelength of light. For that reason, any green laser that was purchased would need to have a lower power rating to still be considered safe. It is possible that some of this loss

in power may be offset by a digital camera's increased sensitivity to green light, but that was not tested in this research.

In addition to the lasers, the incidence laser section of the monitor includes a 360-degree rotational stage manufactured by Siskiyou with ±1 degree of accuracy. This stage featured a central location for mounting fabricated components with a standard quarter-twenty bolt. For the project a one-inch diameter aluminum cylinder was drilled and tapped to fit the fastener on the rotational stage using a lathe. A hole sized to fit the diameter of the laser diode was drilled perpendicular to the length of the cylinder. This mount held a single laser diode. For multiple laser work an aluminum block was drilled with multiple holes, fitted with multiple laser diodes, and attached to the rotational stage.

For laboratory work, the rotational stage and laser was able to be mounted directly onto a Newport breadboard with granite platform (Figure 3.4). In the field a bracket was fabricated that allowed the stage to be rotated in two perpendicular dimensions, with the stage itself rotating in the third dimension, allowing for easy aiming at the target. The fabricated bracket was designed to be affixed directly to a rock wall (Figure 3.5).

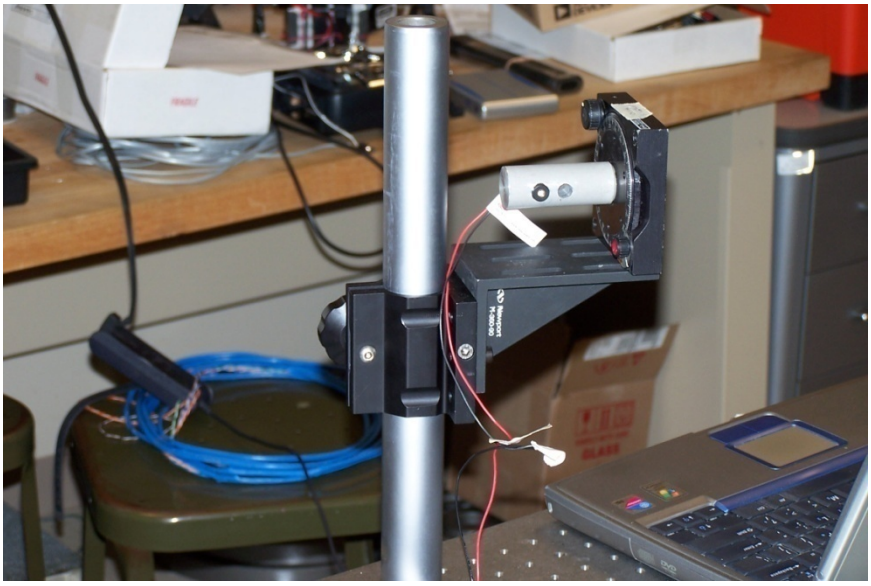

Figure 3.4: Laser diode and rotational stage mounted to an optical experimentation table in the laboratory.

Figure 3.5: Three incidence lasers mounted directly to a rock wall.

3.1.5. The Computer. The final section of the HRTMM is the computer. Throughout the duration of this research project this consisted of a Dell Inspiron 600m Laptop. The computer is used not only to run the HRTMM software for determining centroid movement of the incident laser, but it also stores the data in real time and operates the camera.

The HRTMM software looks at each pixel in the image individually and compares them to the surrounding pixels in order to determine laser spot location. This is a rather processor-intensive procedure. The configuration of the Dell laptop used included a 1.60 GHz Pentium M processor with 1.25 GB of random access memory. This proved to be sufficient for the task, though processing was occasionally slow with images containing well-lit and/or complex backgrounds. The laptop was also outfitted with a USB 2.0 port for the camera connection and a wireless network card for the optional wireless interface with the D200, though this connection was not used for this research.

Other software used on the laptop includes the previously mentioned Nikon software specifically designed for controlling the camera. The aptly named Nikon Capture Control version 4.4.0 was used to completely control the D200. The program allows for remote control of the image capture as well as all camera properties via USB port and USB cable. Captured images can be automatically named and saved to specified folders. The program also allows the user to program a series of images to be taken at specified times, which would be ideal for a monitoring program. The program could automatically capture an image every 30 minutes indefinitely, as long as storage space was unlimited. Finally, remote control of the camera eliminates human contact with the camera during data capture and the vibrations that the contact creates. This was shown to

be a problem in prior research [6]. The entire camera and computer setup can be seen in Figure 3.6.

Figure 3.6: Sensor mount and laptop computer used with the HRTMM.

3.1.6. The Mounting Brackets. Three of the four sections of the HRTMM are designed to be mounted to a rock wall. For this purpose, custom-built mounts were fabricated with the intent to make them strong and ridged, so that they should be able to withstand being installed in an underground mine. The sensor platform and the target

each have a wall mount made out of steel that extends approximately 16 inches from a nut welded to the mount. The 16-inch extension is necessary to allow the tripod heads free movement without hitting the wall. The nut welded to the rear is of the size that it can be threaded onto 7/8-inch threaded rock bolts, or 5/8-inch rock anchors with an adapter. Installation of the monitor simply consists of screwing the wall mounts to the bolts or anchors mechanically fixed in the wall, and then attaching the sensor platform or target respectively. The wall mounting bracket can be seen in use in Figure 3.3.

The mounting bracket for the incidence lasers consists of a square piece of stainless steel with a nut similar to the ones described above welded onto one side. A hole is drilled perpendicular to the nut through which a quarter-twenty bolt is threaded. This bolt fastens directly to the rotational stage holding the incidence lasers themselves. Adapters were also created to let the wall mounts be used with a wider variety of threaded anchors. These were simply created from a bolt with a smaller nut welded onto the head (Figure 3.7).

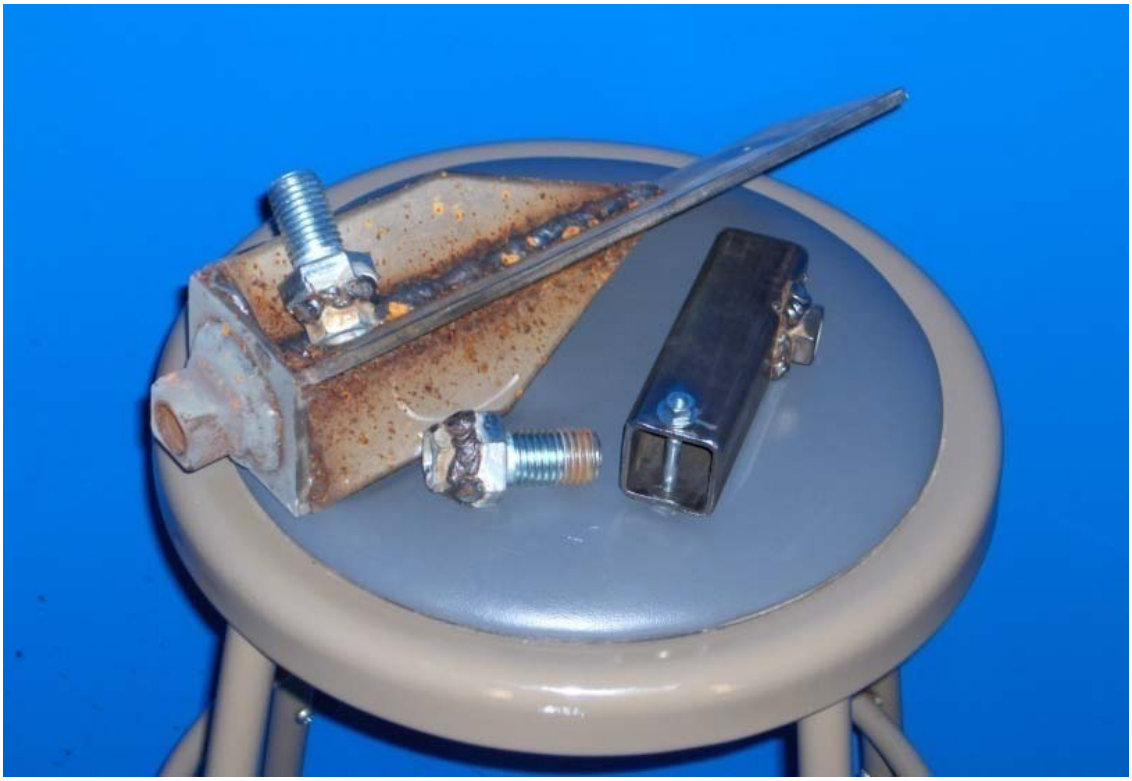

Figure 3.7: A wall mount for the target or sensor platform (left). The wall mount for the incidence laser(s) (right). Thread adapters (resting on top).

3.2. HRTMM SOFTWARE

The HRTMM software was custom written for this monitor application as part of a separate thesis [6]. The software is operated on the laptop computer and is responsible for computing the locations of the laser spots within the image. The location of each laser spot is referenced according to the X and Y coordinates of the image pixels. The coordinate system is oriented so that the X value increases from left to right across the image and the Y value increases moving from top to bottom. This orientation places the origin of the coordinate system in the top left corner of the image.

This project is partially in response to the initial recommendations of the software author. Very little testing was done on the software for use as a monitor beyond the basics required to prove that the software functioned correctly and that the concept was viable. The knowledge gained through this project has played a large part in determining the necessary changes to the software for it to become a practical movement monitor for the mining industry.

3.2.1. Software Procedure. The basic flow of the HRTMM software from start to finish is as follows. First the code loads an image of a specific format. The image itself can be in a wide range of formats, including but not limited to bitmap, jpeg, portable network graphic, etc. The image contains a target or object on which the laser light is shining, creating "spots" which are brighter than the background due to the light intensity and contrast. Once all of the image data is loaded into the computer, it is converted to a grayscale image based on the color planes of the image. The program then applies a user-specified threshold to the image so that for each pixel in the image the pixel is changed to black if the pixel value is below the threshold value or changed to white if the pixel value is above the threshold value [6, 58]. The threshold value is compared to the pixel's brightness value.

The software is able to detect essentially any number of laser spots in the image as long as processing time and power are unlimited and the spots do not overlap. Although there are multiple ways of accomplishing this with techniques such as the use of blob-labeling algorithms [59], the current system utilizes a sliding window function of user-specified size to sweep through the image and locate and record white pixel locations. Once all white pixel locations are found, the software begins to group together

all coordinates which are adjacent to one another. By performing this operation, the software locates and groups together all white pixels within a cluster, which represents a spot. The software then creates a sub-image containing all white pixels within the image.

After determining the clusters within the image, the final step of the program is to use the total area created by each cluster of white pixels and the total of the X and Y coordinates to determine the centroids of the clusters according to Equations 5 and 6. This process is repeated until centroids have been determined for all clusters.

$$X\ Centroid\ Coordinate = \frac{\sum X\ Coordinates}{Area} \quad (5)$$

$$Y\ Centroid\ Coordinate = \frac{\sum Y\ Coordinates}{Area} \quad (6)$$

Figure 3.8 shows a blown up version of a sample image which was taken using three lasers, producing three laser spots (only one of which is shown in the figure). The blue boxes represent the window function searching the image. The red box around the entire spot is the area within which white pixels were included when determining the centroid of the laser spot. The red bulls-eye represents the location of the detected centroid.

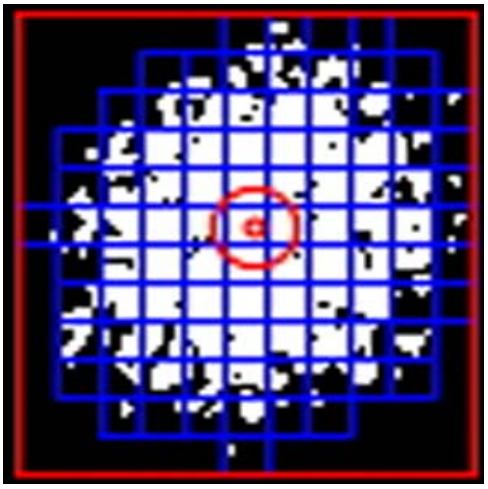

Figure 3.8: Example of a laser spot returned by the HRTMM program.

3.2.2. Data Return. This method of tracking laser movement has the potential to yield extremely high levels of accuracy in terms of its ability to detect relative distance changes between the monitor and the target. When the program calculates the centroid of a laser spot it does so with sub-pixel resolution. The resultant centroid returned by the HRTMM program is calculated by an algorithm that uses the discrete pixel locations of all the pixels in the laser spot and so yields an extremely precise calculation.

Upon completion of the operation, the HRTMM program returns a great deal of data concerning the image and the laser spots it contains. The centroid of each laser spot is returned, along with the number of windows necessary to enclose it and the total number of pixels located within that particular spot. The coordinates of the corners of the red outlining box seen in Figure 3.8 are returned and data concerning the number of extraneous pixels found in the image is returned.

In addition to numerical results, the program also automatically saves a copy of the thresholded version of each image; a black and white version of the image showing the white spots on the black background. Finally, the program saves a copy of the image showing the pixel, centroid, sliding windows and red bounding box. These images are very useful for troubleshooting purposes and for judging the quality of the user-specified threshold and window size.

3.3. MONITOR CONFIGURATION AND INSTALLATION

The typical configuration of the HRTMM monitor is with the sensor mounted opposite the target or object being measured so that the line-of-sight of the sensor is perpendicular to the plane of the target or object. This orientation helps to reduce the error of the monitor from poor alignment. If the target or object being measured is not perpendicular to the sensor line-of-sight then, when the sensor and target converge or diverge, there will be an error introduced into the measurement dependent on the angle of the target off perpendicular. This occurs because the point at which the target intersects the incident laser beam moves closer or further from the sensor due to its off-angle as well as due to any convergence or divergence imparted to the target. As the off-angle approaches zero, the error will also approach zero. As the off-angle approaches the incidence angle of the incidence laser beam the error approaches infinity. This can be anticipated and removed by calculating the true perpendicular movement based on trigonometric identities.

Since the perpendicular alignment of the sensor with the target is essential for optimum performance of the monitor, a simple method of achieving perpendicularity has

been devised. In order to assure said alignment a temporary mirror is affixed to the surface of the target. The sensor and the target are aligned so that when turned on, the targeting laser on the sensor platform reflects off of the mirror and back to the source aperture. This method of determining perpendicularity is considered to be accurate enough for the purposes of aligning the sensor and the target.

The position of the incidence laser mount around the sensor is not important. The laser could even be mounted directly above or below the sensor without ill effects. This would only change the path that the laser spot would take across the target or object being measured. The only location factor that matters to the sensitivity of the monitor is the angle at which the incidence laser intersects the target. A larger incidence angle will result in a greater sensitivity. The converse of this statement is true as well.

The monitor components are designed to be installed on the end of threaded rock bolts or mechanical anchors and are described in the previous section. While they were not tested during this research, other methods of component mounting can be considered. It is possible that a method could be used to attach the monitor to previously installed rock bolts with a strong magnet. Permanent mounting stations could also be installed according to the specifications set forth by the Army Corps of Engineers for survey control points [43]. This would be especially useful if the monitor were used for slope monitoring in a surface mine.

As a back monitor the target should be installed on the back, with the target itself being set in the horizontal plane, or perpendicular to the direction of expected convergence in the area. This will allow for the most accurate readings of convergence. The camera or other sensor would be best installed near the floor, to allow for easy access

for power and data cables or for data retrieval if cables are not used. Monitor performance will improve if the camera line-of-sight and the target are perpendicular.

In underground mining, especially in a low-coal application, installation of the monitor requires a bit more imagination. Due to the low clearances between many pieces of machinery and the back in low-coal seams it may be possible to create a cavity in which the camera could be installed, if the geotechnical conditions of the area allow for creation of such a cavity. In this instance the camera should be the monitor component installed in the back, with the target being mounted directly in the floor. This arrangement does have a disadvantage in that installation of the target in the floor allows for machinery and foot traffic to come into contact with the target, potentially altering its orientation or eroding the surface from friction and abrasion. Gravel, mud and dirt can also be transported onto the target interfering with data acquisition.

In a low-coal application, a more practical installation would be with the target fixed directly on the back and with the camera installed near the floor on one side of the cavity being monitored and the incident laser being installed near the floor on the other side. This configuration does not allow for a perpendicular orientation between the camera and target to be achieved, but is more practical. In order to eliminate damage to either camera or incident laser these can be installed behind a heavy shield or outcrop, or a cavity can be created in the rib if safe to do so.

4. MONITOR SENSITIVITY

4.1. CALCULATION OF SENSITIVITY

The HRTMM is primarily a convergence monitor, needing a physical convergence or divergence of the sensor and the target in order to detect movement. Ultimately the purpose of the monitor is to determine the magnitude of said convergence or divergence in terms of a standard unit of measurement. While this may be the ultimate goal, the monitor itself is incapable of returning direct data concerning the distance between the target and the sensor in its current form. In reality a change in distance is derived from the results obtained by the monitor, which in simple terms merely calculates the location of the centroid of a light source in a digital image. A meaningful result in the form of a convergence or divergence distance is accomplished during post processing. Since it is the case that the monitor is determining convergence based on the centroid location in a digital image, to understand the monitoring capabilities of the HRTMM it is necessary to first look at the method in which monitor sensitivity is calculated.

4.1.1. Sensitivity Definition. The sensitivity of the HRTMM is defined by the smallest change in target position that the monitor is able to resolve. Since the monitor calculates a change in movement based on how far across a digital image the centroid of a light source moves, and digital images are made up of a discrete number of pixels, the smallest change that the monitor should able to detect is a movement of one pixel. For example, if a light source appeared on the image to take up an area of one pixel, in order for the monitor to sense that the light source had moved the light source would need to change position in the image by moving to an adjacent pixel. Under these circumstances it is understandable that the maximum sensitivity, or minimum movement discernable by

the HRTMM, would be equal to the distance the target would have to move in order to cause a movement of one pixel on the image.

In the event that a light source produced a spot larger than one pixel in area, the HRTMM software is capable of determining the centroid of the spot with sub-pixel accuracy. Similar to the example provided above, the maximum sensitivity of the monitor is determined by comparing the distance that a light spot moves across an image to the real movement required to produce the corresponding centroid shift. In this case the monitor sensitivity, s, is equal to the distance the target moved, ΔD, divided by the total centroid movement across the image, C. This is shown in Equation 7. This equation is used in order to determine experimental sensitivity values.

$$s = \frac{\Delta D}{C} \tag{7}$$

It has been suggested that there are two different methods of calculating C from the returned centroid data [6]. In the first suggested method, the centroid of the laser spot before movement and after movement are both compared to the origin of the image (defined as the upper left corner). With this method the distance calculated is not Euclidean and C varies with the position of the two centroids within the image. The second method simply determines the direct Euclidean distance between the two laser spot centroids before and after movement. The first method follows Equation 8 while the second follows Equation 9. In both equations C is the centroid movement across the image (in pixels). X_1 and Y_1 are the centroid locations along the respective axes before

movement, and X_2 and Y_2 are the positions of the centroid after a target movement. In order to determine the true sensitivity of the monitor Equation 9 must be used (method 2).

$$\boldsymbol{C = \sqrt{(X_2{}^2 + Y_2{}^2)} - \sqrt{(X_1{}^2 + Y_1{}^2)}} \quad (8)$$

$$C = \sqrt{(X_2 - X_1)^2 + (Y_2 - Y_1)^2} \quad (9)$$

4.1.2. Sensitivity Variables. Due to the nature of the HRTMM, it is impossible to provide a single maximum sensitivity for the monitor. There are many variables that affect the sensitivity and therefore give the monitor a different maximum sensitivity for every situation in which it is placed.

Two types of variables affect the sensitivity of the HRTMM; fundamental and nuisance variables. A fundamental variable is one which has the ability to either increase or decrease the sensitivity of the monitor. It is dependent upon the configuration of the monitor's parts, settings and location relative to the target. Generally, a fundamental variable requires an actual physical change in the alignment of the monitor's parts or in the settings or components the monitor is using. A nuisance variable is something that negatively affects the capabilities of the monitor. These variables are incapable of improving the monitor's sensitivity and are caused by the environment and other influences extraneous to the monitor. Improving a nuisance variable serves only to reduce the error in the monitor's measurements, thus improving the measurements themselves.

4.1.2.1 Fundamental variables. Fundamental variables include the distance between the target and the camera, the angle of incidence of the incidence lasers (measured relative to the normal of the target), the focal length of the lens, the cross sectional dimension of the image along the line of centroid movement (expressed in pixels and more easily referred to as the "pixel-width" of the image), and the width of the camera's sensor (in millimeters).

The fundamental variables affect the sensitivity of the monitor in three different ways. The distance between the camera and target and the focal length of the lens both affect the sensitivity of the monitor in a similar way. Both variables increase or decrease the amount of real target movement necessary to cause the centroid of a light source to move in a discernable manner across the image. In both circumstances the scene appears to move "nearer" or "further" to the camera, effectively decreasing or increasing the area of the target recorded by each pixel, thus altering the sensitivity. Decreasing the distance between the target and the camera accomplishes this in a physical manner - truly moving the target closer to the camera. Increasing the focal length of the lens accomplishes this optically by channeling the light from the scene through the lens or a set of lenses, allowing the camera to perceive that the distance to the target is less. While this isn't actually the case, the principle is the same.

The angle of incidence affects the sensitivity by controlling the rate (centroid movement per unit of measurement target movement) at which a laser will move across the target if target movement occurs. This is generally expressed in pixels/mm or pixels/in.

The pixel dimensions of the image sensor affect the monitor sensitivity by increasing or decreasing the number of distinct measurement points, or pixels, the monitor is utilizing to record data. The camera views a scene with a defined field of view that has a given height and width. For each dimension there are a given number of pixels on the sensor that each record a portion of that scene. As the number of pixels being utilized increases, the percentage of the total scene area recorded by each pixel diminishes. This has the effect of decreasing the real target movement necessary in order for the centroid of a projected light source to move across the image, thus increasing the sensitivity.

The physical dimensions of a camera's imaging chip are mostly related to the use of digital cameras as a sensor. Most mechanical cameras were designed to use film that was 35 mm in width. Lenses sold for these cameras do not act the same when used with a digital camera where the imaging chip is not 35 mm wide. The term "effective focal length" is used to describe the apparent focal length of a lens when used with an imaging chip that is not 35 mm wide and is determined by multiplying the 35 mm focal length by the following equation (Equation 10) where *F* is the effective focal length, *f* is the focal length, and *w* is the width of a camera's imaging sensor. All units are expressed in millimeters.

$$F = f * \frac{35}{w}$$

When determining the width of the camera's imaging sensor it is important to base this on the effective resolution of the camera. This is best explained with an example. The Nikon D200 uses a DX format imaging chip that is 23.6 mm wide by 15.8 mm tall. It has a resolution of 10.92 million pixels and 10.2 million effective pixels. This is the number of pixels on the imaging chip that are actually part of a captured image and have light from the lens fall upon them. The effective width of the camera's imaging sensor is based on the effective pixels of the sensor. For the Nikon D200 this effective width (the width of the 3872 pixels used in the maximum resolution image) is 22.6 mm based on the known effective resolution and the known 3:2 image format.

4.1.2.2 Ideal sensitivity. The ideal sensitivity of the monitor can be determined from optical lens equations and is based on the equation used to calculate the field of view of a lens at any distance (*FOV*) [60]. The field of view is defined as the far-field (at the distance of the target, t_d) width of the scene that is captured by a sensor using a lens of a given focal length. It is defined by Equation 11.

$$FOV = \frac{w}{f} t_d \tag{11}$$

If the far-field width of the field of view at the target distance can be determined, Equation 12 shows it is a simple matter in order to determine the far-field width of a single pixel (w_p) as long as the number of pixels along the cross sectional line of the image sensor are known (p_w). The cross sectional line is defined as the line created on the

image or image sensor drawn between two laser spot centroids, before and after target movement, extended in both directions to the edge of the image.

$$w_p = \frac{FOV}{p_w} \tag{12}$$

Based on Equation 7 it is understood that the maximum sensitivity of the monitor is equal to the target displacement required for a single pixel centroid movement. It is also known from Equation 12 what the far-field width of a single pixel is. It can be reasoned that the maximum sensitivity (due only to variables of focal length, target distance, sensor size and horizontal pixel count) is equal to w_p.

$$C = w_p \tag{13}$$

The far-field pixel-width is related to target movement, ΔD, by the tangent identity where θ is the angle of incidence.

$$\Delta D = \frac{C}{\tan\theta} \tag{14}$$

Substituting Equations 11,12 and 13 into Equation 14 yields a single equation that will produce the ideal sensitivity that could be determined by the monitor based on the

five fundamental variables. The equation is determined for a centroid movement of a single pixel so $\Delta D = s$.

$$s = \Delta D = \frac{wt_d}{fp_w \tan\theta}$$

15

4.1.2.3 Nuisance variables. Nuisance variables include such things as ambient light levels, particulate matter or water vapor in the air, vibrations, temperature, humidity, barometric pressure, air movement, target texture, target color, and laser thermal drift. Each of these variables are influences outside of the monitor itself that can impart error to the data.

High ambient light levels act to reduce the contrast between the projected laser spot and the surrounding scene, making it more difficult for the HRTMM software to properly locate the centroid of the spot. Particulate matter and water vapor in the air can scatter the incidence laser light reducing the amount that impacts the target and is returned to the sensor. It can also refract the light path altering the location of the laser projection on the target. Vibrations harm data by falsely changing the location of the camera, target and/or incidence laser platform. Temperature, barometric pressure and air movement are environmental variables that cause error. Temperature can cause thermal expansion of the monitor components, changing their positions. Humidity and barometric pressure can both cause refraction through the air by changing its density and therefore its index of refraction. Increased target texture can increase random scattering of the light as it refracts and can also alter the shape of the laser spot, confusing the true location of the

spot centroid. Depending on target color different amounts of laser light are absorbed or reflected back to the sensor. This can have the effect of changing the amount of light recorded by the sensor and thus changing the size of the spot recorded and possibly the centroid as well. Finally, as a laser diode's internal components warms up the direction of the projected laser beam can be altered slightly. This is referred to as thermal drift and obviously alters the position of the laser spot on the target. Each of these errors will be considered in more detail.

4.2. EFFECTS OF SENSOR PIXEL DIMENSION

Of course, sensor resolution plays a part in the sensitivity of the monitor, but more specifically, it is the dimension of the image sensor expressed in pixels that is important. In the case of the Nikon D200 the effective resolution is stated as being "10.2 megapixels" by the manufacturer but the dimension of the camera's image sensor is 3872 pixels wide by 2592 pixels tall (on its highest setting).

To show the effects of camera resolution on the sensitivity of the monitor, two tests were completed, one with the Konica Minolta DiMAGE A2 digital camera and one with the Nikon D200. The A2 and D200 both have the capability of adjusting the resolution used to capture data between three different image resolutions. In order to judge the effect of resolution on the sensitivity of the monitor, data was collected with each camera in each of their three resolution settings.

4.2.1. DiMAGE A2 Resolution Test. For the first test the DiMAGE A2 was used. This camera has settings to capture images that are 3264 by 2448 pixels, 2560 by 1920 pixels, and 1600 by 1200 pixels in size. For this test the distance between the

camera sensor and the target was 2.000 m and the distance between the camera and the incidence laser was 1.000 m. The camera was set to use a 10-second delay between pushing the shutter button and actually activating the shutter. This was in order to allow time for vibrations imparted by pushing the shutter button to die down. The target on the micrometer was moved away from the camera 8.00 mm in 1.00 mm increments and an image was captured at each location, including the zero position, at each camera resolution setting. This test was repeated 5 times, making a total of 45 data points per resolution setting or 135 total data points all showing centroid movement at a given resolution setting due to target movement. All images were analyzed using a window size of 7 and a threshold of 120.

Analysis of the data gathered from the test proceeded as follows. Once the data was imported into a spreadsheet the X and Y values of the laser centroids were input into Equation 8 in order to determine how far the centroid moved with each change in target position. The average sensitivity and standard deviation of the sensitivity for each resolution was then found (Table 4.1). The ideal model produced different results for the expected sensitivities at each resolution setting.

Table 4.1: Monitor sensitivity due to camera resolution from the DiMAGE A2 Digital Camera. Accuracy is the difference between the experimental and the ideal sensitivity. Precision is equal to one standard deviation of the experimental sensitivity values.

	3264 Pixels	**2560 Pixels**	**1600 Pixels**
Average Sensitivity in mm. (n=80)	0.217	0.282	0.444
Expected Sensitivity (mm)	0.054	0.068	0.110
Accuracy (mm)	0.163	0.214	0.334
Precision (mm)	0.019	0.017	0.061

The graphed data shows that there is a positive relationship between the resolution of the camera and the movement of the laser spot centroid (Figure 4.1). The plotted trendlines indicate a linear relationship, and that the rate of movement of the centroid increases with higher camera resolutions. This result is rational, as increasing the number of pixels in an image will decrease the distance the spot centroid needs to move in order to be located on an adjacent pixel.

Unfortunately, there was some systematic error involved in the readings from this test. Looking at the data from each resolution data set shows that the error must be caused by a systematic shift upwards or downwards in the data. The slope of the erroneous data points still matches the overall slope of the dataset, supporting its systematic nature. In the right half of the data sets these errors are especially evident.

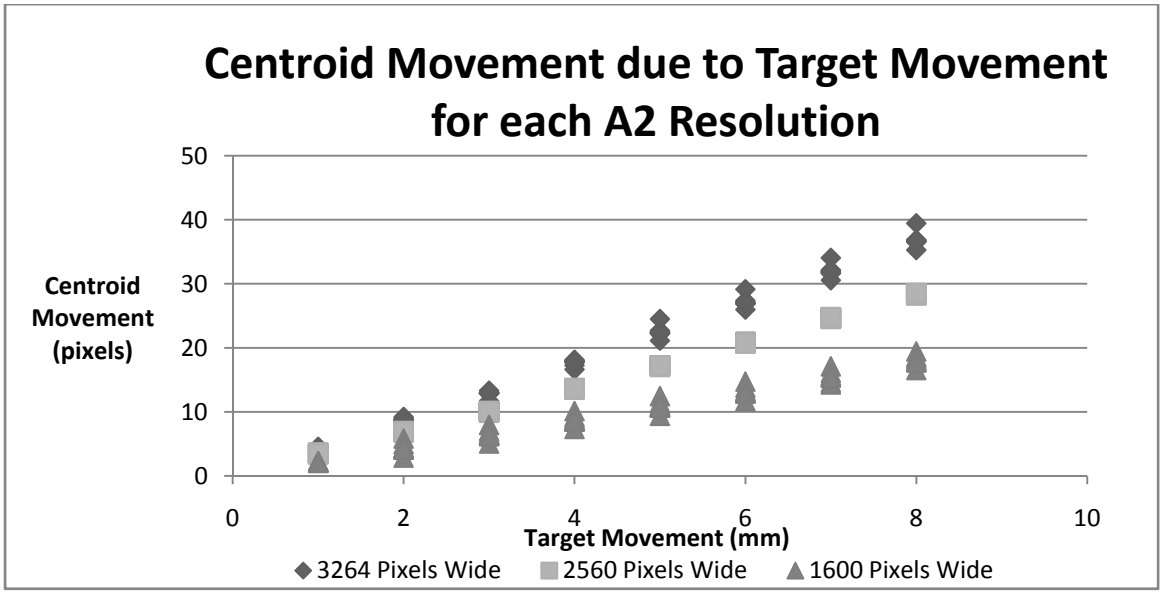

Figure 4.1: The general trend is that increasing a camera's resolution will increase the rate at which a laser spot centroid moves across the image, thus increasing the sensitivity of the monitor.

Even though no specific error sources were noted during data collection, an educated guess can be made concerning the cause of the error. The systematic nature of the error eliminates atmospheric variables as the source, as there was too much uniformity of condition within the laboratory for it to be the cause of such a short term error. It also eliminates camera or laser vibration as the source as those sources contain too much randomness. It is highly unlikely that one of the components was bumped, because the error does not remain constant after one point in time, rather it appears in the middle of the data sets and then disappears or shifts, but remains systematic in form.

The most probable cause of this error is that since the micrometer was manually operated, a change in the point-of-view of the researcher while collecting data could have resulted in the data being corrupted in this form. A parallax error during micrometer operation would have increased or decreased the actual distance that the target was moved, but because no other variables would have been changing the slope of the data points would have remained the same. An example of this would be if one set of data were collected with the researcher viewing the micrometer from above in a standing position, while a second set was collected viewing the micrometer from the side while sitting down.

The differences between the expected and measured sensitivities with this camera are very large, large enough to eliminate the systematic errors as the source of the difference. It is likely that the camera is the source of the error. The A2 includes both a 2X digital zoom and image stabilization function. Both of these use computer algorithms in order to alter an image to either make it the scene appear closer or to eliminate vibration.

4.2.2. D200 Resolution Test. The magnitude of the error in the DiMAGE A2 data set makes it unsuitable for drawing conclusions, but the data does support the idea that a positive trend must exist between the camera resolution and monitor sensitivity. Support is also necessary for the theory that the error between the expected and experimental results was due to the camera. For these reasons a second set of data was collected using the D200.

For the D200 testing the experiment using the DiMAGE A2 was recreated using the 0.500 m between camera and incidence laser and 1.000 m between camera image plane and target. The camera settings included ISO 250 and exposure $^{1}/_{100}$ of a second. The focal length of the lens was 300 mm and the aperture was set to F/5.6. The camera was controlled remotely via USB cable, with the computer controlling the shutter to eliminate vibration.

For this test it was decided that due to the general linearity of the data collected up to this point, it was unnecessary to collect data at 9 different target positions. For this reason only three target locations were used, the zero position, 4.00 mm away from the camera, and 8.00 mm away from the camera. The D200 has three resolution settings available including 3872 by 2592, 2896 by 1949, and 1936 by 1296 pixels. For each of these settings the target was moved through its three-position cycle and data was collected 10 times, for a total of 90 data points. Extreme care was taken to eliminate parallax error in the manual target movement.

The data was analyzed using the same methods used with the DiMAGE A2, and the results were much better. In fact, when the data was analyzed there was a correlation coefficient of 1.0000 between the target movement and centroid movement and a

coefficient of determination of 1.0000 for each of the three camera resolutions. The graph of the resolutions shows perfect linearity between the data for each resolution, and the increase in rate of movement of the centroid is seen from the increased positive slope as the camera resolution increases (Figure 4.2).

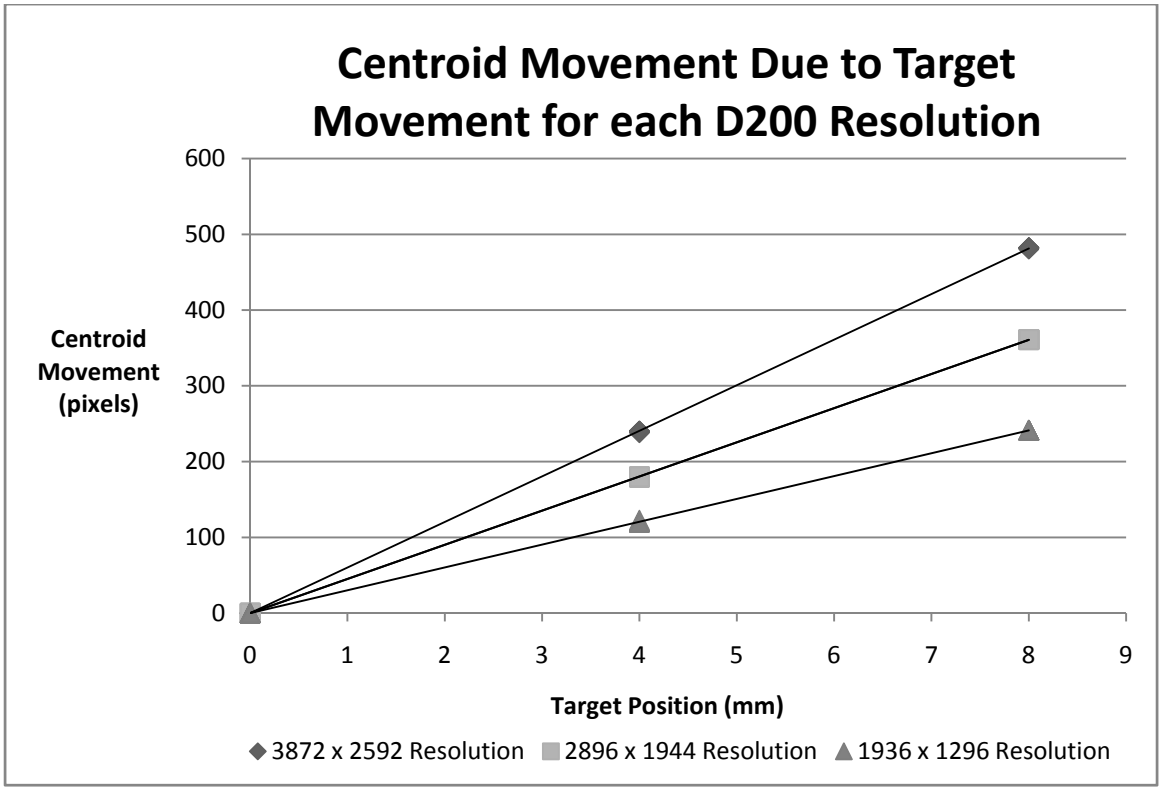

Figure 4.2: D200 resolution test. Note that this graph includes all 90 data points, 30 for each resolution.

Since the focus of interest is actually on determining the effect of the camera resolution on monitor sensitivity, the sensitivity of the monitor from this experiment was calculated from the recorded movement values using the method outlined in Equation 8.

Results from this test, along with the expected sensitivities from the ideal model, are presented in Table 4.2.

Table 4.2: Sensitivity data for the D200 sensor resolution test.

Pixel-Width	Expected Sensitivity (mm)	Experimental Sensitivity (mm)	Accuracy (mm)	Precision (mm)
3872	0.0224	0.0149	0.0075	9.65 E-6
2896	0.0229	0.0199	0.0100	6.54 E-6
1936	0.0448	0.0298	0.0150	10.1 E-6

It can be seen that the difference between the experimental and modeled sensitivity values is much less than what was experienced with the DiMAGE A2. In this case the difference values located in tables Table 4.1 and Table 4.2 represent the error of the system due to p_w.

Regression was used in order to determine the expected difference (error) between the ideal model and the experimental results. It was found that the form of the equation is a negative power function where the ideal model conforms to Equation 16 while the experimental data conforms to Equation 17.

$$s = \frac{90.49}{p_w} \quad (16)$$

$$s = \frac{57.43}{p_w} \quad (17)$$

The difference between these two equations is equal to the sensitivity error due to changes in p_w.

$$s_e = \frac{90.49}{p_w} - \frac{57.43}{p_w} = \frac{33.06}{p_w}$$

18

4.3. EFFECTS OF LENS FOCAL LENGTH

Changing the focal length of a lens has the ability to make a scene appear nearer or further away similar to changing the target distance. In the case of the HRTMM this has the ability to increase or decrease the sensitivity of the monitor. Understanding the effect of focal length not only provides a deeper understanding of the variables influencing monitor usage, but will simplify sensor and/or lens selection should a decision be made to use sensors or lenses other than those used in this research.

A simple experiment was run in order to determine the effect of lens focal length on monitor sensitivity. The Nikon D200 was used to collect images of the target with both the standard 28-70 mm lens and the telephoto 70 – 300 mm lens. The camera was set to its highest resolution of 3872 pixels wide by 2592 pixels high (p_w=3872). The laser incidence angle was set to 42.62 degrees. This angle was calculated from measured distances of 923 mm between the sensor and the laser, and 1003 mm between the sensor image plane and the target in its zero position. The incidence laser was warmed up for more than one hour.

Data collection was completed first with the telephoto lens. The lens was set at a focal length of 300 mm and 10 images were captured of the laser spot. The target was

then moved away from the sensor 5.00 mm with the micrometer movement stage. Following target movement 10 additional images were captured of the laser spot. This process was completed for four focal lengths, 300, 200, 100 and 70 mm, each of which are clearly marked on the lens body. After this initial data collection was completed, the standard lens was substituted and the process was repeated for focal lengths of 70, 50, 35 and 28 mm. The reasoning behind this was both to gather data about a larger number of possible focal lengths, but also to allow for comparison of the two lens types.

The images were processed with the HRTMM program with a window size of 7 and a threshold of 55. Post processing of the data was completed following Equation 9. Sensitivities were calculated for each of the focal lengths tested on each lens and the results were graphed against focal length. This graph is seen in Figure 4.3: The effect of lens focal length with the D200 on the sensitivity of the monitor..

From the graph it is evident that the two lenses did not act identically. It was expected that the two points shown at a focal length of 70 mm would have matched perfectly. The graphed lines of the two lenses do appear to follow the same trend, but there is a noticeable offset between them. One possible cause is that this could be a small misalignment error imparted at some point during the substitution of the standard lens for the telephoto lens. Switching lenses during monitoring would never be recommended under normal circumstances. This could have been caused by bumping the sensor.

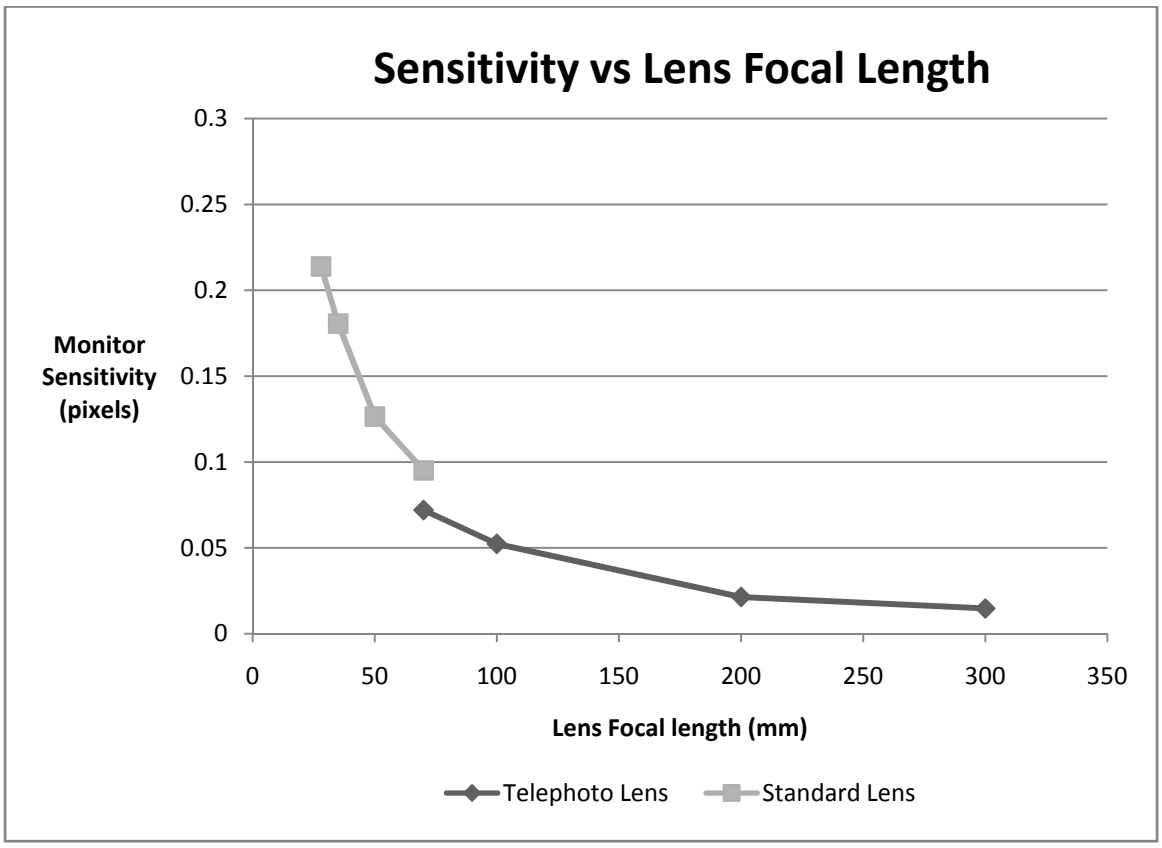

Figure 4.3: The effect of lens focal length with the D200 on the sensitivity of the monitor.

Another possible source of the error could have been a difference in the manufacture of the lenses such as a small imperfection in the curvature of the elements incorporated in the lenses. In any case it was necessary to determine which line, if any, had the proper location and the error of the two lines. This was accomplished by determining the expected sensitivity based on the ideal model.

It is also possible that the error could simply have been caused by incorrect settings when using the lenses. The markings on the lenses that show the position of each focal length were not that precise and an error could have been made by improperly setting the focal length. For the highest and lowest focal lengths of each lens this would

not have been as large of an issue, as in each case the setting is accomplished by turning the lens to its mechanical stopping point. However, as the lens focal lengths were not verified, it is still possible that these focal lengths were not exactly 300, 70, or 28 mm.

For each tested focal length the sensitivities were calculated and the values were graphed along with the experimental values in order to compare them (Figure 4.4). The actual values and the experimental values are all shown in Table 4.3 along with the error for each focal length found by subtracting the experimental value from the modeled value.

Table 4.3: Lens focal length experimental data.

Focal Length (mm)	Lens Used	Expected Sensitivity (mm)	Experimental Sensitivity (mm)	Accuracy (mm)	Precision (mm)
300	Telephoto	0.0221	0.0147	0.00742	2.57E-05
200	Telephoto	0.0332	0.0214	0.0118	3.58E-05
100	Telephoto	0.0664	0.0523	0.0141	1.67E-04
70	Telephoto	0.0949	0.0720	0.0229	2.18E-04
70	Standard	0.0949	0.095	-0.000260	2.79E-04
50	Standard	0.133	0.126	0.00636	3.20E-04
35	Standard	0.190	0.181	0.00916	6.10E-04
28	Standard	0.237	0.214	0.0233	7.84E-04

The results of the experiment show that the telephoto lens clearly provides sensitivity values lower than those obtained with the standard lens. Due to the longer focal lengths the telephoto lens is able to improve sensitivity to a level where at a 300-mm focal length even the highest error experienced with the telephoto lens still provides a sensitivity value below the best obtained with the standard lens. The standard lens did have lower error overall, but the sensitivity improvements gained from using the 300-mm focal length are enough to justify the lens with the larger error.

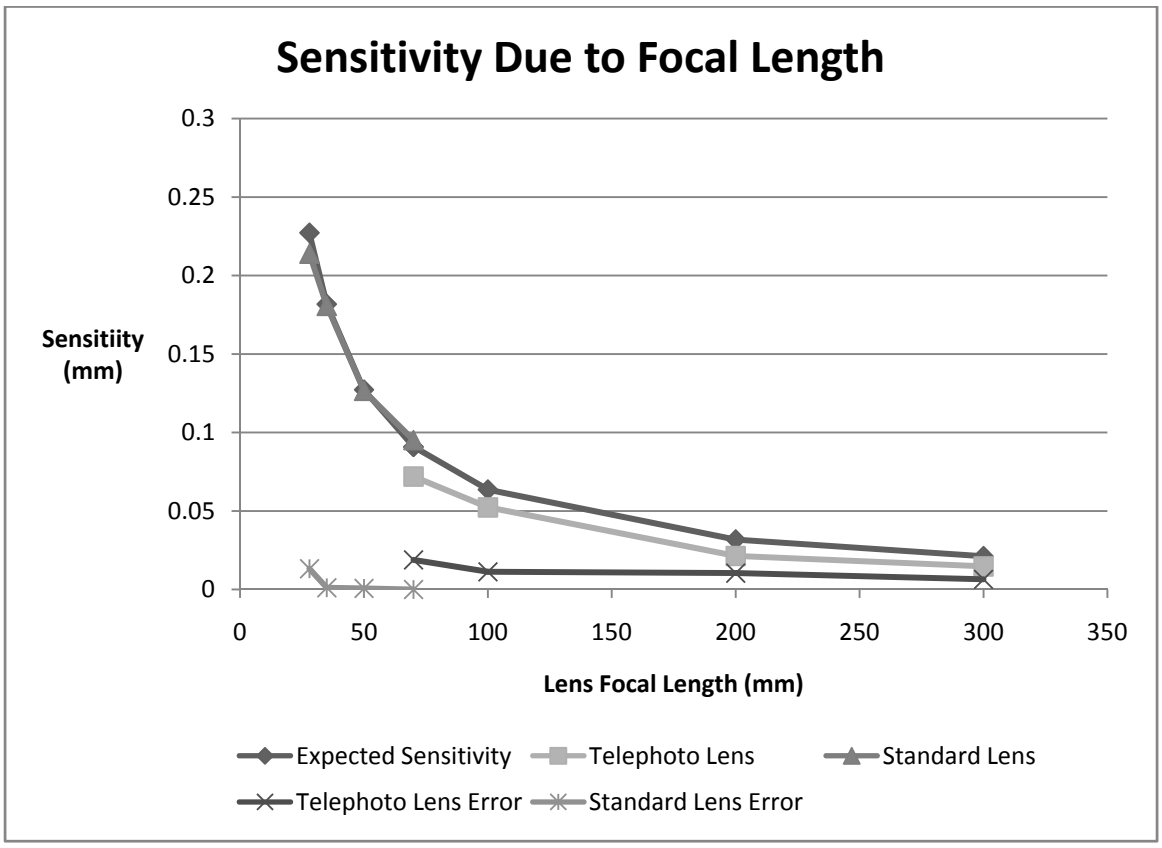

Figure 4.4: The expected sensitivity of the monitor compared to the values obtained from each lens. It is clear that the standard lens matches the expected values best, though the error with the telephoto lens set to 300 mm is similar to the standard lens error.

It is also important to note that while the telephoto lens had larger error overall, at the 300-mm focal length the lens error was very similar to that obtained with the standard lens. Both lenses experienced increasing error with increasing focal length. This is likely due to the increased manufacturing precision necessary for a quality image at longer focal lengths than for shorter focal lengths and the fact that the Sigma lens was not expressly designed for use with Nikon cameras.

A secondary error not actually researched in this project would be vibration error due to focal length. While a longer focal length certainly does not cause the vibration

itself, a longer focal length will respond to vibrations more vigorously than a shorter focal length. It is possible that this may eventually preclude super-telephoto (focal lengths longer than 300 mm – generally 1000 mm or higher) lenses from use as the sensitivity of the monitor to vibration from air currents and other natural vibrations would degrade data quality quickly. Use of registration markers fixed directly to the target in combination with the incident laser would allow for elimination of this error, though truly remote monitoring would be sacrificed. Image stabilization systems in many digital cameras might also assist in elimination of this imparted vibration error.

4.4. EFFECTS OF SENSOR-TARGET DISTANCE

Extended distance testing was completed early in the morning in the gymnasium of the Missouri University of Science and Technology. The location was chosen for its large distances and uninterrupted views. The time was chosen as one when few people would be using the facility in order to minimize the potential for error from floor vibrations, people walking in front of the incidence laser beam or sensor line-of-sight, or from accidental disturbance of the monitor components.

The test set-up utilized three stable tripods to support each of the three main components, the sensor, target, and incident laser. Each tripod was set to the same height and placed in general positions using the lines painted on the gymnasium floor as guides. The laser-mirror reflectance technique was utilized to fine tune the alignment of the three components in order to form a right triangle with all three components all residing on the same horizontal plane in space. This process was repeated each time that the components needed to be moved throughout the morning.

Originally a metric micrometer was planned for the target platform but due to an accident it was broken and an imperial micrometer had to be substituted. Measurements with this device were accurate to 0.001 inch. Distances between the components were measured using a surveying tape in metric units but in order to keep systems of measurements consistent throughout the experiment imperial target distances of 25, 50, 75, 100 and 125 feet were converted to metric and used. The final results were dealt with in metric in order to be consistent with the other experiments of the project. Each tripod was located over the tape with the use of a plumb bob. The target and sensor were located on the long side of the triangle with the sensor being located at the right-angle corner. The incidence laser was located in the third corner (Figure 4.5).

Measurement of the laser incidence angle was completed in two fashions. First a constant 30-degree incidence angle was measured using the rotational stage. This provided a measurement accurate to 1 degree. Next the measurement was refined by calculating the lengths of the triangle legs trigonometrically. This method gave angular measurements accurate to within 0.003 degrees for the closest target when considering that the smallest unit measurable on the survey tape was 1 mm.

The sensor used for this experiment was the Nikon D200 with the Sigma telephoto lens. The focal length for all images was 300 mm, the ISO was 250, and exposure was $^{1}/_{60}$ of a second. The camera was set at its maximum resolution and manual focusing was completed because the automatic focus had difficulty focusing on the small target.

Measurements were taken with the target at 7.62, 15.24, 22.86, 30.48 and 38.10 m. (25.00, 50.00, 75.00, 100.00, and 125.00 feet) from the sensor. At each target distance

an image was captured with the micrometer in the 0.000 inch position and then the micrometer was adjusted 0.300 inches away from the sensor and another image was captured. This process was repeated 10 times at each target location. The purpose of the repetition was to allow for averaging of the data during post-processing, helping to eliminate errors

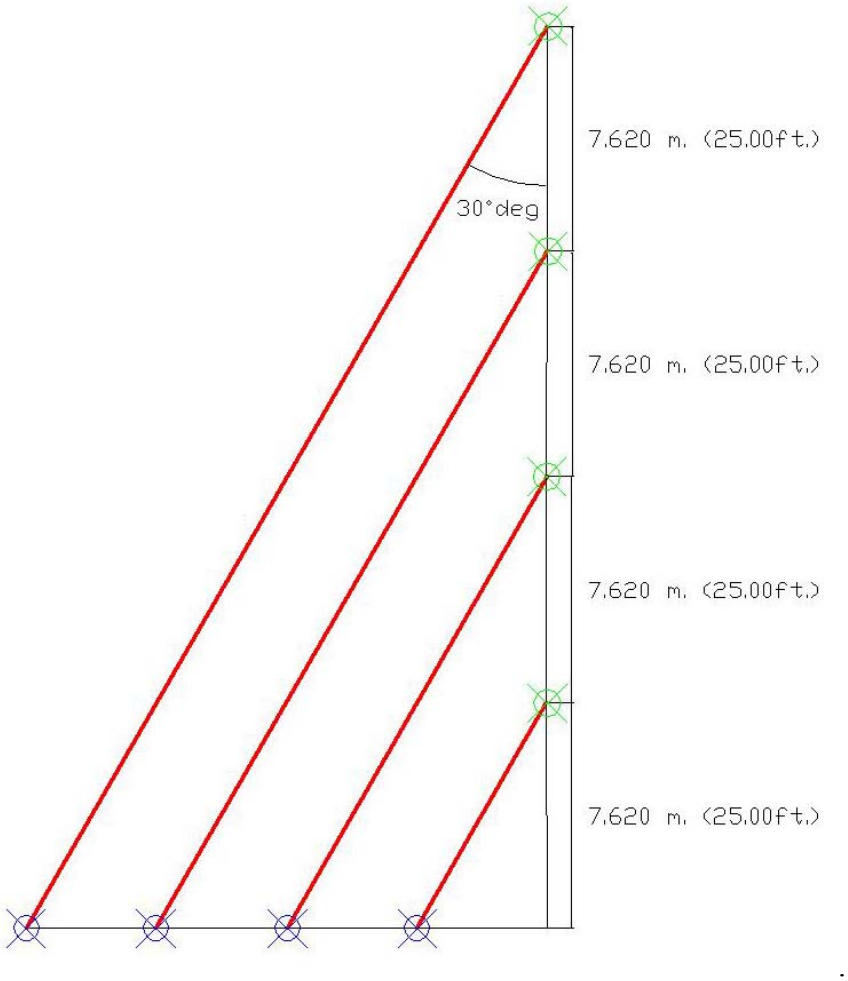

Figure 4.5: Experimental set-up for the gymnasium distance tests. Blue points along the bottom represent incidence laser positions; Green points along the right represent target positions. Red lines represent laser path. The camera was located in bottom right corner.

Each image was analyzed using the HRTMM program and returned results which were then stored in a database and transferred to a spreadsheet for further manipulation. Recall that each target position includes a total of 20 images, captured in the sequence of one at the 0.000 inch position and then one at the 0.300 inch position, repeated ten times. Each pair of images makes up one image pair. One complete pair is required in order to determine the sensitivity of the monitor. Once the distance between the laser spot centroids in each image pair were determined for each image pair the values were averaged. Graphing these values for all of the images shows the average centroid movement for each target distance (Figure 4.6).

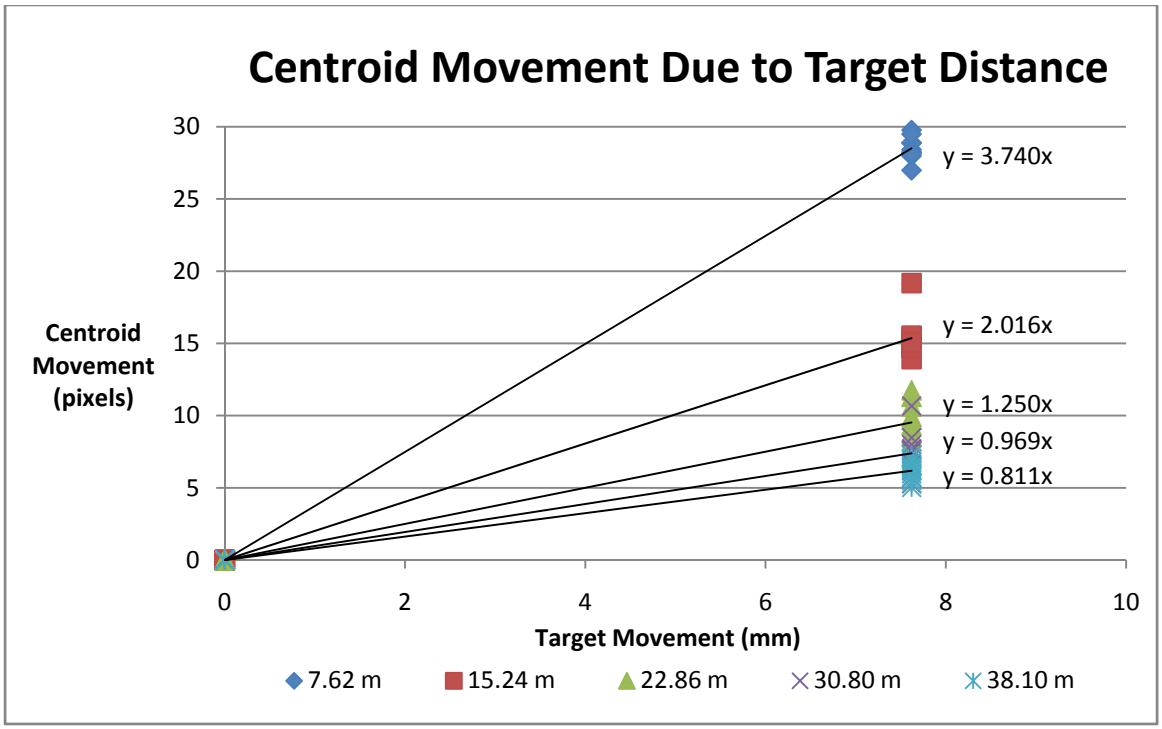

Figure 4.6: Centroid movement from 0.300 inches (7.62 mm.) of target movement for each of the five target locations. All 10 image sets for each distance are included in the graph.

Upon graphing the results of the target movement it became apparent that the slope of the line created by the centroid movement and the target movement decreased as the distance between the target and the sensor increased. This is rational because as the target moves further away the far-field area covered by a single pixel increases.

While the data points on the right side of the graph do have some spread in the Y direction, the linear regression associated with each distance is thought to be a good model of the slope for that distance. Correlation coefficients showed that there was an extremely strong linear tendency and the coefficient of determination shows that almost all of the variation is accounted for by the models (Table 4.4).

Table 4.4: Statistics concerning the performance of the linear regression for each target distance.

Target Distance	Correlation Coeff.	Coeff. of Determination
7.62 m. (25.000 ft.)	0.999	0.998
15.24 m. (50.000 ft.)	0.992	0.985
22.86 m. (75.000 ft.)	0.980	0.961
30.48 m. (100.000 ft.)	0.962	0.926
38.10 m (125.000 ft.)	0.971	0.979

After determining the centroid movements for each of the distances the results were used to calculate the monitor sensitivity for that distance according to Equation 7. These sensitivity values can be compared to the ideal sensitivity as calculated from Equation 15. Standard deviations for the data at each measurement distance were also calculated. The experimental data is quite accurate as it corresponds very well with the

ideal values. With the exception of the 15.24 m distance the ideal sensitivity is within one third of a standard deviation of the measured sensitivity (Table 4.5).

Table 4.5: Sensitivity of HRTMM in mm.

Distance (m)	Expected Sensitivity (mm)	Experimental Sensitivity (mm)	Accuracy (mm)	Precision (mm)
7.62	0.268	0.267	0.001	0.006
15.24	0.536	0.496	0.039	0.039
22.86	0.804	0.800	0.005	0.127
30.48	1.072	1.032	0.041	0.217
38.10	1.341	1.232	0.108	0.379

Graphing the recorded data, ideal values, and the standard deviations (plus and minus) of the recorded data provides a visual means of checking the accuracy of the monitor. In this case the error of the monitor increases as the distance between the camera and the target increases. This is very sensible and the trend of the standard deviations give a general representation of the random error associated with increasing target distance (Figure 4.7).

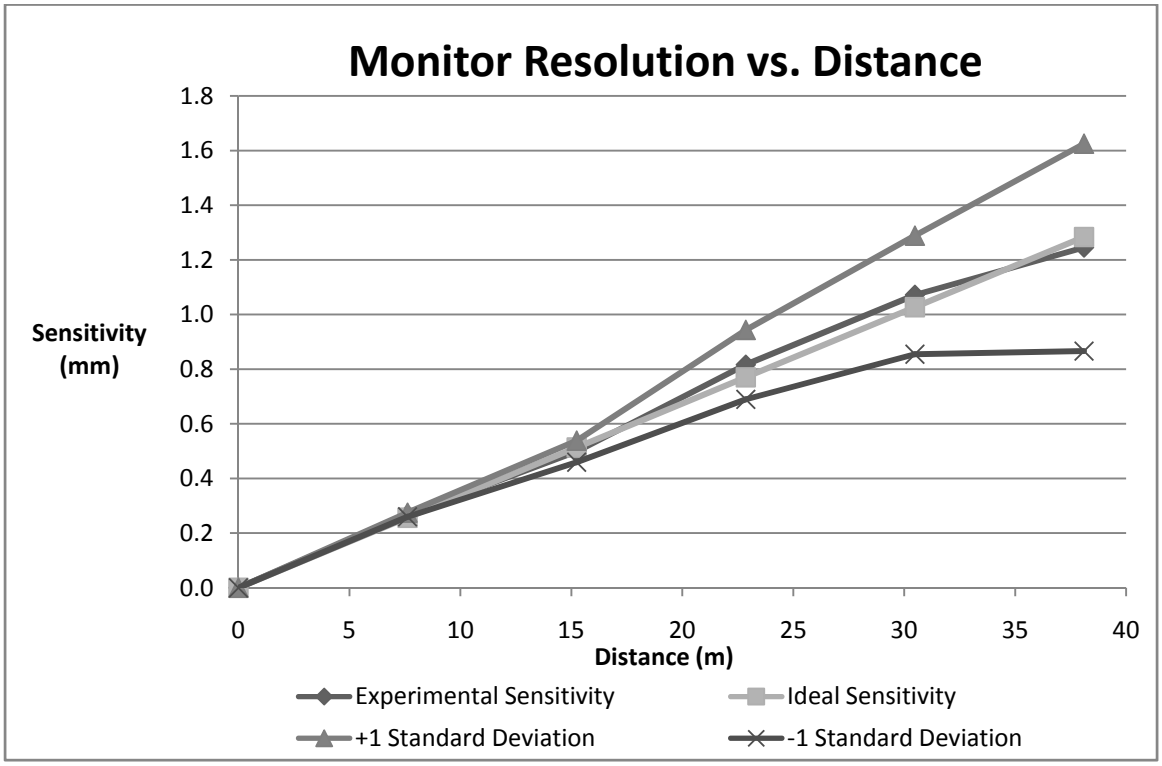

Figure 4.7: The monitor corresponded rather well with the ideal data. Experimental results were consistently within one standard deviation of the ideal sensitivity.

If linear regression is used to determine a best fitting line to the average experimental sensitivity values the equation can be used to predict the average sensitivity of the monitor under the test conditions defined for this distance test (equals 0.033 times the target distance). A similar regression can be used to determine the random error (where error is one standard deviation from the sample mean) due to distance. This test shows that the random error due to distance for the monitor is 0.008 mm per meter between the sensor and the target. Stated another way, the accuracy of the monitor is approximately 0.039 mm ±0.008 mm/m. It is important to reiterate that the average sensitivity and random error value quoted here is only valid for the test conditions used.

4.5. EFFECTS OF LASER INCIDENCE ANGLE.

Beyond target distance and sensor resolution, the angle of the incidence laser with respect to target normal has a very significant impact on the sensitivity of the monitor. As the incidence angle becomes larger, the monitor's sensitivity increases [58, 61]. In order to demonstrate and understand this effect, extensive testing was completed under laboratory conditions with the hope of actually modeling the effect of laser incidence angle on monitor sensitivity and understanding the errors involved.

The laser angle tests were carried out on the optical vibration elimination table and made use of the Nikon D200 digital camera sensor under laptop computer control. The distance between the target and the sensor was measured to be 1.008 m while the location of the incidence laser varied depending on the angle being tested. The vibration elimination table is fitted with a metric breadboard that makes locating components of an experiment simple to accomplish and to measure, thus all measurements were completed in millimeters. All angles were then determined by measuring two legs of a triangle and solved for trigonometrically. Figure 4.8 shows the location of the incidence laser relative to the camera and target. While the distance between the incidence laser and target did not remain constant, this should have no substantial effect on the sensitivity of the monitor due to the coherent nature of the laser and the short ranges. This experiment was detailed in the September 2007 issue of the Journal of Geotechnical and Geoenvironmental Engineering [61].

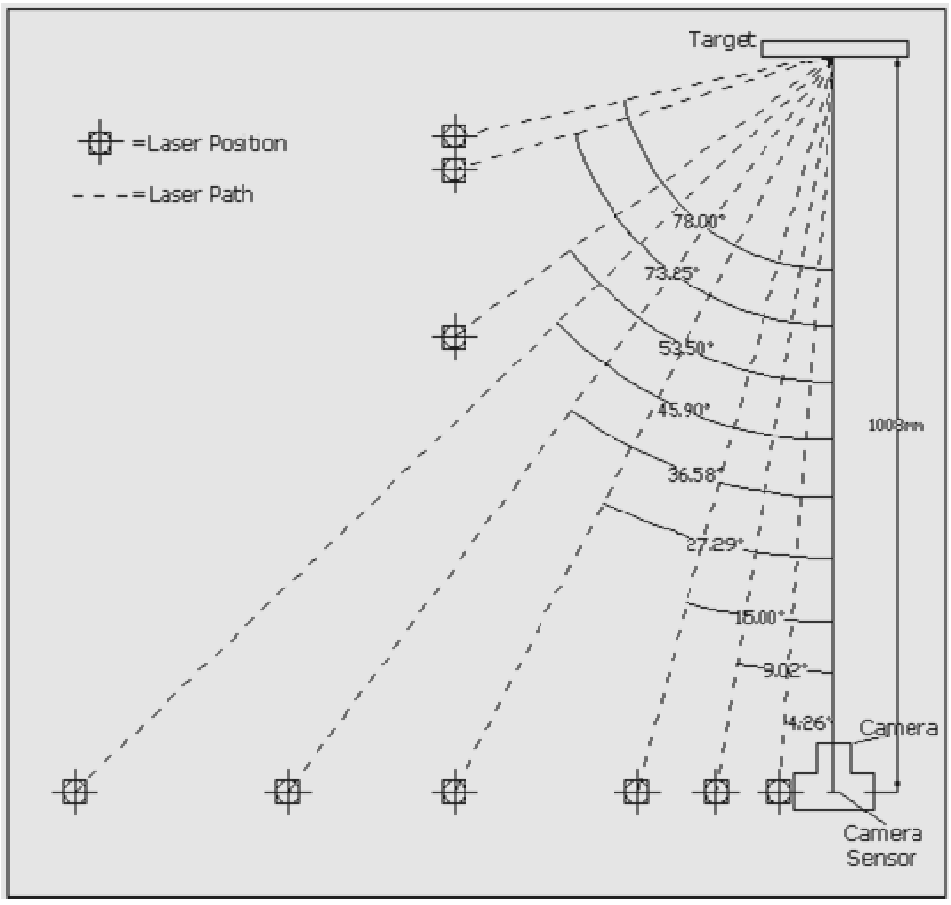

Figure 4.8: Positioning of the incidence laser with respect to the sensor and the target, adapted from [61].

For this experiment the D200 was placed perpendicular to the target and used the Sigma telephoto lens set to its full zoom of 300 mm. The camera ISO was set to 250, the exposure was set to $^{1}/_{100}$ of a second, and the resolution was set at maximum. The aperture of the lens was set to F/5.6 and the lights were on in the room. The data was analyzed with the HRTMM program with the window size set to 7 and the threshold set to 120. The incidence laser was allowed to warm up for approximately 1 hour before beginning data collection.

Alignment of the system was completed with a series of laser reflections. Two optical experimental quality mirrors were positioned around the incidence laser. One was located directly next to the sensor to help align the laser on the same horizontal plane as the sensor. The second mirror was situated so that the mirror and the incidence laser formed a line parallel with the line-of-sight of the camera. Before beginning any data collection the incidence laser was aligned so that as it turned counterclockwise on its rotational stage it would pass first the mirror next to the sensor, next the target, and finally the second mirror. The laser was adjusted until it would reflect off of each mirror and back to its source. This assured that the laser was sighted along the same horizontal plane as the sensor. The laser was then aimed at a marked spot on the target.

Tested angles were chosen to provide a generally even spread across the total possible range. The largest angle possible was 78.00 degrees. At this angle the rate of movement of the laser spot across the target was so fast it completely transversed the camera's field of view. Higher angles would be possible with a longer distance between the sensor and the target or with a shorter focal length, either of which would widen the field of view and reduce the monitor sensitivity. The lowest angle limit was 4.26 degrees because the mounting platform for the laser could not be positioned any closer to the sensor without interfering with the camera's line-of-sight to the target.

The sequence of data capture for each angle was as follows: An initial image was captured with the target in the zero position. Subsequent images were captured with the target adjusted manually away from the target in 1.00 mm increments. Eight subsequent images were captured making total target movement equal to 8.00 mm with nine total

images captured. This completed one cycle. For each angle 10 cycles were completed totaling 90 data points for each angle.

Analysis of the data during post-processing produced some interesting results. Calculation of the monitor sensitivity from each incidence angle verified that monitor sensitivity increases as laser incidence angle increases. Comparison with the ideal sensitivity showed that the lower the incidence angle the more inaccurate the monitor is. The random error (standard deviation) of the monitor's readings was similar in that the highest random error was found with the lowest laser incidence angles. The random error decreased as the incidence angle increased until the 73.25 degree data set, where the random error increased slightly.

A graph of the experimental and ideal sensitivity at each incidence angle can be seen in Figure 4.9, while the actual data is detailed in Table 4.6. It can be seen that the monitor always records a reading that is below the ideal sensitivity. Creating a ratio with the ideal sensitivity divided by the experimental sensitivity shows that on average the ideal sensitivity is approximately 1.44 times greater than the value given by the monitor. This fact itself might be considered disturbing except that the magnitude of the errors is so small that the discrepancy is considered unimportant. The combination of accuracy and random error due to incidence angle is less than 0.01 mm for all angle values above approximately 32.5 degrees (Figure 4.10). Most tape extensometers currently in production and used for ground control purposes are only capable of relative measurements of 0.01 mm or greater [62, 63].

Table 4.6: Monitor sensitivity and error due to incidence laser change.

Incidence Angle (degrees)	Expected Sensitivity (mm)	Experimental Sensitivity (mm)	Accuracy (mm)	Precision (mm)
4.26	0.263	0.169	0.094	0.022
9.02	0.123	0.095	0.028	0.013
15.00	0.073	0.050	0.023	0.004
26.29	0.038	0.025	0.013	0.000
36.58	0.026	0.018	0.008	0.000
45.90	0.019	0.013	0.006	0.000
53.50	0.014	0.010	0.004	0.000
73.25	0.006	0.004	0.002	0.000
78.00	0.004	0.003	0.001	0.001

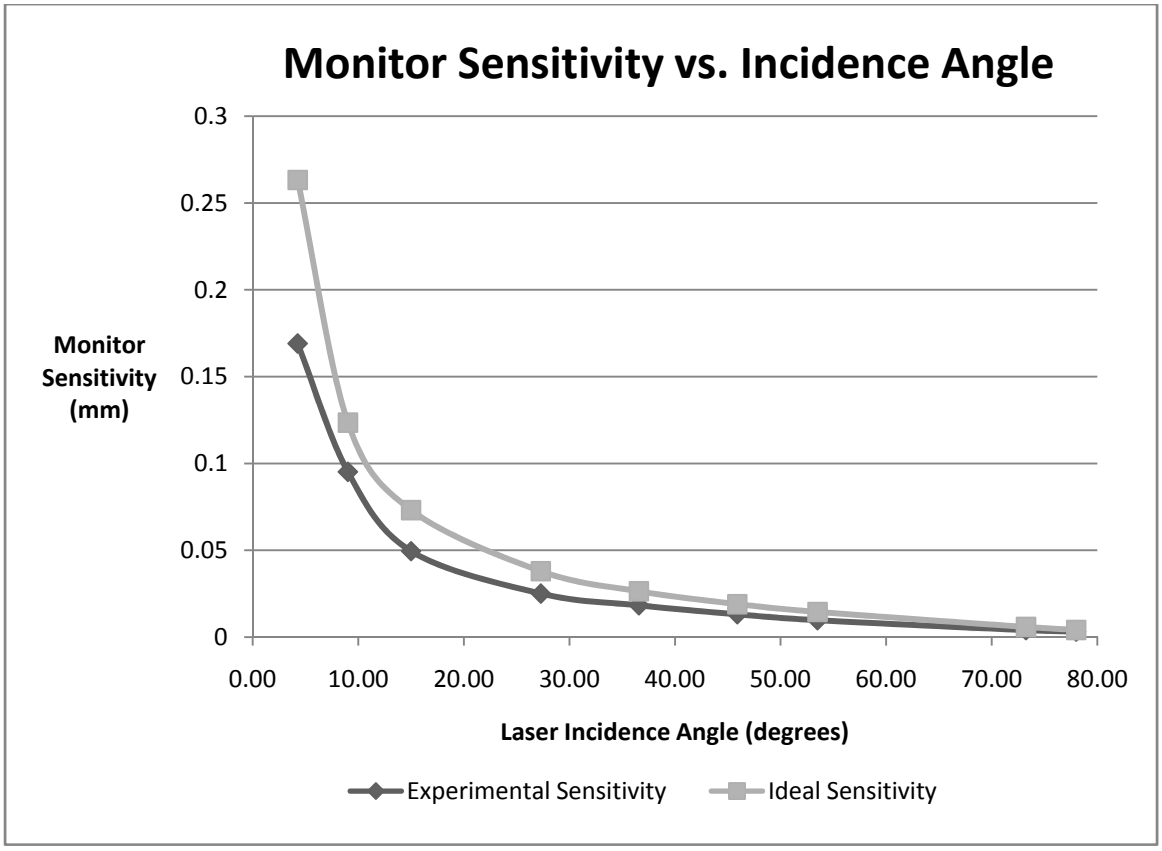

Figure 4.9: Monitor sensitivity due to laser incidence angle with target at 1 meter.

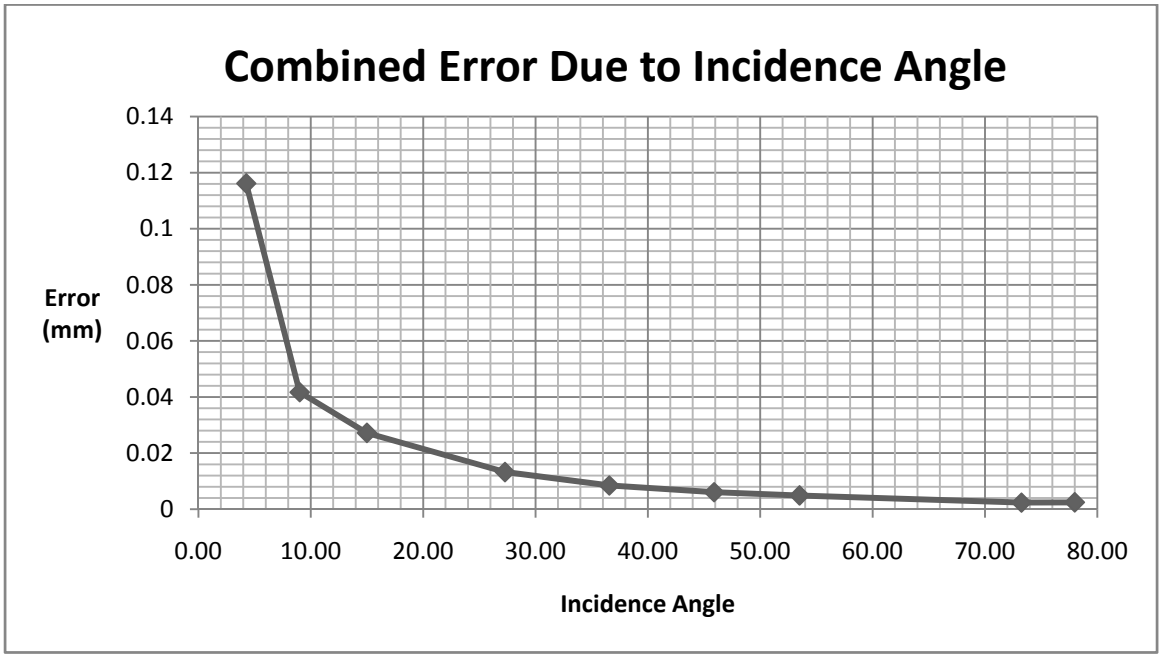

Figure 4.10: Combination of both accuracy and random error dependent on incidence angle.

The sources of the error for this experiment vary depending on the incidence angle being used. At small incidence angles error is primarily due to the small distance the laser spot centroid moved over the target. When the laser intersects the target it is diffusely reflected. The scatter created by this imperfect reflection introduces error into the readings collected by the monitor as it can cause small changes in the location of the laser spot centroid. At larger laser incidence angles the magnitude of the centroid travel across the target is much greater than the error caused by the typical scattering from the stainless steel target surface. At small angles the error introduced by scattering remains unchanged, but the movement of the centroid is large enough to prevent the error from harming the measurements.

Because the light source for these experiments is a nearly coherent laser there is also laser speckle that is a source of error. Laser speckle is caused when a coherent beam reflects off a surface. If the surface is rough enough to have surface variations greater than the magnitude of the wavelength of the laser it will create a speckle pattern. The speckle pattern is formed by interference caused by reflection off the rough surface. This pattern will change as the relative positions of the laser, target and sensor change, causing small movements in the position of the laser spot centroid.

At large incidence angles, error is caused by reflection of the laser light across the stainless steel target. In this case the incidence angle is so large that reflection of the diffusely reflected laser light illuminates a portion of the target directly opposite the laser. This illumination changes very slightly as the target moves and introduces error in the location of the laser centroid. However, because the magnitude of the laser spot movement across the target is so great at these high incidence angles, the relative magnitude of the error is very small, allowing it to be virtually ignored.

4.6. INCIDENCE ANGLE AND TARGET DISTANCE VERIFICATION

The data that was collected for the target distance test had one major shortfall. While the data provided a high-quality model showing how the sensitivity of the monitor reacted at extended target distances, the entire data set was taken with a 30-degree incidence angle for the lasers. Likewise, while the incidence angle data displayed in section 4.5 was of similarly high quality, it was all collected from a distance of only one meter. It was therefore necessary to produce a model incorporating both variable distance and variable incidence angle. To this end a separate test was designed.

4.6.1. Test Setup. The combined target distance/incidence angle test was conducted in the 2nd floor lobby of McNutt hall on the campus of the Missouri University of Science and Technology. Data collection was completed on a Sunday morning during the summer semester. As with the initial extended distance test, this time and place was chosen as a controlled environment inside a building that would have very few people in the area to create vibrations that could disturb the measurements. If a person happened by during image capture activities data collection was suspended until the area was clear of those not assisting with the project.

The system was arranged in much the same fashion as for the initial extended distance testing. Floor tiles provided a convenient method for basic alignment of the three components of the monitor while the same surveying tapes were used for refining the distance between monitor components. A plumb bob was again used to locate components over the surveying tapes. These tapes were affixed to the floor to eliminate some measurement errors.

The target and sensor setup were identical to that used in the initial extended distance test and were as described in section 4.4. The incident laser was arranged on a movable platform instead of a tripod. The same alignment procedures were followed as those previously described, though the system was aligned to the height of the incidence laser on the platform instead of to an arbitrary level[64][64][64].

To correlate the data better to that collected in the initial extended distance test, the target movement was again measured with the imperial micrometer to a distance of 0.300 inch. The target distances used in this test were 4.572, 7.620, 10.363, and 14.935 m (15.00, 25.00, 34.00 and 49.00 ft). The distances corresponding with 34.00 and 49.00 feet

were used due to miscommunication between people helping to collect the data. The original planned values were for 35.00 and 50.00 feet. This change had no effect on the results as it was noticed before data analysis began.

For each target distance, data was collected at four different incidence angles, 15, 45, 60 and 75 degrees. The data reported in Section 4.4 was distance test data with an incidence angle of 30 degrees, so it was not re-collected. The angles were chosen in order to evenly span the most probable range of use for the monitor. Angles were determined trigonometrically and were measured using a metric tape measure accurate to one millimeter. This gives angular measurements accurate to within 0.003 degrees at the 4.572 m distance and 15.00 degree incidence angle. Other degree calculations would all give accuracies higher than this value.

Alignment of the system's components occurred in much the same way as it had for the experiments outlined in section 4.5. Once the sensor and target had been located over their proper places on the survey tape using the plumb bob, they were aligned using the targeting laser on the sensor platform and the temporary mirror on the target. This mirror was removed before data collection began. Once the incidence laser was placed it was turned on its rotational stage to ensure that it illuminated the image plane on the D200 and the center of the target in the same arc. This verified that all three components were on the same horizontal plane. This also provided an opportunity to double check the location of the incidence laser with the degree gradations on the rotational stage.

The D200 was attached via the USB cable to the laptop computer for remote control. The shutter speed was set to $^{1}/_{100}$ of a second, ISO was 250, and the aperture set to F/5.6 using the telephoto lens at its maximum focal length. The camera was set for its

highest resolution and manual focusing was completed. The incidence laser was activated 1.5 hours previous to beginning data collection.

At each specified distance the incidence laser was set and calibrated. Data collection proceeded exactly as in the original extended distance test. After all 20 images had been captured at that location the incidence laser was reset for another angle, recalibrated, and data collection continued until all distance/angle combinations had been completed.

4.6.2. Data Analysis and Results. The images from the test were analyzed by the HRTMM program with a window size of 7 and a threshold of 120. The resultant centroid data was used to determine the sensitivity of the monitor for each target distance/incidence angle combination using Equation 7. The calculated sensitivity values are located in Table 4.7. Error component values were also calculated both as an accuracy (Table 4.8) and as random error in millimeters (Table 4.9).

Table 4.7: Monitor sensitivity in millimeters.

Sensitivity (mm)		**Laser Incidence Angle (degrees)**			
		15.00	**45.00**	**60.00**	**75.00**
Target Distance (m)	**4.572**	0.3762	0.0994	0.0548	0.0256
	7.620	0.5867	0.1643	0.0938	0.0427
	10.363	0.8746	0.2131	0.1247	0.0553
	14.935	1.0980	0.3136	0.1790	0.0817

Table 4.8: Accuracy error determined from the ideal sensitivity value minus the experimentally determined value.

Accuracy Error (mm)		Laser Incidence Angle (degrees)			
		15	45	60	75
Target Distance (m)	4.572	-0.0442	-0.0105	-0.0034	-0.0018
	7.620	-0.0334	-0.0160	-0.0082	-0.0029
	10.363	-0.1222	-0.0115	-0.0083	-0.0013
	14.935	-0.0136	-0.0230	-0.0113	-0.0038

Table 4.9: Random error (precision) equal to one standard deviation of the experimental results.

Random Error (mm)		Laser Incidence Angle (degrees)			
		15	45	60	75
Target Distance (m)	4.572	0.0132	0.0011	0.0004	0.0002
	7.620	0.0180	0.0029	0.0009	0.0003
	10.363	0.0626	0.0015	0.0008	0.0003
	14.935	0.1288	0.0048	0.0012	0.0005

The sensitivity of the monitor increased not only as the distance became smaller, but also quite substantially as the angle became larger. When a graph was made of all of the data, including the original 30-degree extended distance data, a method for predicting the sensitivity of the monitor at any distance and with any incident angle became apparent. This method is based solely on experimental data.

The slope of the lines in Figure 4.11 actually represent the rate of increase of monitor sensitivity for that particular incident angle. Also, the change in distance between the sensor and the target is obviously a linear relationship, which matches perfectly the data shown in Figure 4.7. Building on the results from the first extended distance test, this evaluation allows the conclusion that that the linear trend for increasing target distance holds for any incident angle and makes developing an experimental model for predicting

monitor sensitivity simply a matter of determining the slope of the line when monitor sensitivity is graphed against target distance.

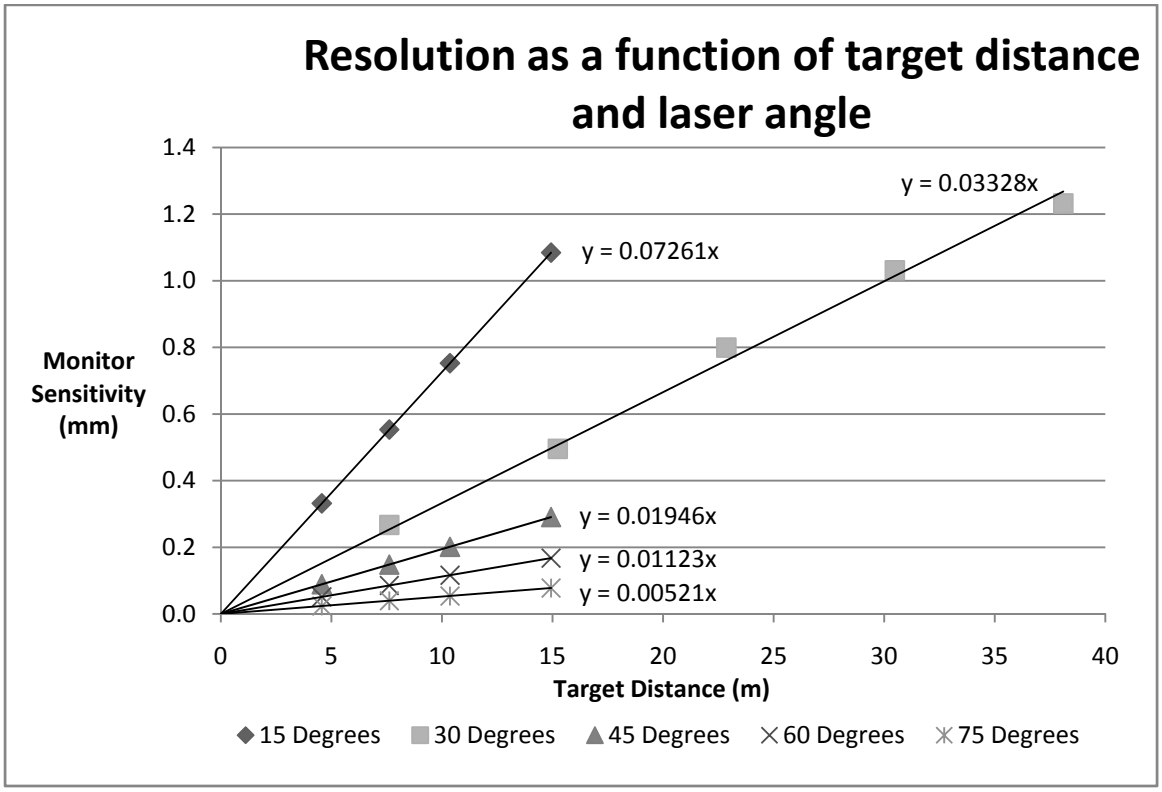

Figure 4.11: This graph demonstrates how the slope of the line changes due to laser incidence angle. Predicting this would allow for prediction monitor sensitivity.

Looking at Figure 4.11 the observation can be made that larger incident angles cause the slope of the line to increase, but that the increase is not equal between each 15-degree increment. In other words, the difference between the slope of the 15 degree line and the 30 degree line is 0.03933 while between 60 and 75 degrees it is only 0.00602.

This means that there is not a linear increase in the rate of sensitivity increase with incident angle.

Considering the way that the laser centroid is known to move across the target when the target moves gives a clue about the type of function used to predict the slope. As the incidence angle of the laser approaches zero degrees (normal to the target and parallel to the line-of-sight of the camera) there should naturally appear to be zero movement of the centroid before and after target movement. However, if the laser incidence angle approaches 90 degrees the rate of centroid movement will increase until it eventually moves an infinite distance from any target movement at the point when 90 degrees is reached. The laser centroid moves in a direction away from the laser source if the target moves away from the sensor (backwards) and towards the source if the target moves towards the sensor (forwards).

Theoretically, if the incidence angle were to be set at 91 degrees (also considered 89 degrees when viewed from the back side of the target) the centroid movement would move a near infinite distance, but would move *towards* the laser source when the target was moved backwards and *away* from the source when the target moves forwards. In effect, the movement of the laser centroid due to incidence angle is described by a tangent function.

This can be shown graphically by using the slope of the lines created by target movement at a particular laser incidence angle as a variable (shown in Figure 4.11). This variable is referred to as the Resolution Coefficient (R_c) and is plotted against the angle of incidence for that line. The plot returned is indeed a tangent function (Figure 4.12).

The resolution coefficient is the increase in sensitivity for the monitor for a target distance increase of 1.000 m at a given incidence angle. It can also be said that the resolution coefficient is the sensitivity of the monitor for a given incidence angle at a distance of 1.000 m. Calculating the sensitivity of the monitor at any distance and incidence angle can be accomplished by determining the resolution coefficient for that incidence angle and multiplying this by the target distance in meters. This is only true for the monitor parameters used in the set of data upon which the resolution coefficient is based: focal length of 300 mm, image sensor width of 22.6 mm, and the cross-sectional pixel-width of 3872.

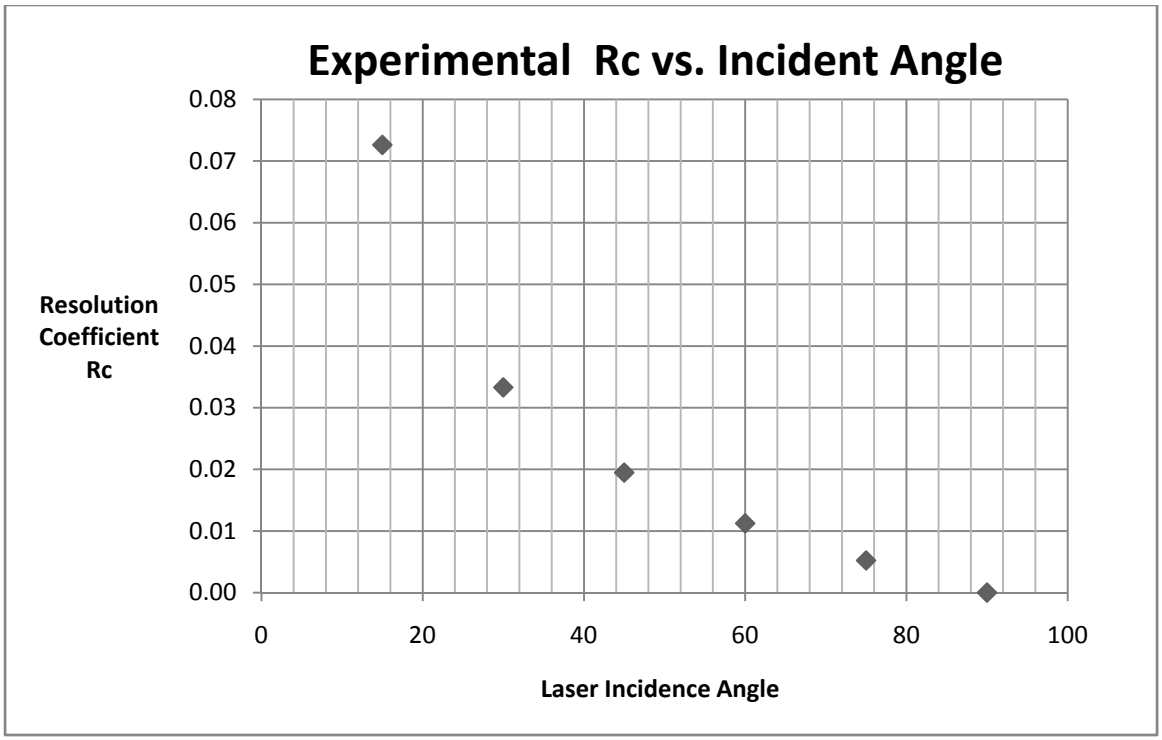

Figure 4.12: The resolution coefficient derived from incidence angle tests. A data point could be assumed at (0.000, 90), though it was not actually recorded during data collection.

By analyzing Figure 4.12 it was possible to determine the form of the equation for predicting R_c. This is shown in Equation 19.

$$\boldsymbol{R_c = -\tan(\theta - 90)} \quad (19)$$

While the form of Equation 19 does correspond with the derived resolution coefficients, it required a modifying coefficient to optimize the experimentally based model. In its current form the model overestimates the experimental R_c at every value except when the incident angle equals 90 degrees, in which case both are necessarily equal to zero. The overestimation was especially bad near the lower incident angles. The modifying coefficient multiplied by the tangent function changes the shape of the function and flattens the curve, bringing it into close agreement with the experimental data.

Optimization for the model can be simplified by first manually approximating the modifying coefficient, M_c. In the case of the collected data the approximated coefficient was equal to 0.02196. This was chosen as a number that made the model more or less visually match the derived resolution coefficients on a graph. This manual first step is not necessary, though it significantly reduces the number of iterations necessary in order to reach optimum.

To begin the optimization process, let $\boldsymbol{a}$ be a vector containing the incident angles at which data is known.

$$\boldsymbol{a} = \begin{bmatrix} \boldsymbol{\theta_1} \\ \boldsymbol{\theta_2} \\ \vdots \\ \boldsymbol{\theta_n} \end{bmatrix}$$

20

Next, substitute $\boldsymbol{a}$ into Equation 19 and form a new vector, $\boldsymbol{b}$ where:

$$\boldsymbol{b} = -\tan(\boldsymbol{a} - \mathbf{90})$$

21

Let c be a vector containing R_c values such that each of the n values recorded in $\boldsymbol{a}$ has a corresponding m value in $\boldsymbol{c}$ and that m equals n.

$$\boldsymbol{c} = \begin{bmatrix} \boldsymbol{R_{c1}} \\ \boldsymbol{R_{c2}} \\ \vdots \\ \boldsymbol{R_{cm}} \end{bmatrix}$$

22

The next step is to multiply M_c by the result of Equation 21. These results are stored in a new vector, $\boldsymbol{d}$, which now contains the modified resolution coefficients, R'_{cn}.

$$\boldsymbol{d} = \boldsymbol{M_c} * \boldsymbol{b} = \begin{bmatrix} \boldsymbol{R'_{c1}} \\ \boldsymbol{R'_{c2}} \\ \vdots \\ \boldsymbol{R'_{cm}} \end{bmatrix}$$

23

After this the original resolution coefficients stored in $\boldsymbol{c}$ are compared with the newly modified coefficients found in $\boldsymbol{d}$. This is accomplished in Equation 24 and the resultant values are termed $\boldsymbol{R''_{cn}}$.

$$\boldsymbol{e = c - d = \begin{bmatrix} R''_{c1} \\ R''_{c2} \\ \vdots \\ R''_{cm} \end{bmatrix}}$$

24

The next step is to determine the average of the values contained in $\boldsymbol{e}$.

$$\boldsymbol{\overline{x} = \frac{\sum_1^m R''_c}{m}}$$

25

If the calculated average is less than zero then the modifying coefficient must be decreased and it must be increased if the average is greater than zero. Through iteration of this entire process the modifying coefficient eventually reaches the point where the average equals zero out to a specified precision. At this point the model matches the data points as closely as it can and is considered optimized. Using a spreadsheet the entire process can be automated and completed in just a few minutes with a high degree of precision. The completed and optimized model can be found in Equation 26 in general form.

$$\boldsymbol{R_c = -M_c \tan(\theta - 90)}$$

26

This optimization process would be successful for incident angle/target distance data collected with any sensor resolution and focal length. In the case of the data collected and presented within this project the modifying coefficient eventually calculated was 0.019398307. This provided that the average difference between the model and the data was equal to zero out to 9 decimal points. The completed model is shown in Equation 27.

$$\boldsymbol{R_c = -0.019398307 \tan(\theta - 90)}$$

27

Using this equation, the model was plotted in addition to the data already found in Figure 4.12 in order to form a new graph (Figure 4.13). It can be seen that the model accurately matches the data gathered for this second extended distance test. The ideal sensitivity model was also used to calculate the expected sensitivity at angles spanning the entire range of the graph. The range used for the ideal model was 1.000 m in order to correspond with the resolution coefficient. They are superimposed upon the other two values. The extremely close match of the experimental data, the experimental model and the ideal values is encouraging.

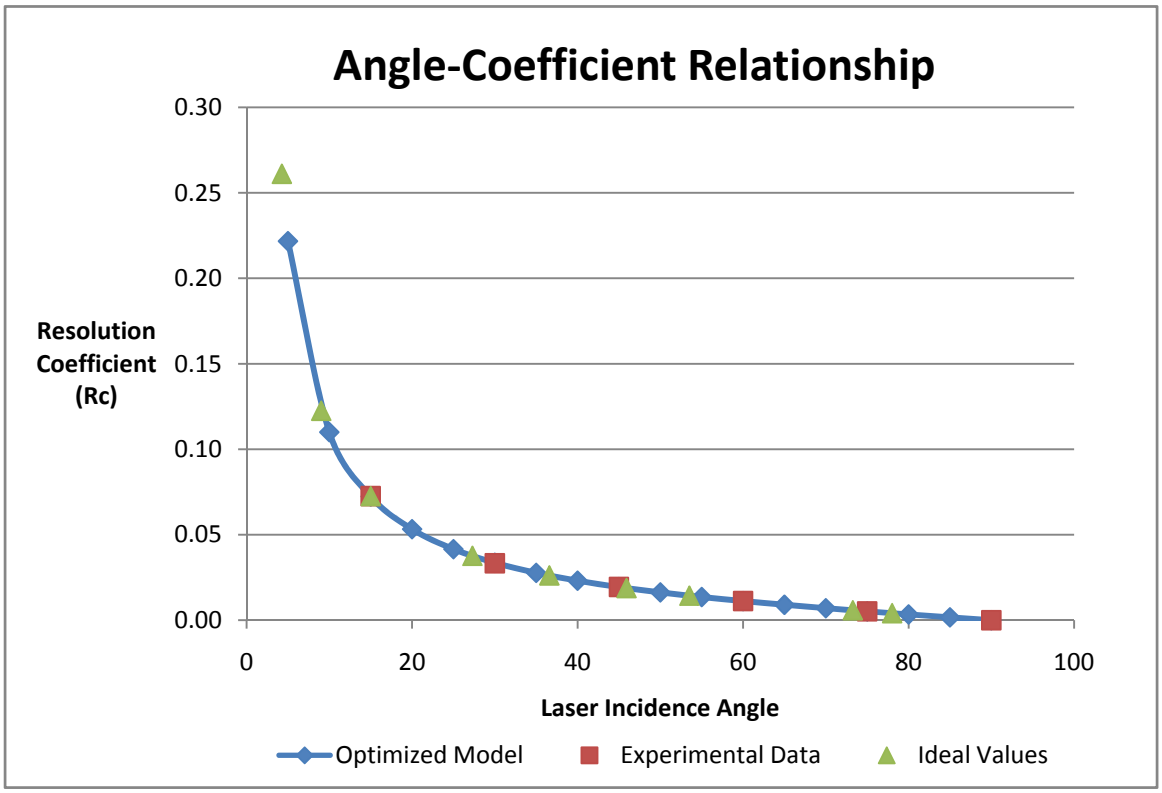

Figure 4.13: The optimized model for predicting the resolution coefficient based on the experimental data can be seen in this graph with the actual data points superimposed on top. Also superimposed is the data from the original incidence angle testing in the lab.

As stated previously the three graphed sets of values are extremely similar. However, there is a slight difference between the experimental model and the ideal model. At an incidence angle of 15 degrees the difference is 0.000215 mm, with the differences decreasing as the incidence angle gets smaller until the difference is only 0.0000150 mm at 75 degrees, while the models match exactly at 90 degrees. This comparison serves to show that the experimental model developed from this test data can be used as an alternative method of estimating the sensitivity of the HRTMM.

Sensitivity prediction with the experimental model takes place according to Equation 28 where the sensitivity, s, is equal to the resolution coefficient multiplied by the distance between the target and the sensor, t_d. The sensitivity result is given in millimeters.

$$\boldsymbol{s = R_c t_d} \tag{28}$$

5. ERROR SOURCES, RECOMMENDATIONS, AND CALIBRATIONS

5.1. LASER POINTING ERROR

Laser pointing error is the error that is introduced into a measurement when misalignment, atmospheric turbulence, or thermal changes in the body of the laser cause the beam to move away from its true aiming point. In high-precision measurement or communications systems this can be of extreme importance as some components of the error grow in magnitude as the distance between the laser aperture and the target grow. A pointing error of only 20 arcseconds represents a far-field inaccuracy of approximately 0.01 mm at a range of 100 m.

Pointing error has a number of causes including atmospheric conditions and laser warm up. The method used to launch the beam from the laser can also create pointing error, though this only effects the behavior of the of the beam after it leaves the laser diode and does not alter the beam direction [43].

The launching method of the laser only effects the dispersion of the beam over distance and so will not affect the accuracy of the HRTMM program to correctly locate the laser in an image. The basic premise is that for a given distance a laser beam with a long wavelength will grow in diameter faster than one with a short wavelength, and the larger the initial diameter of the laser aperture the less the beam will spread. This dispersion is governed by Equation 29 where ω_o is the initial beam radius, ω_z is the laser beam radius at a distance z from the source, and λ is the wavelength of the laser [65]. This information is included for the sake of completeness.

$$\omega_z = \omega_o \sqrt{1 + \left(\frac{\lambda z}{\pi \omega_o^2}\right)^2}$$

29

Atmospheric conditions have the ability to alter the path of a propagating laser beam. This takes place due to the inhomogeneous nature of the Earth's atmosphere and can have a very detrimental effect on the accuracy of optically based measuring equipment, especially if it is used over a long distance. The cause of the inaccuracy can be in the form of beam movement or quivering, or in the form of scintillation, which is a variation in the intensity of light over time.

Movement of the laser beam as it passes through the atmosphere is caused by refraction and is partially described by the refractive index. The refractive index, *n*, is the ratio of the speed of light in a vacuum to that in a medium and is always greater or equal to one. This plays a part in determining the direction and magnitude of any change of direction of an optical wavefront within an inhomogeneous medium according to Snell's Law. Snell's Law describes the interaction of a ray of light with the boundary between two media of refractive indices n_1 and n_2 where θ_1 is the angle of incidence and θ_2 is the angle of refraction (Equation 30) [66].

$$n_1 \sin\theta_1 = n_2 \sin\theta_2$$

30

This relationship shows how the change of direction of light is thus influenced by changes in the refractive index of either medium. The three largest influences on the

refractive index (n) that concern this research are the temperature in degrees Kelvin, T, the atmospheric pressure, P, and the water vapor pressure (humidity), H. Pressure and vapor pressure are expressed in millibars. An equation relating the three variables with the refractive index is shown in Equation 31 [43].

$$\boldsymbol{n = 1 + 10^{-6}\left(\frac{79}{T}\right)\left[P + \left(\frac{4800H}{T}\right)\right]} \quad (31)$$

Little can be done in order to eliminate error due to water vapor pressure or atmospheric pressure short of limiting monitoring to time periods matching predetermined and acceptable ranges for those variables. This is not a viable option for a convergence monitor acting as an early warning system. Measurements made to monitor the strain rate of an opening or slope must be made continuously in order to sense increases in this rate. Compensating for these variables or for temperature can be done, but is impractical. This type of correction is generally made for monitors located at a single location.

Whether used on the surface or underground, it is very possible that the incident laser, target, sensor and the distances in between could all have different atmospheric variables. Making the necessary measurements in order to complete these corrections accurately for every HRTMM reading would be impractical and also would defeat the purpose of having an inexpensive, remote movement monitor.

While total removal of atmospheric error is likely impossible, steps can be taken to minimize the error. Temperature refraction effects are most pronounced when the line-

of-sight between monitor and target is within 2 m of the ground surface. It is also unwise to install a monitor so that the line-of-sight runs parallel and very close to any long objects such as tunnel walls which might exaggerate a temperature gradient across the distance being measured. The line-of-sight should also not come near to objects of drastically different temperature than the surrounding air. All of these instances increase the temperature effect [43].

A propagating laser will remain on its initial course until it is refracted, after which time, the new course will be followed until the laser beam either refracts again or intersects with the target. Thus, changes in the propagation of a laser will have a much larger impact on monitor error if they occur near to the emitting laser than they would if they occurred near to the sensor. Due to this, installation of the monitor components should be completed so that the incident laser propagates away from one of the previously described surfaces as quickly as possible. An ideal example of this would be to install the incident laser so that the direction of propagation was normal to the surface on which the laser was mounted.

Terrestrial scintillation can also cause a laser beam to wander from its true aiming point. In 1959, Tatarski published research identifying how air velocity affects scintillation. It is caused by very small bodies of air with varying refractive indices moving across the beam path. The worst error is found when air movement is directly perpendicular to the beam path, with higher wind velocities causing greater disturbance. Any monitor installation should be set to minimize this arrangement, which is a much more feasible option in underground mines where the air directions are strictly controlled than on the surface. The importance of taking air velocity into account while measuring

with the monitor cannot be understated. Operators should take every effort to collect data while mine fans are in their normal operating condition and should expect variations in measurements with the monitor if the normal operating condition is not met. Even this being said, taking repetitive measures and averaging should help to eliminate scintillation error due to the rapidly changing nature of its source [43, 67].

During surveying activities, both atmospheric refraction and scintillation are frequently minimized by completing measurement only at night. Unfortunately this is not a viable option for the HRTMM if it is being used as a convergence monitor for early warning purposes. If HRTMM measurements are not required on a strict periodic timetable, setting the system to measure only at night on the surface or between shifts underground would help to eliminate scintillation and thermal errors.

Pointing error can also be caused by the thermal warm up of the incident laser. In the thesis disseminating the information concerning initial software development of the HRTMM program, laser thermal drifting was identified as one of the possible sources of calibration error [6]. Thermal drifting occurs, as the components of the laser warm up, from the expended energy causing small movements of the components due to thermal expansion or contraction. It is dependent upon the ambient temperature, laser design and output power.

The author of the thesis conducted an experiment to characterize the extent of thermal drifting that might be encountered. In the experiment three Roithner-Lasertechnik lasers (see section 3.1.4) were shown on a white target. After a 15-minute warm up period five images were captured, one every three minutes (a total of 15 minutes of data capture), in order to track the drifting of the laser. While the experiment itself may

have been worthwhile to conduct, it was not carried out fully and the only conclusions that can be drawn from the data are that the incident laser spot does in fact change position, likely from thermal drifting, and that multiple lasers of the same type seem to behave similarly. No useful trend concerning laser spot movement can be determined due to the small number of data points and no conclusion can be reached concerning laser warm up time because within the time scale of the experiment thermal stability of the laser was never reached.

Due to the importance of understanding thermal drift, the experiment was repeated during this research using one of the same Roithner-Lasertechnik lasers. For this experiment the Nikon D200 was utilized. The camera was set 2000 mm from the target and the incident laser set so that the beam was parallel to the line-of-sight of the camera. This orientation was chosen in order to eliminate any exaggerated spot movement due to the laser impacting the target at an angle. The camera was set to capture images exactly every two minutes; a total of 58 images were captured. The laser was left turned off until immediately before the experiment began. At the conclusion of image capture the images were analyzed using the HRTMM program.

The data showed that the laser did have a warm up time and eventually stabilized 68 minutes into the test (Figure 5.1). The centroid of the laser spot in the initial image was located at X and Y coordinates of [1687.08, 1569.7] while the final average position was located at [1675.93, 1553.1] and had a standard deviation of [0.223, 0.392]. The average position was calculated by determining the average X and Y positions of the 24 images taken after stabilization occurred, with the same being true of the standard deviation.

The same test was repeated using the 5 mW BEA laser. The laser movement in this test did not produce a clean line as in the test with the Roithner-Lasertechnik laser. Images were still taken 2 minutes apart, but based on the results of the previous test only 45 images were taken spanning 88 minutes. This lower number of images did prove to be enough for the lasers to reach thermal stabilization.

Stabilization was reached earlier with the BEA lasers than with the Roithner-Lasertechnik version. In approximately 46 minutes the lasers reached a stable condition.

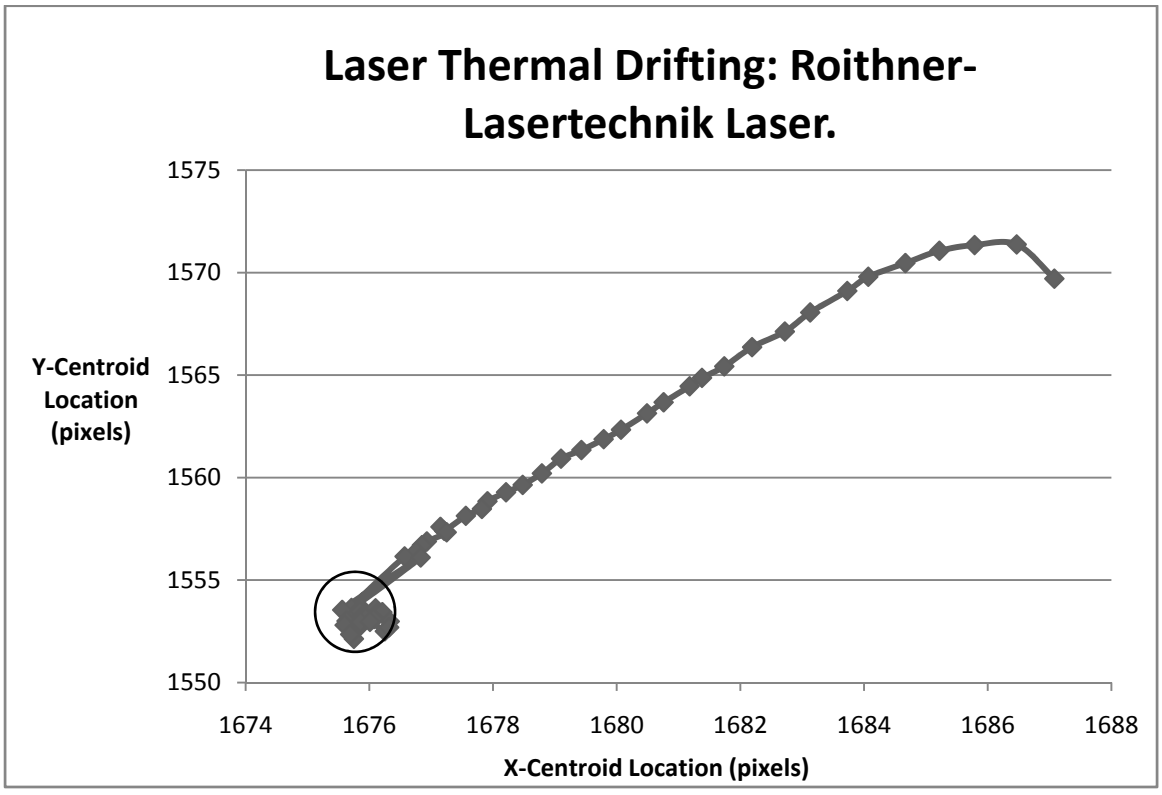

Figure 5.1: Thermal drifting causes the centroid of the incident laser to move across the target. The first image taken in this test is the point on the right-most end of the line. The circle shows the area after stabilization.

The laser spot in the initial image had a centroid location of [2092.23, 1242.6] and the average centroid of the 22 images after stabilization was located at [2087.81, 1238.1]. The standard deviation of the stabilized spot locations was [0.176, 0.192] in the X and Y dimensions respectively. The results from the BEA laser test are shown in Figure 5.2, but are displayed in 10 minute long segments in order to facilitate easier understanding of the travel path of the laser.

In general, the BEA laser had much less difference in the locations of the laser spot between each image. The laser stabilized faster and upon reaching stabilization had a smaller standard deviation. The BEA laser actually reached the level of variability (standard deviation) equal to that found with the Roithner-Lasertechnik laser approximately 17 minutes after the test began and continued to stabilize to a precision much greater than that ever achieved with the other laser. It is interesting to note that this faster stabilization time and higher performance comes even though the BEA laser is rated at a power output of ≤ 5 mW while the Roithner-Lasertechnik is rated at ≤ 1 mW.

Given the results of these tests, it is understandable that each type of laser used with the HRTMM as an incident laser could have a different thermal stabilization or warm-up time. While many laser diodes come with a specified warm-up time from the manufacturer, that is not always the case. It is recommended that any laser used as an incident laser with the HRTMM be allowed to warm up for at least 90 minutes in order to guarantee thermal stabilization has occurred. Note that thermal stability is not necessary for the aiming laser attached to the sensor platform as it is in use for such a short time that thermal drifting with a magnitude large enough to disrupt the monitor is highly unlikely.

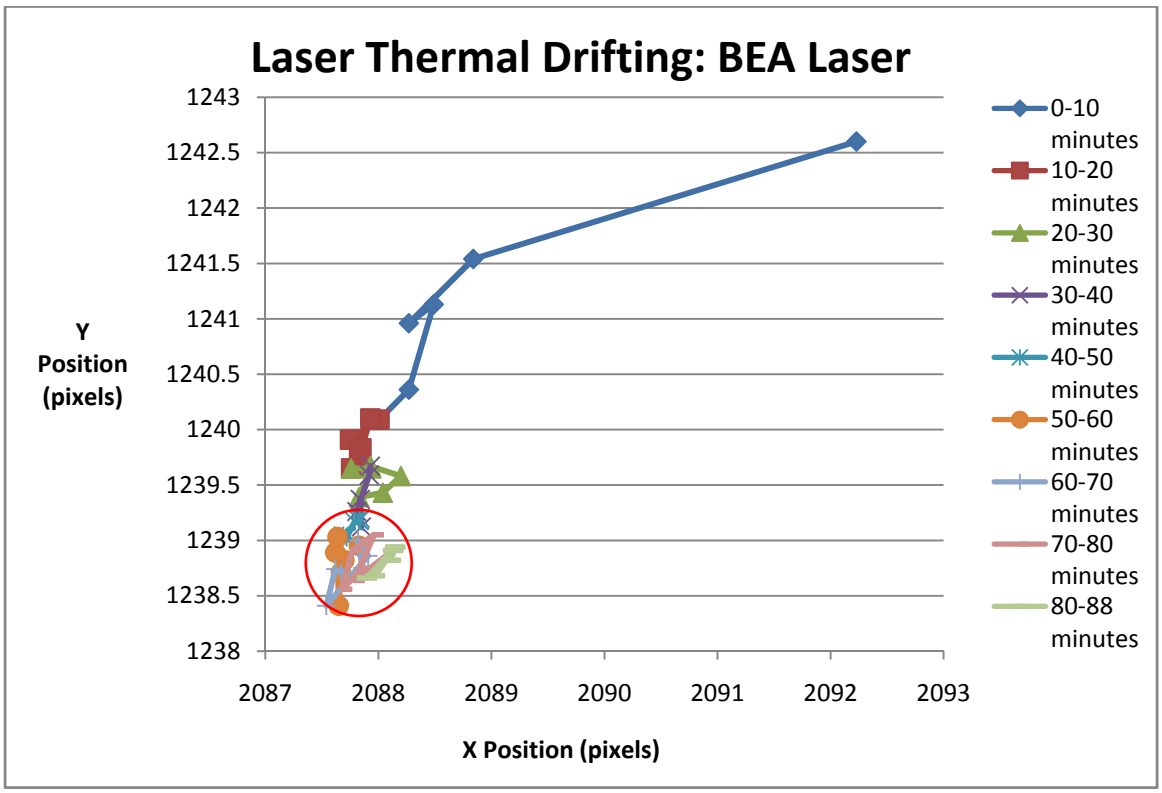

Figure 5.2: Laser spot movement across the image shown according to passing time. Circle shows area after stabilization.

5.2. CAMERA FOCUS

At the beginning of this research the assumption was made that the best accuracy and least error would occur when the camera was focused directly on the target and the incidence laser spot was in clear focus. This assumption was untested and work proceeded throughout the project always under that same assumption. Near the end of the project a set of images was accidentally taken with the camera out of focus and the situation was not noticed until after data analysis was complete. The results brought the assumption of camera focus into question and a test was designed to estimate the differences between monitor operation with the laser spot in and out of focus.

For this examination of camera focus, the camera was placed 1003 mm from the target, which was held stationary for all images. The incidence angle was calculated to be 42.62 degrees. The laser was warmed up for longer than one hour and the camera settings were the standard ISO 250, exposure speed $^{1}/_{100}$ of a second, and aperture of F/5.6. The telephoto lens was used and set to a focal length of 300 mm.

The test began with the laser spot in focus. Twenty computer-controlled images were taken of the laser spot. The focal plane of the camera was then shifted to a point approximately 30 cm behind the target and twenty more images were taken. Finally, the focal plane was shifted to a point approximately 100 cm behind the target and a final twenty images were taken. These images were analyzed in order to determine the precision of the centroid location.

Data analysis began by determining the average X and Y position of the centroids of the twenty images for each of the focus points. These averages were used to normalize each data set. The average deviation from the mean, standard deviation and variance was determined for each data set (Table 5.1).

Table 5.1: Comparison of the precision and repeatability of the HRTMM with changes due to camera focus.

	Average Deviation from Mean (pixels)	**Standard Deviation (pixels)**	**Variance (pixels)**
In focus	1.05	1.60	2.59
30 cm out of focus	0.836	0.457	0.209
100 cm out of focus	0.617	0.289	0.083

It is clearly seen that contrary to the initial assumption under which almost the entire project was completed, setting the camera so that it is slightly out of focus

definitely had the ability to improve the quality of the data returned. Using the ideal sensitivity equation and Equation 7 the standard deviation can be translated into a plus or minus random error value for this monitor setup (Table 5.2).

Table 5.2: Random error for the monitor as a function of camera focus.

	Standard Deviation (pixels)	Random Error (±mm)
In focus	1.60	0.0339
30 cm out of focus	0.457	0.00969
100 cm out of focus	0.289	0.00613

The expected reason for the improvement in precision is due to the fact that when the camera is placed out of focus it expands the area of the image plane that is covered by the light that enters the camera. In the case of the incident laser light, the same amount of light enters the camera at any focus setting, but when the camera is slightly out of focus the laser spot appears much more circular and much more consistent in color. Areas of overexposure are eliminated and small imperfections in the shape of the laser spot are eliminated, removing a source of tiny centroid movements. Typically these small spot imperfections are created by circular interference patterns, laser speckle, reflections off of the target and interference created within the camera lens, which might be removed by using a different lens. An example of the image improvement can be seen in three spots from this test (Figure 5.3).

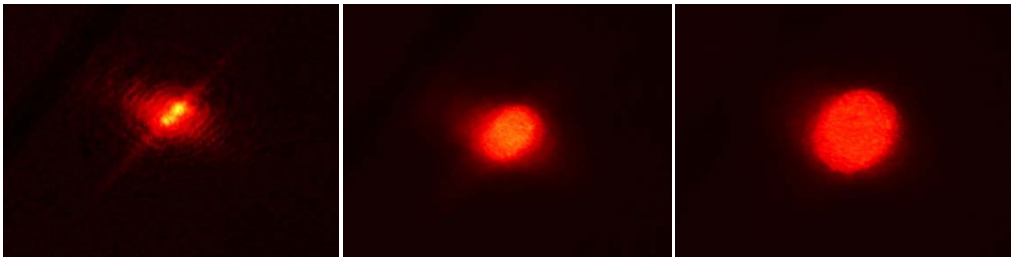

Figure 5.3: Crops of three laser spots with three different camera focus settings; in focus, approximately 30 cm out of focus, and approximately 100 cm out of focus, respectively, left to right.

While the performance of the monitor does improve substantially by setting the camera to be slightly out of focus, this improvement will not continue indefinitely. As the camera is set further and further out of focus the overall image quality will decline as less and less light reaches the image plane. Reducing the light that reaches the image plane will have the effect of making the image appear cloudy and reducing the potential range of the monitor.

5.3. VISIBILITY

5.3.1. Contrast Theory. A typical wall movement monitoring system records data systematically throughout the day. Sampling periods can range from a few minutes to a few hours. Even in the case of a relatively short sampling period (i.e. 15 minutes) it is to be expected that the lighting conditions during sampling will not necessarily remain constant. Factors that can affect the lighting conditions of the target include changing sun position, star light, weather influences, dust, or manual interferences such as vehicle headlights or a miner's cap lamp directed at the target.

The methods used by the HRTMM to detect each laser position depend on high contrast between the light intensity of the laser and the intensity of the background or ambient light, making an understanding of the variables influencing this contrast important. Table 5.3 lists variables known to influence contrast. Lens aperture was initially set as a constant for this project in order to simplify the visibility problem. It was held at an F stop of 5.4.

Table 5.3: Variables known to influence laser spot/ambient light contrast.

Visibility
Target ambient lighting conditions
Laser output power
Camera shutter speed
Camera ISO setting
Target reflectivity
Lens Aperture

Visibility is generally defined as a decrease in contrast between the background and an object. Decreases in contrast are caused by either the introduction of light into the sight path of a dark object, or loss of light from the sight path of a light-colored object [68]. In visible wavelengths, light loss or gain is caused by combinations of scattering, absorption, and an atmospheric extinction coefficient, k, which measures radiation lost per unit distance according to Beer's Law, where I_o is the initial irradiance, I is the reduced irradiance, and x is the distance (Equation 32).

$$I = I_o e^{-kx}$$

32

In the case of the HRTMM, light is lost from the laser twice - once while the laser transmits from the monitor to the target and once again when it reflects from the target back to the monitor. This doubled distance allows scattering and absorption to have a greater effect than they would if the light source was emitted from the target. Mie scattering and absorption due to dust and moisture particles in the air all affect the visibility of the laser. These influences will be considered later.

Another important aspect of visibility is that of threshold contrast, which is the point at which an object becomes visible and the viewer or monitor is able to distinguish between the target and the background [69]. This discrimination can be made through color change (red words on white piece of paper) or through a noticeable change in light intensity (a bright light in a dark room). The HRTMM relies on the latter of the two principles to detect the presence of a laser spot; thus, increases in ambient lighting naturally make it more difficult for the HRTMM to locate a laser light, which is emitted at a nearly constant intensity. The threshold contrast of the HRTMM is limited by the total range of intensity values in the image being analyzed divided by the 255 different intensity values the pixels are assigned during the program's image gray-scaling process. This process is used to eliminate color effects from the image and to simplify and accelerate computer processing [6].

Each of the variables in Table 5.3 affects contrast differently. Through evaluation it has been found that increasing the output power of the laser from 1 mW to 5 mW has the tendency to increase the contrast. This comes as no surprise. In any given lighting

situation, the sensor of the camera records light from all parts of the field of view. If the ambient lighting remains constant and the output of the laser increases, the contrast between the background and the laser spot necessarily increases.

It has also been found through experience that increasing the shutter speed of the camera or decreasing the ISO setting of the camera each have the effect of increasing contrast between the laser spot and the background. Increasing the shutter speed decreases the amount of time that light is incident on the camera sensor. The laser spot is generally a higher intensity than the background, so the decrease in exposure does not affect the laser light captured as much as it does the background light. The ISO of the camera imitates the "speed" rating of standard film where a higher speed film has a faster chemical reaction to light than a lower speed film would. In the same manner decreasing the ISO setting of the camera sensor means that more light is necessary to achieve a given intensity value on the digital image. By adjusting the exposure or ISO settings of the camera it is often possible to achieve an image where the laser is the only thing visible on an otherwise black picture, even in a bright room (Figure 5.4).

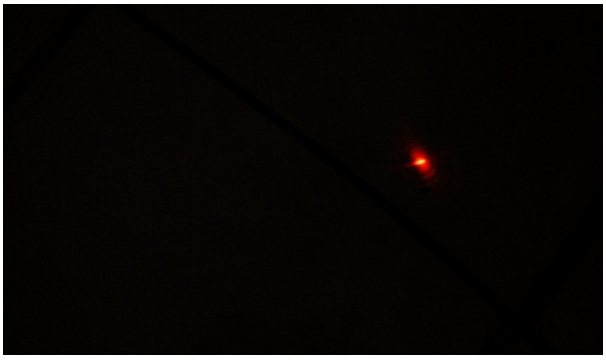

Figure 5.4: Image of laser spot on target. All lights in the room were on (ambient approximately 1000 Lux), Nikon D200 was used to acquire the image set at F/5.6, $^{1}/_{200}$ second, ISO 250.

5.3.2. Shutter Speed and Ambient Light Interaction. A series of tests were prepared to evaluate how the ambient light incident on the target would affect the monitor. The monitor was set up on the optical vibration elimination table with a target distance of 1.010 m. The incident laser was placed 0.567 m away from the camera, forming a right angle between the laser and the target with the camera at the right corner and pointed at the target. This resulted in a laser incidence angle of 29.3 degrees. The camera was the Nikon D200 and was connected to and operated through a laptop computer using the program Nikon Capture Control Version 4.4.0. This allowed for hands-free operation of the camera to eliminate further vibration.

A set of two 500 W high-intensity halogen work lamps were placed 0.400 m away from the target and pointed directly at the target. These work lamps were wired with a dimmer switch so that the light output could be controlled. A digital lux meter was affixed to the target so that it was directly beneath the laser spot, but out of the field of view of the camera. One lux is equal to one lumen per square meter.

Testing was performed by varying the amount of light ambient on the target and taking repeated pictures of each target without moving the camera or the target. With the room lights on and the work lights turned to full power the ambient light was measured to be 13,850 lux. The tests were performed at 10-percent intervals of this maximum value. At each ambient light level a total of 105 pictures were taken. These consisted of three different sets of 35 pictures each. Each set used one of three different camera exposure speeds known to allow for successful detection of the laser spot. The goal of these experiments was to determine if exposure speed would have any influence on the quality of the results, given that the camera was set up to properly acquire an image for use with the HRTMM, and to determine if the monitor could successfully be used under varying lighting conditions. Table 5.4 shows the configurations used. The camera was set at a constant ISO of 250 and aperture of F/5.6.

Table 5.4: Ambient light test parameters. Exposure speeds expressed in seconds. Shaded cells were captured on day one before the camera battery was removed, recharged, and replaced. Clear cells were captured on day two with a fresh battery.

Lux	**13850**	**12560**	**11110**	**9790**	**8410**	**7020**	**5640**	**4250**	**2870**	**1485**
Speed 1	1/2500	1/1600	1/1600	1/1250	1/1250	1/1000	1/800	1/800	1/640	1/500
Speed 2	1/4000	1/2500	1/2500	1/1600	1/1600	1/1250	1/1000	1/1000	1/800	1/640
Speed 3	1/6400	1/4000	1/4000	1/2500	1/2500	1/1600	1/1250	1/1250	1/1000	1/800

During testing it was necessary to remove and recharge the camera battery, with the remainder of the test being accomplished on the next day. This was accomplished approximately half way through testing, with 595 images taken previous to recharge and

the remaining 490 images taken afterwards. The image sets shown in Table 5.4 were taken in order; beginning in the lower left corner of the table moving upwards and then left to right across the table.

The design of this test only varied the camera speed and the ambient light incident on the target. The camera speeds that were chosen were all tested prior to the test for each corresponding ambient light level and were shown to be viable camera speeds for the HRTMM program to successfully isolate the laser spot from the image. To determine if there is an appreciable change in data quality specifically due to either the ambient light level or the camera exposure speed a factorial analysis of variance (ANOVA) was conducted. ANOVA is a method of determining the variance in a data set due to individual variables and assumes three things; independence of the data sets, normality, and homogeneity of variances between data sets. In this case independence was a factor of the test design, normality was verified through the use of both the Kolmogorov-Smirnov and Anderson-Darling goodness-of-fit tests, and homogeneity of variances was confirmed through the use of Levene's Median test at a significance level of 0.05 [70-72].

Results of the ANOVA are found in

Table 5.5. The variances for each ambient light level and each camera speed are very similar with only four exceptions. These are the total variance for ambient light level 7020 and the total variance for shutter speeds $^{1}/_{1000}$ of a second through $^{1}/_{1600}$ of a second. While these total variances are extremely high compared to the others, the variances of the individual data sets can be seen to be very similar to all of the surrounding data and were shown to be the same through Levene's Median test.

Table 5.5: ANOVA results from the ambient light-shutter speed experiment. Shaded data was collected prior to battery replacement.

	Shutter Speed Denominator ($^1/_X$ of a second)									
Lux	**500**	**640**	**800**	**1000**	**1250**	**1600**	**2500**	**4000**	**6400**	**Total**
1485	0.040	0.029	0.037							0.069
2870		0.072	0.056	0.020						0.091
4250			0.050	0.040	0.028					0.052
5640			0.055	0.035	0.340					1.321
7020				0.054	0.208	0.046				159.078
8410					0.015	0.042	0.030			0.148
9790					0.034	0.060	0.051			0.094
11180						0.054	0.030	0.039		0.245
12560						0.086	0.092	0.022		0.115
13850							0.129	0.068	0.091	0.277
Total	0.040	0.087	1.318	118.046	154.923	112.237	0.310	0.346	0.091	

Explanation for the four extremely high variances resides in the fact that the battery recharge and replacement occurred after completion of the $^1/_{1000}$ data set at the 7020 lux light level and before the $^1/_{1250}$ second data set at the 7020 lux light level. When the camera was replaced on the mount it was not returned to the exact same position (the mean centroid distance from the top right corner of the image was 1977.70 and1952.94 pixels before and after battery replacement respectively).

A number of conclusions can be drawn from this test. Firstly, it is shown that the variance (quality) of the data collected at any given camera shutter speed can be considered the same when the camera is set at a single ISO. As long as the shutter speed-ISO combination is sufficient to allow the HRTMM program to successfully analyze the data the monitor will work. Secondly, it is shown that the monitor will work under a wide range of ambient lighting conditions from total darkness up to 13850 Lux without effecting the output of the monitor. Third, the importance of having a stable mount for

the camera is illustrated. Even with an extremely stable platform and a mount designed specifically to hold the camera including both a mounting nut and a locking pin, it was impossible to replace the camera to exactly the same location. This shows that any movement or battery change that must be made should be done at the end of a particular test. In this case it was unavoidable due to the length of the test. Normalization of future data by subtracting the initial data set from the mean of a data set after camera movement would eliminate this problem and would be a viable method since the variance of each data set is the same.

Similarly, it is important that the camera speed remains the same throughout a test. Since the camera speed plays a direct role in determining how much light is collected by the digital camera, changing the speed will not only change the condition of the ambient lighting, it will also affect how much of the incident laser light is collected, affecting the contrast. A brighter laser spot on the image will produce a bigger spot after the thresholding process and could also change the shape of the spot. This has the potential to falsely alter the laser spot's centroid, imparting severe error to the data.

The test procedure evaluated the HRTMM under ambient light levels between 1485 and 13850 lux. While the variances of the data sets collected for this test were shown to be the same, there does seem to be a general trend of increasing variance with greater ambient lighting conditions. Using the lux monitor, the ambient light of the sun was recorded to be an average of 109,800 lux. This reading was taken at noon on a cloudless day in direct sunlight and could be used as an approximate maximum ambient light level that the target might be subjected to. Though this eventuality hasn't been

tested, it is expected that with the right camera settings, a long enough focal length lens, and a strong enough laser, the monitor should work with little difficulty.

5.3.3. Contrast Enhancement with Optical Filters. Increases in the variance of collected data with increasing ambient light levels indicate that a method might be necessary in order to guarantee low variance at any lighting condition, especially if the monitor will be used in surface mining conditions. The results from the ambient light evaluation suggest that even in an underground mine where it is typically completely dark, problems might be encountered if vehicle headlights or a miner's cap lamp were pointing directly at the target or sensor during image acquisition. The simplest method of addressing the error associated with bright surroundings is by using standard optical filters to limit the light that is transmitted through the camera lens and onto the camera sensor.

The purpose of these filters is to increase the contrast between the ambient light levels and the light of the laser. Ideally only a small band of wavelengths surrounding the primary laser wavelength is allowed onto the camera sensor. This drastically reduces the amount of ambient energy included in each image while it leaves the laser light relatively unaffected. These filters can either be an integral part of the camera or added as an accessory attached to the end of the camera lens.

A typical camera sensor is made of silicon and is much more sensitive to near infrared (NIR) light than to the visible portion of the spectrum, with a peak spectral sensitivity in the range between 1000 nm and 1100 nm. This increased sensitivity necessitates the use of NIR blocking filters to reduce the amount of NIR light that actually reaches the sensor. Contamination from NIR light will tend to show up in the red

band of a digital camera due to its close spectral proximity. The primary wavelength of the lasers used by the HRTMM is 650 nm and is also recorded in the red band of the camera. NIR contamination would thus show up in the images used by the monitor and would increase error. The reduction or elimination of NIR contamination would be beneficial.

NIR contamination within the camera's red band is so common that it is frequently taken into consideration during the course of digital camera design. In the case of the Nikon D200 a filter is an integral part of the camera [73]. Installed directly above the camera's CCD sensor, Nikon has included a NIR cut filter to reduce the NIR light that is recorded in an image. In standard visible light photography NIR contamination can cause fogginess and erroneous saturation values in an image as well as reduce image sharpness. While all information concerning the spectral sensitivity of the sensor and cut filter installed in the D200 is considered proprietary by Nikon, some general assumptions can be made.

Through qualitative comparison, users have determined that Nikon's line of digital single lens reflex cameras has had progressively stronger cut filters installed with each successive model. The D200 is the second most recent release in this line of cameras and is found to have a very sharp cutoff point, meaning that the transition from near full light transmission to near zero transmission occurs quickly as the wavelength of the incident light increases. The D300, the most recent release, is also recently available and has even more stringent filtering against NIR light. This camera was unavailable at the beginning of this project. While tests with infrared light sources completed during this research show that the D200 is still sensitive to NIR light of at least 950-nm wavelength,

long exposure times and high ISO settings were required to acquire the images. This suggests that 950 nm is on the very end of the rolloff for the integral cut filter.

Human eyesight is sensitive to light up to wavelengths around 700 nm [74]. In this range humans are naturally able to view some of the contamination from the NIR wavelengths and total removal of all NIR energy in an image would cause some sensitive people to notice chromatic aberrations. Alternately, if a camera were to allow too much NIR light to pass into an image these same people might again object. For this reason the assumption can be made that the integral cut filter would have a 50 percent transmission point somewhere around 750 nm – high enough to provide realistic looking images without increasing image error beyond acceptable levels and also low enough to just barely allow 950-nm wavelengths to be sensed by the camera. A 50-nm transition zone is estimated for this filter from 725 nm to 775 nm.

In addition to the integral NIR cut filter in the D200, which sets the upper bounds for wavelengths recorded by the CCD, two accessory filters attached to the lens set the lower bounds (Figure 5.5). The first filter is a Hoya R-60 high-pass glass filter designed with a 50 percent cutoff at 600 nm. The transition zone of this filter is approximately 50 nm from 575 nm to 625 nm. The second filter is a clear glass UV cutoff filter used primarily to protect the camera lens and R-60 filter from damage. It has a 50 percent cutoff located at approximately 385 nm and a transition zone 50 nm wide [75, 76]. It is assumed that the same luminous intensity is found at each wavelength, 1 candela (cd) per nanometer.

Using the transmission curves of the three filters, it is possible to create a rough estimate of relatively how much light energy is allowed to the CCD sensor with and

without the filtering and to obtain an understanding of how much contrast can be improved by using this method. The spectral range that most digital cameras are sensitive to ranges from about 300 nm to 1100 nm. In order to estimate how the contrast is improved with the use of filters it is necessary to integrate under the curves of the filter transmittance profiles to determine how much light they will allow to reach the sensor. The manufacturer-provided transmittance curves do not include equations for said curves so the areas under the curves are roughly determined graphically. Transmittance is a ratio of the incident luminous intensity, I_o, to the transmitted luminous intensity, I. The SI unit for luminous intensity is the candela.

$$T_r = \frac{I}{I_o}$$

33

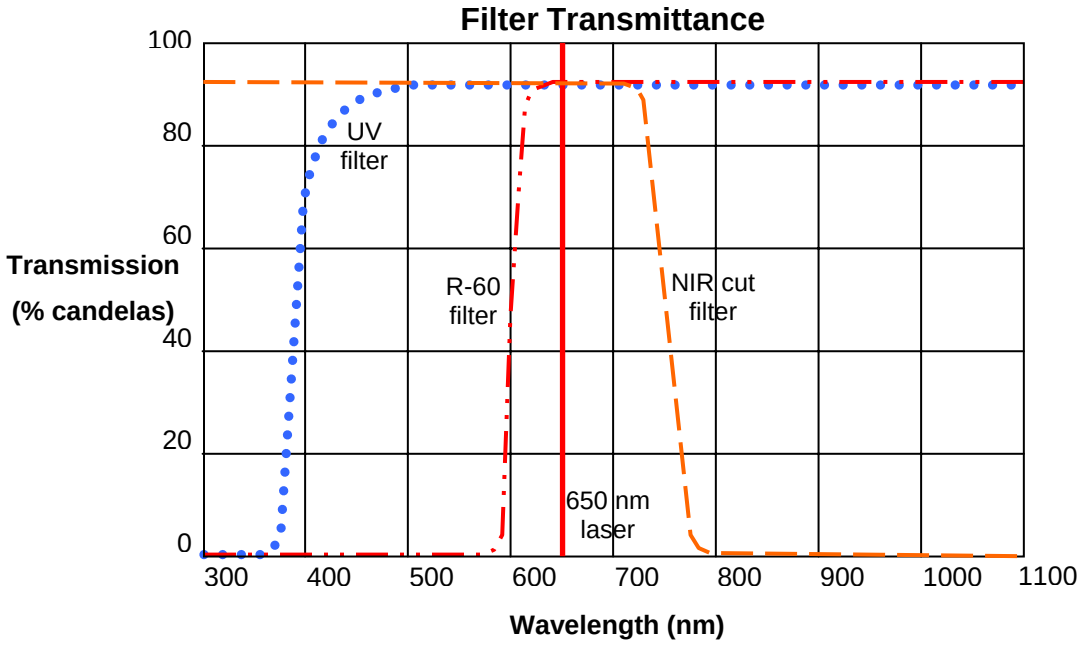

Figure 5.5: Filter transmittance curves for the Hoya R-60, UV filter, and the determined transmittance curve for the D200 integrated IR cut filter. The red line located at 650 nm represents the wavelength of the HRTMM laser.

All filters are assumed to have an upper transmission of 90 percent. The transition zone for the red filter begins at 575 nm. Below this it is assumed that zero light energy reaches the camera sensor. The ambient light allowed to reach the camera sensor is described as follows in Table 5.6: Ambient light filtration with UV, Red and integrated NIR filters. Below 575 nm, the UV filter is ignored for simplicity. Its primary purpose on the monitor is actually to provide an inexpensive lens protector against scrapes, dust, and other misfortune.

Table 5.6: Ambient light filtration with UV, Red and integrated NIR filters.

Wavelength Range (nm)	Equation	Total Light Allowed (cd)	Total Light Blocked (cd)
300 to 575	(575-300)*90%*90%*0%	0	275
575 to 625	(625-575)*90%*90%*50%	20.2	29.8
625 to 725	(725-625)*90%*90%*90%	72.9	27.1
725 to 775	(775-725)*90%*90%*50%	20.2	29.8
775 to 1100	(1100-775)*90%*90%*0%	0	325
	TOTAL	**113.3**	**686.7**
Laser Light %	72.9/100	72.9%	27.1%
Ambient Light %	113.3/(1100-300)	14.2%	85.8%

The laser that is used on the HRTMM is a 650 nm laser diode with a variance of ±5 nm. The entire wavelength range for the laser lies within the heart of the pass-band for the filters so the band is multiplied by (90 percent)^3 to account for the filters. The passed portion of the laser light is 72.9 percent of its original luminous intensity. For the ambient light a total of 14.2 percent is allowed to pass the filters while 85.8 percent is blocked.

Without the R-60 and UV filters the allowed ambient light would be 50.6 percent. Of the laser light 90 percent would be allowed to reach the camera sensor. However, when comparing the absolute values (still assuming one candela per nanometer of wavelength) this would mean 404 cd of ambient light compared with 90 cd of laser light. It can be seen that when using the optical filters much more of the laser light is preserved allowing for increased contrast between the laser spot and the background and increased detail of the laser spot as well. If images taken with and without the filters are converted to black and white to remove color effects (as with the gray scaling process) these improvements can be seen in Figure 5.6: Left image taken without filters. Right image taken with R-60 and UV filter combination. Notice the increased detail and darker tone of

the right image. Both images have been grayscaled as would be done with the HRTMM.. Monitor reliability increased with the addition of these filters.

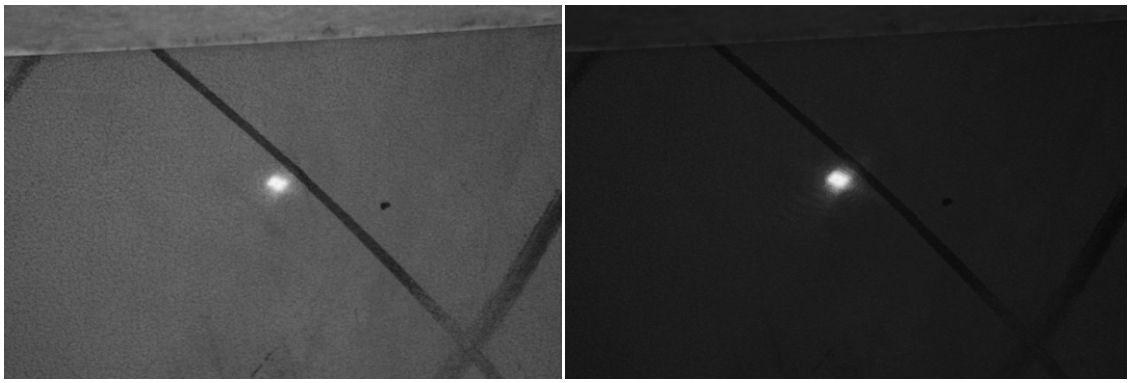

Figure 5.6: Left image taken without filters. Right image taken with R-60 and UV filter combination. Notice the increased detail and darker tone of the right image. Both images have been grayscaled as would be done with the HRTMM.

It is relatively common for the HRTMM program to identify some instances within an image as laser spots even when no laser spot is present at that location. This is most frequently caused by small, naturally reflective surfaces that direct ambient light towards the sensor more so than if the light were truly ambient. The frequency of these false laser spots increases strongly with more intense ambient lighting conditions. While it has been shown that the monitor still locates the true laser spot successfully, the false laser spots can drastically increase processing time, act as unwanted noise within the image, and require manual location of the real laser spot from among the results.

A set of 10 images was collected for each possible filter combination – no filter, UV filter only, R-60 filter only, and the UV/R-60 filter combination. The experiment was repeated with the camera in both automatic exposure mode and with the exposure set

manually at F/5.6, $^{1}/_{160}$ second shutter speed, and ISO 250. In both instances the camera used the telephoto lens set at 300 mm. The data from the images were analyzed and the total number of pixels found by the HRTMM program that were part of the true laser spot and that were part of false laser spot(s) were calculated for each image. The averages for each filter type or combination were determined. The results for the experiments are located in Table 5.7: Automatic exposure results and Table 5.8.

To be considered a success for this experiment, it was expected that the ratio of pixels that were part of false laser spots to the pixels that were part of the true laser spot should be less than 0.01. This ratio is one that could allow a future version of the HRTMM program to reliably and automatically determine which laser spot is the correct laser spot in the event that more than one laser spot is located by the program.

Table 5.7: Automatic exposure results

Trial	Average False Pixels	Average True Pixels	Ratio
No Filter	20941.4	45811.3	0.4571
UV Filter Only	12709.4	40844.3	0.3112
R-60 Filter Only	55.9	22246.6	0.0025
UV and R-60 Both	64.2	21339.1	0.0030

Table 5.8: Manual exposure results

Trial	Average False Pixels	Average True Pixels	Ratio
No Filter	13.0	17513.7	0.0007
UV Filter Only	40.8	17564.1	0.0023
R-60 Filter Only	24.0	19014.2	0.0013
UV and R-60 Both	7.3	18237.4	0.0004

The results provided by the filter testing are very encouraging. For the majority of the trials that have been conducted in other than total darkness, strict manual control was necessary in order to ensure that the HRTMM program was able to successfully locate only a single laser spot. This presents challenges if the monitor were ever to be set up to automatically collect data. Surface mines would have constantly changing sun positions and other lighting influences. Underground mines may have headlight or cap lamp interferences or monitoring may occur in a lighted area. In a truly automatic application the monitor would need to be able to self-correct for these changes in lighting condition. The ability to use the light meter and auto exposure features of the D200, which is suggested by the data in Table 5.7, provides a potential solution to this problem.

While all of the false pixels detected by the camera are indeed part of false laser spot detections, the size (expressed in pixels) of the false laser spots is insignificant relative to the size of the true laser spot. Algorithms should be developed and incorporated into the programming of the HRTMM to automatically locate and isolate only the true laser spot(s). Simply accepting the largest located laser spot(s) is an unacceptable method for determining true laser spots, as the HRTMM is specifically designed to be able to function with multiple lasers. One envisioned method of accomplishing this is to store the area of the largest laser spot found, A_M , and subsequently compare it to the area of each other located spot, A_D , using the ratio, φ, as the rule for false laser spot selection (Equation 34). Spots that produce a ratio larger than 0.01 are accepted while all spots not meeting this criteria are ignored.

$$\varphi = \frac{A_D}{A_M}$$

34

A similar method of comparison could be developed to judge the overall quality of the image. A quality factor might be developed where the ratio of the laser spot (or average of multiple laser spots) could be compared to the sum of all false spots. This would allow for an automatic ratings system to be developed to judge the quality of the monitor's imagery.

The program can also be improved to include an input parameter specifying the number of lasers being used at one time. At any time that the program locates more "true" laser spots than this parameter, a warning message can be displayed calling the attention of the technician or engineer managing the system.

5.3.4. Target Reflectivity. The reflectivity of a target is dependent upon the target color and texture. Two types of reflection are possible, diffuse and specular. The difference between the two lies in how a wave front acts upon intersecting the target. A specular reflection acts like a mirror where a single incoming wave of light energy reflects as a single outgoing wave where the angle of incidence equals the angle of reflection. This type of reflection occurs when the target texture is "perfectly" smooth. In mining, this type of reflection can occur from equipment windows, shiny metal, and from individual crystal faces in the rock. It could also be caused by total internal reflection in water or other liquids.

Diffuse reflections are found when light is reflected in many different directions at once. This happens on curved surfaces, and surfaces that have "rough" textures. Most

surfaces create diffuse reflections and the examples in the mining industry are widespread.

Both diffuse and specular reflections are susceptible to absorption. Light energy can be absorbed by a surface, which is partially responsible for the appearance of colors. The skin of a green apple absorbs light energy from each part of the visible spectrum except for green, which it reflects. Each color absorbs different amounts of light energy from the spectrum as a function of that color's albedo, with darker colors absorbing more than lighter colors.

Color has an effect on the HRTMM and is shown in a test done using large colored paint tiles taped to the target. The color samples used were all Olympic Brand paints and are shown in Table 5.9. For this test the D200 was set up on the vibration elimination table with the incident angle set to 47.5 degrees and the target located 1008 mm away from the camera's imaging plane. The telephoto lens was attached to the camera with all optical lenses attached. The incident laser was warmed up for 1 hour. Focal length was set to 300 mm and the aperture was F/5.6, while the shutter speed was set to $^{1}/_{100}$ of a second with an ISO of 250. The camera was placed in its highest resolution setting. Images were analyzed with a window size of 7 and a threshold of 50.

Table 5.9: A record of the paint colors and codes, along with their common names used in this experiment

Color	Paint Name	Paint Code	Color Number
Black	Black Magic	D58-6	1
Blue	Cobalt Stone	A52-6	2
Green	Leap Frog	A66-6	3
Brown	Fudge	D27-6	4
Violet	Byzantine Purple	A43-6	5

Red	Sunset Skyline	A31-6	6
Orange	Pumpkin Pleasure	A22-6	7
Yellow	Sunflower	A16-6	8
White	N/A	Typing Paper	9

Each color was placed on the target one at a time and 10 images were taken for each color. The target was held stationary. With the HRTMM, reflectivity of a particular color shows as a change in the number of particles composing each laser spot. Following data collection each image was analyzed and the average spot size (number of particles) was determined and graphed (Figure 5.7).

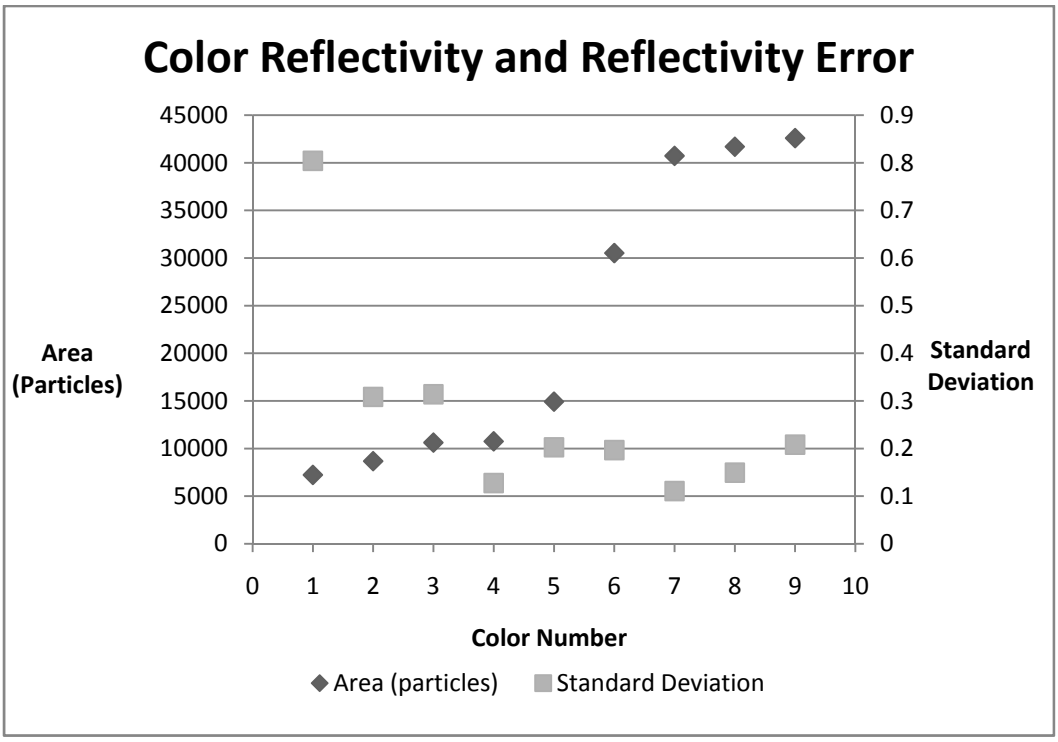

Figure 5.7: Reflectivity is expressed as a function of the particle size of the laser spot. Error is shown as the standard deviation of the centroid locations.

The results of this experiment clearly show that the HRTMM responds directly to the color reflectivity of a target. It also shows (as might be expected) that higher error is associated with darker colors. Alternately stated, darker colors reflect less light, thus returning less “data” to the sensor, thereby increasing the error.

Specular reflections did not need to be included in this test as targets used by the HRTMM will be specular in nature with extreme infrequency. Specular reflections are part of the light seen by the monitor, but the light source for the reflection is ambient light as opposed to incident laser light. In this case the specular reflections show up as error in the image and are treated by the program (in its current form) as other laser spots. These are the false laser spots that are mentioned in section 5.3.3.

Previously unmentioned, the moisture content of a surface has the ability to change the color of said surface. A rough surface that is absorbent like most rocks, soils and dusts, will appear darker when wet. This is caused by a number of properties including diffuse and incomplete reflection, absorption, and total internal reflection within the liquid at the surface. Each of these factors assists in decreasing the intensity of reflected light. In the experiment each color sample was dry [77-79].

Due to the results of this reflectivity experiment, it is clear that light colored targets should be used as frequently as possible with the HRTMM. While some rock types may be considered light-colored enough to keep error within acceptable limits, other rock types, including coal, would certainly not. In these cases an installed metal target will be of assistance in collecting high-quality data. Since many natural targets in a mine have the potential of being wet from time to time, attempts should be made to chose targets light enough in color to prevent significant error increases. Finally, installation of

a man-made metal target would decrease the effect of wetting, as the surface would be light in color, resistant to absorption, would dry quickly, and would eliminate many of the variations in color that come from natural rock or soil types.

Painting a natural target with multiple light coats of non-glossy spray paint would be an attractive option for eliminating color variation across a target and lightening a dark target to make it suitable for use. Multiple light coats of paint are necessary in order to reduce running of the paint. A drop of paint running down a surface could easily create unwanted artificial roughness. Alternatively, building up thick enough layers of paint could have the effect of reducing small scale roughness and undulations in a natural target. This may be an unexpected benefit that could use clarification in the future.

5.3.5. Visibility Summary. It has been shown that the ambient lighting surrounding the HRTMM can have a significant effect on the reliability and functionality of the monitor. The easiest method for addressing this issue is to use a method to increase the contrast between the laser spot and the background. This can be accomplished by increasing the output power of the laser. Due to regulations regarding the maximum safe output for a laser in an environment where people may interact with the laser and the power limits determined for a laser in an explosive atmosphere, there is a limit to how high the laser output can be. In the case that the highest power laser is in use and the contrast is still not high enough for the HRTMM to successfully locate and track the laser spot, optical filters can be used to limit the amount of ambient light impacting the image sensor.

Optical filters have been shown to increase the reliability of the HRTMM and range of environments in which it can be utilized. They accomplish this by limiting the

total bandwidth of light that is allowed into the camera while not significantly reducing the intensity of the laser light incident on the camera sensor. This creates a very beneficial increase in contrast between the laser light and the background. With the ability to use the HRTMM in increasingly bright environments, it is also possible to make use of the D200's light meter for determining image settings. This had previously been impossible as the camera is designed to create an image fit for human viewing, which caused the image to be too bright and the threshold contrast for the HRTMM could not be reached.

Another possible step that could be taken to increase contrast by elimination of ambient light would be to increase the focal length of the lens used with the system. With increased focal length the field of view naturally becomes smaller in the angular dimension, reducing the total ambient light that is captured by the camera's CCD sensor. This may be necessary in the future as the system has not yet been tested under full daylight, which has ambient light measurements almost 8 times as high as the highest used in these experiments (approximately 109,800 lux, average of 10 measurements, full sun, noon hour).

The target or object chosen for the HRTMM should be light in color. This will reduce the effects of color change when the target becomes wet. It will also decrease the error associated with the high absorption levels of dark colored targets. Installation of a metal target would eliminate many of the effects of wetting and would also reduce color variations found in normal rock, soil and dust. This would be especially important in a coal mine.

5.4. TARGET ROUGHNESS

The roughness of the target or object being measured affects the results of the monitor by creating false movement in the image or by decreasing the quality of the image to a point where the HRTMM has increased error, making measurement difficult.

False movement occurs when a movement of the laser spot is exaggerated or diminished by an uneven surface. This can occur when the laser beam impacts an angled section of the target, effectively altering the expected angle of incidence for the laser. The error imparted to the measurements could be compensated for if the effective incidence angles were known, but on a typical rock surface determination of the angle would require a precise surface profile to be completed and would overcomplicate the installation and calibration of the monitor, drastically reducing its appeal. Installation of a controlled target would be much faster and easier to accomplish.

Data quality can be affected when the laser beam intersects a rough target. The two primary quality problems are illustrated below. The first quality problem can be caused when the incidence laser beam only partially impacts the top portion of a bump. The laser beam will appear to create two separate laser spots in this instance, neither of which would occur in the proper location on the image. This drastically alters the centroid of either laser spot and creates large error in the data. Figure 5.8 shows an illustrated side view while Figure 5.9 shows an actual occurrence during testing.

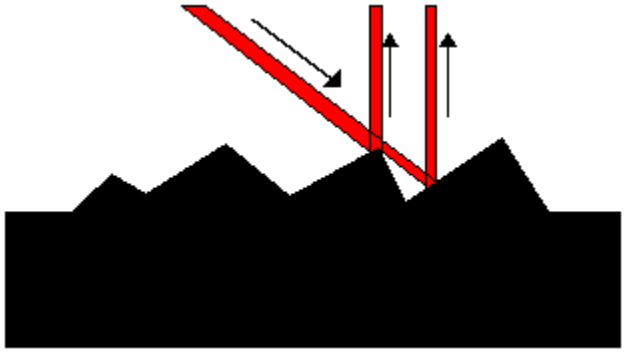

Figure 5.8: It can be seen that the incidence laser beam can potentially create two separate laser spots for the camera. One will be located at the primary point of impact while the second is located at the secondary point of impact, shown as laser beams diffusely scattering back towards the camera (top).

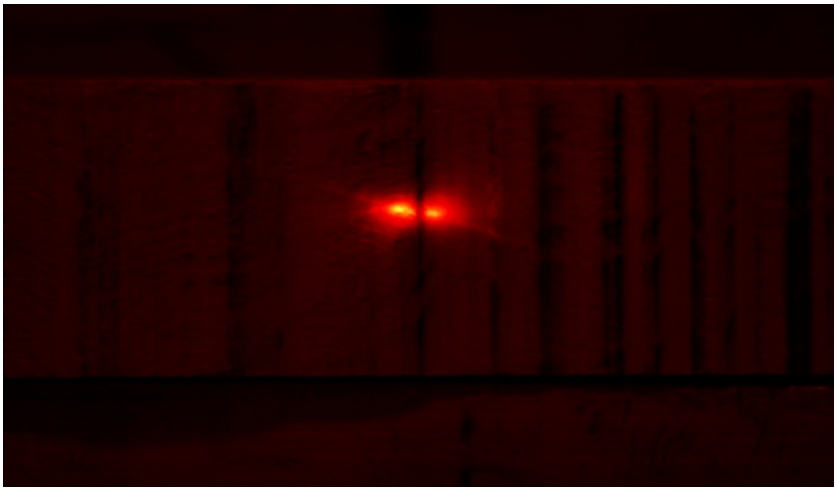

Figure 5.9: An actual example of laser spots created by primary and secondary impact of the laser beam with a rough target.

The second type of quality problem occurs when the incidence angle of the laser is similar to the slope of a bump on a rough target. In this instance two different things can happen. Firstly, as illustrated in Figure 5.10 it can be seen that when the laser is

directly aimed at the tip of the bump it will have the tendency to illuminate the entire slope surface. This will tend to artificially move the laser centroid towards the base of the slope. An actual image of this occurrence during testing can be seen in Figure 5.11. The second error occurs when the target moves either forwards or backwards from the camera. In this case the laser spot would impact with the peak of the bump, move past the slope, and very quickly would impact the base of the next slope. This would have the effect of making the laser spot move across the image much faster than it would otherwise, causing error.

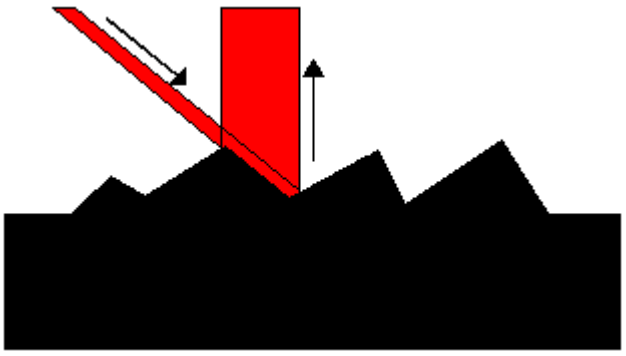

Figure 5.10: In this situation the laser beam is illuminating the entire slope of the bump, creating one elongated laser spot instead of a concentrated oval as if the surface were flat.

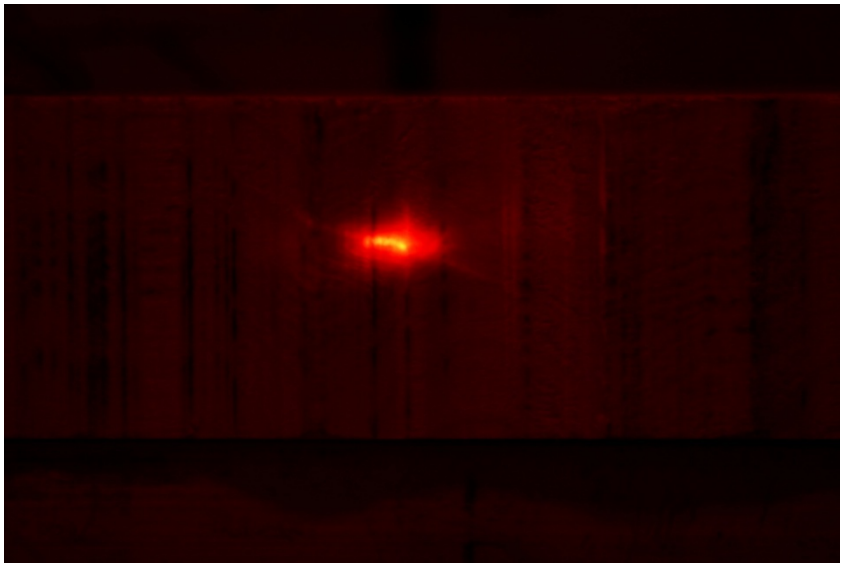

Figure 5.11: An actual example of the error described in previous figure.

In order to demonstrate the impact of a rough target on the HRTMM a test was developed that would compare the HRTMM performance against standardized roughness profiles. The profiles used in this test were based on Barton and Choubey's Joint Roughness Coefficient (JRC). The JRC was initially developed as one of three index parameters used in an empirical equation describing the shear strength of rock joints. This was chosen because it is so frequently used as a method of qualitatively describing the roughness of a rock surface. It takes into account the amplitude, frequency and length of the undulations that typically describe surface roughness [80].

This test was completed by making wooden profiles corresponding to some of the published JRC profiles. These were carved out of wood with a band saw following a trace of the published profiles. This method has been used successfully in previous research

[81]. For this test profiles corresponding to JRC values of 0, 4-6, 8-10, 12-14, and 16-18 were made (Figure 5.12). When in use each profile was secured to the stage micrometer.

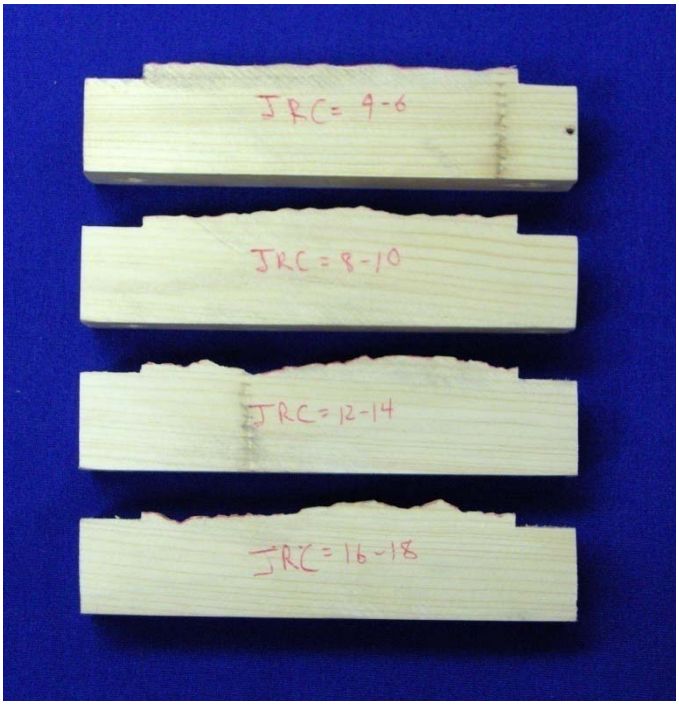

Figure 5.12: Wooden JRC profiles used for roughness testing. JRC zero is a flat surface, so the flat side of one of the profiles was used.

The purpose of this test was to show the importance of having a flat target. For all images taken during this test the Nikon D200 was used under computer control along with the telephoto lens set to a focal length of 300 mm. The aperture was set to F/5.6 and a shutter speed of $^{1}/_{100}$ of a second was used. Each profile was placed one at a time on the micrometer stage set 950 mm between the camera image plane and the base surface of the profile with an incidence angle of 47 degrees measured on the laser rotational stage.

For each profile the length of the profile was divided into 5 segments. Starting at the beginning of each segment an image was taken and then the micrometer stage was moved away from the camera 2.00 mm. This was repeated 4 additional times for each segment making 1.000 cm worth of movement for each segment. This imaging and movement was repeated three times for each segment of the profile. With this method the entire length of each profile was represented in the sample equally and repeatedly.

Analysis of the data was completed according to Equations 7 and 9. The known target movement, ΔD was 2.00 mm. The first profile to be completed was the JRC 0 profile, as it was used as a comparison for all of the other profiles. It represented target movement of a completely flat surface. Once JRC 0 was completed C_0 was calculated and averaged for the entire profile. This acted as a baseline movement value.

Next each other JRC profile was analyzed and the average C was determined. Comparison between other JRC profiles and the JRC 0 profile was completed by subtracting C_0 from the average C value calculated for each other profile. Using this method the average increase in target movement above the baseline value was determined. The results show a steady increase in centroid movement due to target movement as each target increased in roughness. The results are shown in Table 5.10: Increases in the absolute centroid movement value relative to JRC 0 for each other JRC profile in pixels..

Table 5.10: Increases in the absolute centroid movement value relative to JRC 0 for each other JRC profile in pixels.

	C_0	$C_{4\text{-}6}$	$C_{8\text{-}10}$	$C_{12\text{-}14}$	$C_{16\text{-}18}$
C	0.00	16.04	18.09	23.44	33.30

In order to use the HRTMM on a natural rock target (no target installation necessary) a method of compensating for the variation introduced by surface texture must be considered. Thought was given to this question and the fact that the HRTMM has been shown to work with a flat metal target. In reality it is known that no metal target is absolutely “flat”. Microscopic undulations and fluctuations do occur and the biggest difference between the prepared metal target and a natural rock surface is in the frequency and size of these undulations and deviations from being “flat”.

In the case of the prepared metal target, the bumps and undulations are much smaller than the diameter of the incidence laser. In effect, the size of the laser is so much larger than the bumps that those bumps near the center of the laser spot are completely covered and so have no influence on the centroid location, and those bumps near the periphery of the laser create such a small change in centroid position that it does not severely impact the measurement. Additionally, the bumps are small enough and numerous enough that they completely surround the laser spot, creating interference on all edges. The error caused by bumps on one side of the laser spot is canceled by the error caused on the other side. In this manner the roughness of the prepared target has little effect on the accuracy of the monitor.

This reasoning is why the roughness of the prepared metal target was considered as a potential method for dealing with roughness on a larger scale. If the texture must be small relative to the diameter of the laser beam, then increasing the diameter of the laser beam should increase the effectiveness of the monitor on rough surfaces. This thought process was examined using a laser diode with a focusable laser beam. By turning the lens on the end it allowed the diameter of the laser beam to be altered. Four diameters

were chosen relative to the size of the target and the actual diameter was measured afterwards from the magnified images. Each diameter was given a letter to represent it for easier identification (Table 5.11).

Table 5.11: Laser beam diameter and identification.

Identification Letter	A	B	C	D
Approximate Diameter	3.8 mm	6.1 mm	10.4 mm	15.2 mm

The remainder of the test setup was very similar to the previously described test. The Nikon D200 was used in conjunction with the telephoto lens set to a 300 mm focal length. The ISO was set to 250 while the exposure was $^{1}/_{100}$ of a second in duration. The aperture was set to F/5.6. The surface of the roughness profiles was set to be 1005 mm from the image plane and the incidence angle was set to 42 degrees.

For this test, the roughness profiles were moved horizontally across the target without changing the target distance from the camera. Due to the horizontal movement the only potential change in distance between the camera and the roughness profile would be if the laser spot moved left or right due to the surface roughness. If the increase in diameter were to work perfectly, the monitor should show no laser spot centroid movement. This test used the same four roughness profiles and 16 images were taken sampling the entire length of each profile.

A flat surface would return laser spot centroid values that had more or less the same values in both the X and Y directions. In order to compare the roughness profiles each one needed to be compared to a baseline value unique to that profile. In order to

determine this value the first step in analysis was to calculate the average X and Y position for each profile, which was then used to normalize the movement of the laser spot for each image. The normalized movements represent the deviation from a flat surface and were calculated according to Equation 9. The deviations are shown as the number of pixels that the laser spot centroid moved and are shown in Table 5.12.

Table 5.12: Laser spot movement due to surface roughness and laser diameter. Diameter increases from A to D. Results expressed in pixels.

Centroid Movement		**Joint Roughness Coefficient**				
		0	**4-6**	**8-10**	**12-14**	**16-18**
Laser Diameter	**A**	0.79	20.30	53.48	98.52	118.15
	B	0.65	19.10	48.40	82.99	111.83
	C	0.713	25.54	52.99	92.73	96.94
	D	0.62	49.49	45.94	95.01	97.41

From these results it appears that the centroid movement is not affected much by increases in laser beam diameter. JRC 16-18 is the only case where there seems to be a general trend towards elimination of the effects of roughness by increasing laser diameter. JRC 0, 8-10, and 12-14 do not show an identifiable pattern of change between the four laser diameters, while JRC 4-6 actually shows increasing variation with increasing diameter. From these results the only valid conclusion is that the experiment didn't work out very well.

One potential source of error for this experiment was the coloration of the profiles. The JRC profiles were created by tracing the profile onto a block of wood and then using a band saw to cut away the unwanted portion of the wood, leaving the profile behind. On some parts of the profile surface, the wood was slightly burnt or discolored

from the friction of the saw blade. This changing coloration could have altered reflectance of the profile enough that the shape of the returned laser spot would have changed, moving the centroid. Another source of error could have been the direction of movement of the profile as the data was being collected. Due to the arrangement of the monitor components, the incidence laser was aimed along the long direction of the profile, while the saw cuts on the profile were made perpendicular to the long direction of the profile. When the profile was moved in a direction parallel to both the long axis of the block of wood and the aiming direction of the laser, changes in shape of the laser spot might have been exaggerated more-so than on a true rock surface where the roughness does not lie only perpendicularly to the aiming direction of the incidence laser. It is believed that the perpendicular trend of the roughness would have been compensated for if the laser spot could have been made much larger, but this was not possible.

A final test was completed in order to clarify the ability of the monitor to deal with rough surfaces. For this test an aluminum target was fabricated that had a very precisely defined roughness. The target was made to have increasingly rough sections with square cross sections upon which the laser could be aimed. The goal was to see how well the HRTMM reacted strictly to changes in amplitude of the roughness. The square cross section of the rough sections increased in 0.500 mm increments from 0.500 mm to 3.000 mm. The profile is shown in cross section in Figure 5.13.

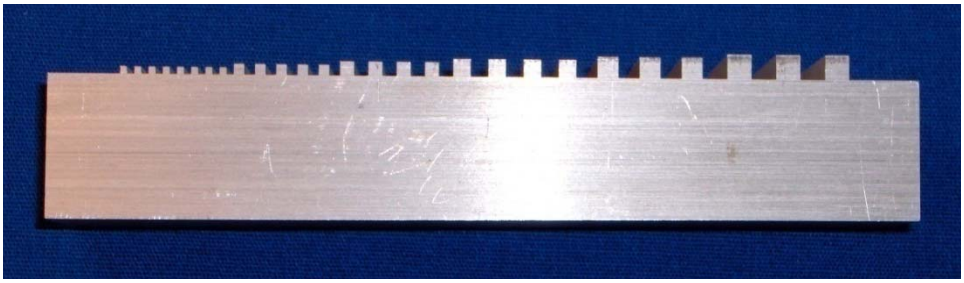

Figure 5.13: Cross-sectional view of the metal fabricated roughness target.

This test was completed in the same manner as the initial laser beam diameter test with one exception. With the fabricated aluminum profile the distance moved sideways between each image was equal to one half the width of the square profile being used at the time. This was done under the assumption that the maximum centroid movement should occur between the peak and valley of two of the square protrusions. Repetitions of measurements between the peaks and valleys allowed for a good estimate of centroid movement for each roughness.

Two diameters of the laser beam were used in this test, approximately 2.0 mm and 5.5 mm. Each laser diameter was used to take 26 images of a section of the roughness profile. Data was analyzed in the same method as for the previous test. Results are shown in Table 5.13.

Table 5.13: Normalized centroid movement due to surface roughness and laser diameter. Results expressed in pixels.

Centroid Movement		**Roughness**			
		0.500 mm	**1.000 mm**	**1.500 mm**	**2.000 mm**
Laser Diameter	**2.0 mm**	19.28	30.84	38.07	41.44
	5.5 mm	16.22	22.44	25.68	26.74

It can be seen from the table that this test was successful in demonstrating that increasing the diameter of the laser beam will help to eliminate error due to target roughness. For all four roughness levels tested, the increase of the laser diameter from approximately 2.0 mm to 5.5 mm significantly decreased the deviation from zero pixel movement, as would be expected with a perfectly flat target.

When the ratio of the roughness to laser diameter was determined and plotted against the normalized pixel movement for each testing combination, a trend becomes apparent. With the exception of the 2.0 mm laser and 0.500 mm roughness combination, a pattern is developed where the ratio is related to the pixel movement with higher ratios having less pixel movement (Figure 5.14). This sort of trend was expected, though the JRC profiles incorporated too much randomness and potential error to make it easily apparent.

Following discovery of this trend the same process was completed with the JRC profile data. The ratio was developed by using the average JRC value as the roughness value, and a roughness of 1 was used for the JRC 0 profile (Figure 5.15). This was done because typically the lowest JRC profile is considered JRC 0-2.

For both graphs, it is difficult to find a particular equation to fit the collected data well. Even with the demonstrated trend, it is considered unlikely that the laser spot could be made large enough in order to ever completely remove roughness error for a surface with a JRC value greater than 4. Increasing the diameter of the laser beam is only an option up to a point because the increase will cause error due to environmental effects to increase as well. It is recommended that a man-made target be installed if a surface appears rougher than a JRC of 2.

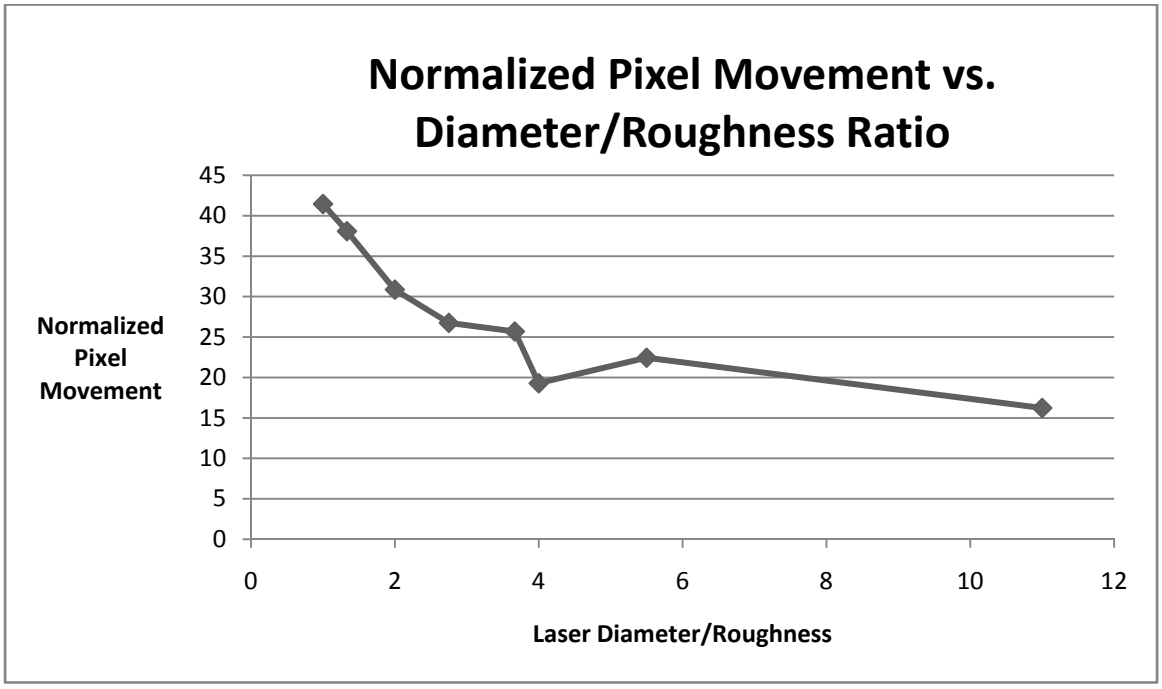

Figure 5.14: A decreasing trend can be seen between pixel movement and Diameter to Roughness ratio.

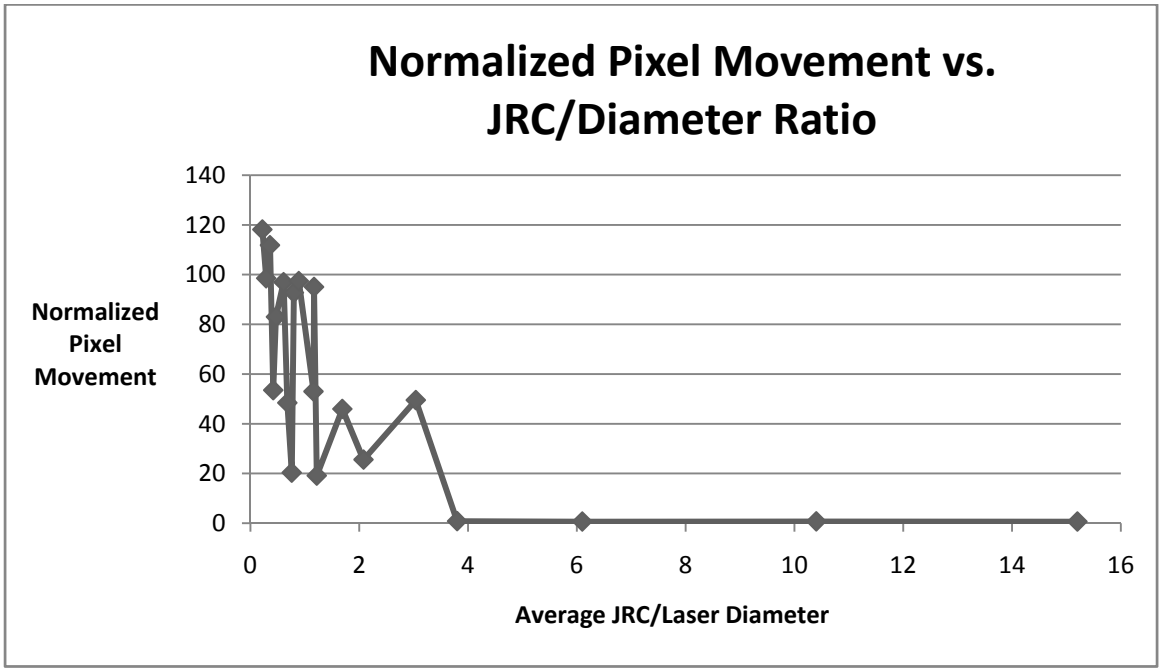

Figure 5.15: A decreasing trend is apparent even though the data seems imprecise.

5.5. MINE FOG AND DUST

Mine fog and dust are two types of particulate matter that negatively affect the readings of an optically-based monitor. As light travels through an atmosphere it will be scattered as it moves through a cloud of fog or dust particles. Generally Mie scattering will apply due to the size of mine fog particulate, which is generally much smaller in diameter than typical surface fog (diameter generally between 1.0 and 10.0 μm as opposed to between 5.0 and 40.0 μm) [82, 83]. Mie scattering is applied when the diameter of the particulate is greater than the wavelength of the light.

Mie scattering is a function dependent upon the physical characteristics of the light, the particulate, and the medium in which the scattering takes place. The scattering coefficient (β_a) is given by:

$$\beta_a(\lambda) = 10^5 \int_0^\infty Q_d\left(\frac{2\pi r}{\lambda}, n'\right)\pi r^2 n(r)dr \tag{35}$$

where *n'* is the real part of the refractive index of the aerosol particles, λ is the wavelength in μm, *r* is the particle radius in cm, *n(r)* is the particle size distribution and Q_d is the Mie normalized scattering cross section [84].

The scattering coefficient is most greatly affected by the radius of the particles. Smaller particles will create more scattering than larger particles. Since mine fog has a general tendency to have smaller particle sizes than surface fog, this helps to explain why similar thicknesses of fog underground have a much higher impact on the absorption and scattering of light, greatly reducing visibility. With respect to the HRTMM, fog and

particulate matter are a much greater concern for underground monitoring than for surface mining.

In order to demonstrate the impact of mine fog on the precision of the monitor, a test was conducted at the Fletcher mine, an underground room-and-pillar lead mine owned and operated by the Doe Run Company. This mine is located approximately 60 miles away from the Missouri University of Science and Technology making it an ideal location for conducting underground experiments in an actual mine setting.

This test was designed in order to see how mine fog would impact the precision of the monitor when an installed target was moved away from the camera exactly 0.500 in. For the test setup a Hilti range meter was used for measuring distances between the three components of the monitor, measured in feet. Three measurements were taken and averaged in order to determine each distance. The fog test was completed in an old section of the main haul road between number 3 and 4 accesses. The setup is located on the corresponding section of the mine map in the figure below. The location was chosen as one of the areas of the mine with the most fog on that day, though the fog was light. It was judged subjectively to have a thickness of 3 out of 10. It was disappointing that the fog was as thin as it was, but it was still sufficient to show the impact of airborne particulate matter on the results of the monitor.

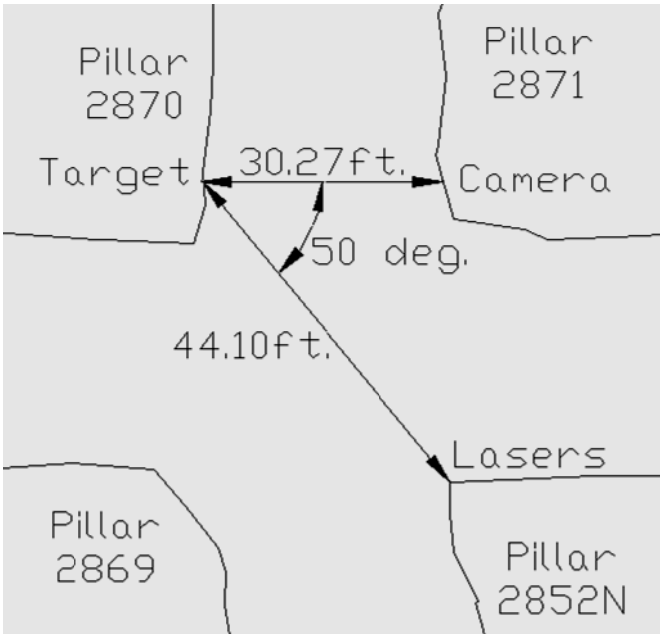

Figure 5.16: A section of the mine map from the test site in the Fletcher Mine. Testing was completed at an intersection between pillars [85].

For this test the camera was set to its highest resolution setting with an ISO of 250, shutter speed of $^{1}/_{100}$ of a second, and an aperture of F/5.6. The camera was operated by computer control. The laser was allowed to warm up for over an hour. While setting up the monitor, the aiming laser was used with the temporarily affixed mirror in order to ensure that the camera line-of-sight and the target were perpendicular.

One major difference between the mine tests and all other testing was the incidence laser. Previously a single incidence laser had been used, while for the underground evaluation three identical lasers were substituted for the single incidence laser. A new aluminum mount was built that held the three lasers in the form of an equilateral triangle and was fixed to the rotational stage.

Testing began once the monitor was set and calibrated correctly. The micrometer movement stage was set at a zero position and 50 images were taken of the incidence lasers. Upon completion, the movement stage was moved away from the camera 0.500 in. Another 50 images were captured with the computer. The purpose of this was to gather a large amount of sensitivity data (150 data points with the three lasers) at a single time in order to achieve more results.

Analysis of the data was completed according to Equation 9 in order to calculate the sensitivity of the monitor. Using the measured values from the monitor setup, the sensitivity (when converted to metric for consistency) was expected to be 0.157 mm. In actuality the experimental sensitivity of the monitor from this field test was 0.121 ± 0.002 mm. This gave a variation of approximately 0.036 mm from the ideal and expected value. This variation was caused by errors.

There were three major potential sources of the error. The first was laser thermal drift. Even though the lasers were allowed to warm up for over an hour as recommended, the data still showed signs of some thermal stabilization taking place (Figure 5.17). This might have been possible because the newly implemented laser mount had a larger mass of aluminum which could have required a longer time to stabilize the temperature of the lasers. It might also have been possible because the environment was not the laboratory environment, it was warmer. This is unlikely to have been much of an influence as the higher temperature would have helped the thermal stabilization to occur faster. Overall, the thermal drifting that was noticed would have given the monitor a higher calculated sensitivity, but since the calculated sensitivity was actually lower than the expected value, this error source could not have had much influence.

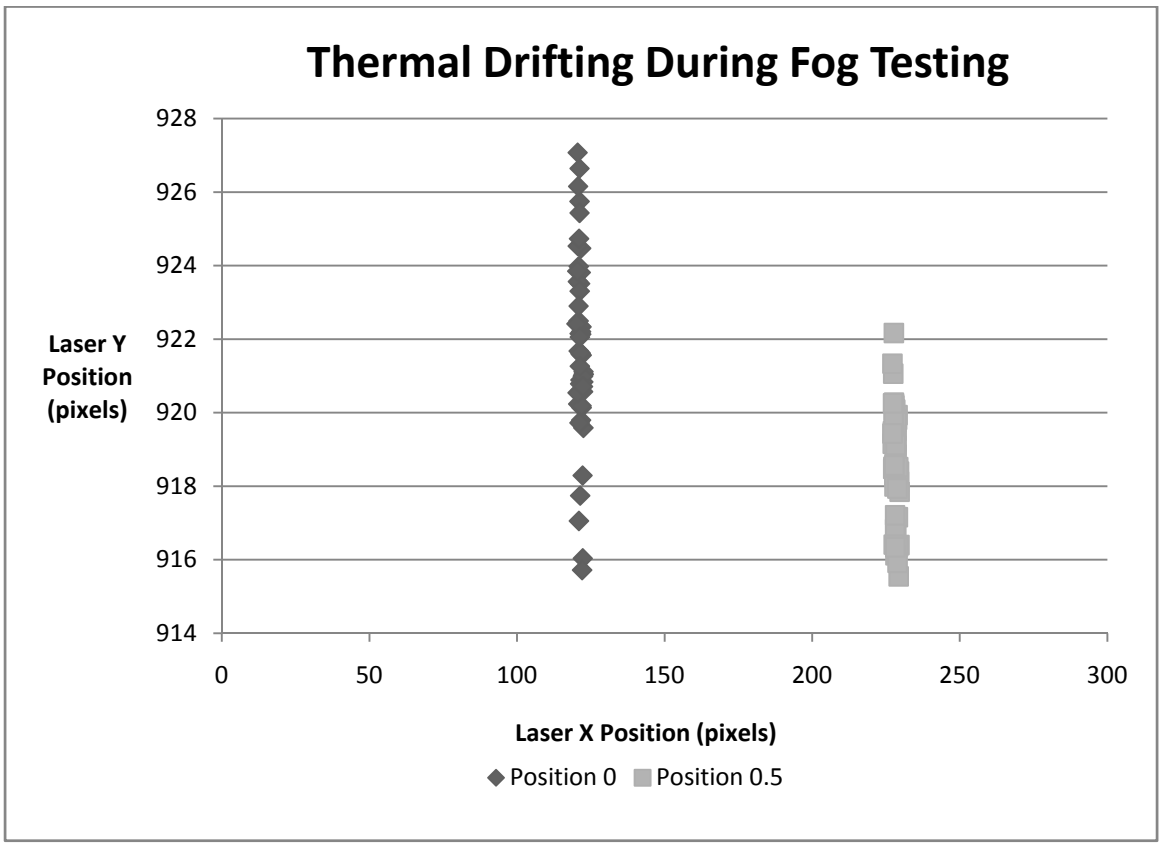

Figure 5.17: Thermal drifting is apparent from the reduction in data spread found in the 0.500 inch target location.

A second potential error source is a small misalignment that was found between the incidence laser beams between the mount and the target. Ideally, the three laser beams would have projected onto the target as an equilateral triangle identical to the triangle formed between the three lasers in the mount. It was noticed, however, that the actual projection formed an acute triangle on the target. This is definitely a source of error as it had the ability to minutely change the angle of incidence between the lasers. Fortunately, this error can be discounted as that minute change in angle can be calculated to create a sensitivity error of approximately 0.0001 mm.

The third error consideration was that the entire system was installed on a horizontal plane within a horizontal roadway with a horizontal air movement. This was considered to be the largest source of potential error. It has been previously stated that air movement can cause scintillation of the laser beam and certainly the suspended fog and dust particles have the capacity to alter the path of the projected laser light. Verification of this supposition was found by examining the correlation between the three incidence lasers in both the X and Y directions.

The graphs of the laser positions in each dimension were graphed against the image number. Both sets of images (before and after movement) were normalized and included on each graph. This provided correlation over the entire collected data set. The correlation of the three lasers in the vertical direction was found to be very good. With very few exceptions, the vertical positions of the three lasers were almost identical (Figure 5.18). However, the correlation of the three incidence lasers in the horizontal X direction was poor comparatively (Figure 5.19). This is a sign that the error imparted to the data is almost entirely taking place in the horizontal plane.

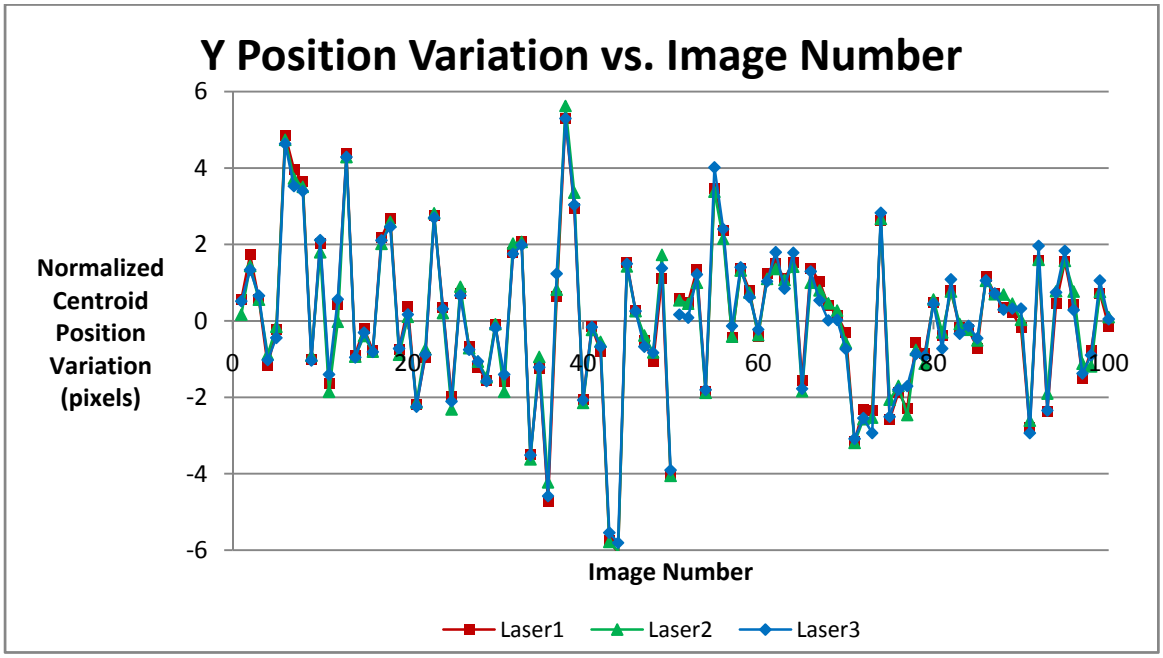

Figure 5.18: Variation of the laser centroid position in the vertical dimension.

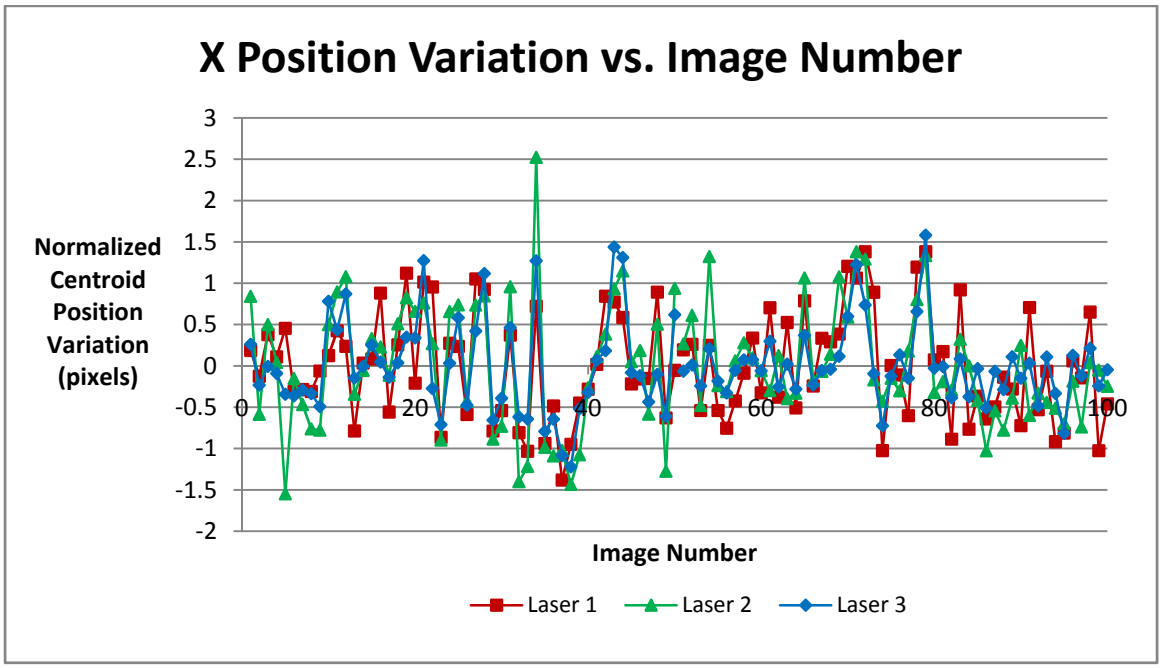

Figure 5.19: Variation of the laser centroid position in the horizontal dimension.

Given the amount of error found in the field test it was considered prudent to compare it not only to the idealized expected value, but also to a similar test completed under controlled environmental conditions. This comparison was completed as a method of examining how the monitor might have reacted in a very similar setup with identical camera settings, but without the influence of mine fog, particulate, or air flow.

The controlled test chosen for comparison was one part of the data collected during the incidence angle/ target distance evaluation completed as part of Section 4.6. In this example the camera settings were all identical, though the distances and incidence angle were both slightly different, but close enough for comparison. The details of the comparison are outlined in Table 5.14.

Table 5.14: Comparison between the field evaluation and a very similar evaluation completed under controlled environmental conditions.

	Target Distance	**Incidence Angle**	**Idealized Sensitivity**	**Experimental Sensitivity**
Controlled Conditions	10.36 m	45 degrees	0.210 mm	0.213 ±0.001 mm
Field Evaluation	9.226 m	50 degrees	0.157 mm	0.121 ±0.002 mm

After noticing the similarity between the two tests the most important observation from the comparison was the variation between the experimental and idealized values. For the controlled evaluation it could be seen that there was only a 0.003 ± 0.001 mm difference while there was a much larger 0.036 ± 0.002 mm difference in sensitivity for the field evaluation. This clearly indicates that since all other factors were nearly

identical, the deviation from the expected ideal values must be caused by the environmental conditions in this Fletcher Mine test.

5.6. VIBRATION

Vibration has been previously identified as a source of error in HRTMM measurements [6]. It was originally determined to be the cause of error during the use of the DiMAGE A2 camera. The error was imparted when the researcher pushed the shutter button on the camera in order to capture the images. In order to help eliminate this error the camera's time-delay function was utilized with a delay of 10 seconds in order to allow the vibrations time to subside. This was an acceptable method of eliminating vibration error though it would be unacceptable for most uses of the HRTMM where automation would be key.

Based on the results of that study, the current version of the HRTMM uses the Nikon D200 attached to a laptop computer which controls all the functions of the camera. Physical contact with the camera is necessary only to set up the experiment. This effectively eliminates human vibration error from the data collection.

Another potential internal vibration source is that of "mirror slap". In a DSLR camera a mirror is set into motion in order to capture an image. The impact of this mirror on the camera frame can cause vibration error. While the manufacturer claims that both the D200 and D300 are have "balanced" mirrors to eliminate this vibration, at extreme equivalent focal lengths (higher than about 500 mm) or short exposure speeds (less than about $^{1}/_{30}{}^{th}$ of a second) these vibrations can still be an issue, causing cloudy pictures and a general loss of clarity. Fortunately, with the HRTMM neither the focal length or the

shutter speed most frequently used places the monitor in danger of this type of error. However, vibration error is still a potential problem for the HRTMM as there are many other external sources of vibration.

There are two types of error caused by external vibration with the HRTMM. The first is similar to the vibration error initially caused by the researcher pushing the shutter button. This error is vibration energy from the external environment and could be caused by human contact, falling debris or air movement that directly pushes the components and removes them from their equilibrium position. The vibration continues until the restoring force and friction return the monitors to their equilibrium conditions. Any images captured during the time period before the monitor returns to equilibrium will have an error imparted to the results equal to the amplitude of the vibration at that moment if only one component is vibrating, and potentially could have error equal to the sum of the amplitudes of two components if both sensor and incidence laser were vibrating out of phase. This error could be referred to as active vibration as the monitor components are moving during data collection.

The second type of vibration error could be caused by an extremely powerful vibration such as that caused by blasting. If a vibration was powerful enough it could have the energy required to actually cause a monitor component to change position and lose alignment with the rest of the monitoring system. An analogy would be if a person pushed on one of the tripod heads enough that the force of the push overcame the frictional force of the tripod head resisting the push, causing the tripod head and thus the monitor component, to rotate a few degrees along some plane. This is actually a vibration error only in the sense that it would be a vibration that was the cause of the misalignment,

but it was considered none the less. This passive vibration error occurs even though all monitor components are stationary at the moment of data collection.

Active vibration error was primarily addressed through the addition of the computer automation. Short of installing a stabilization devise such as a gyroscope or vibration dampening pad, or using a camera and lens with an auto-stabilization feature, there is little that can be done to limit this vibration error. Fortunately, for large vibration sources such as blasting data collection could be programmed around the blasting schedule to eliminate the error from this generally predictable source.

The Fletcher Mine was used again as the site of an experiment that would test monitor's ability to function successfully with both types of vibration errors. The goal of the experiment was to set up the monitor in a heading adjacent to an active heading. Previous to a production blast, the monitor would be used to collect 50 images sequentially. A large production blast would then be initiated causing very high energy vibrations to impact the monitor components. Passive vibration error would be seen in a corresponding set of 50 images taken after the blast and would appear as movement of the laser centroids.

The post blast images would be taken during the mucking of the adjacent heading with a 4.2-4.6 m^3 Caterpillar front-end loader and multiple 36-45 tonne six-wheel-drive Volvo haul trucks working in the area (all components within approximately 50 feet of the machinery) [86, 87]. The target would not be manually moved between collection of either data set so that any change in the centroid positions of the lasers could be attributed to the blast vibration as passive vibration error. The precision of each data set could be compared in order to gain insight into whether external sources such as the machinery

could cause enough vibration to introduce unacceptable active vibration error into the readings.

It is not expected that large error could be introduced to the readings as a result of actual rock displacement caused by the blast. Firstly, the area was known to have relatively competent rock, which was the primary reason behind the selection of that particular heading for the monitor location. In addition, post blast inspection showed very little damage to the monitor heading. Both of these signify that the area had high-quality rock, less likely to show immediate deformation from the blast.

Secondly, the blast was in the end of a heading so the area immediately around the blast was well supported. This blast area remained surrounded on three sides even after the blast was completed.

Thirdly, the camera and incidence lasers were located on the opposite side of the monitor heading from the blast, placing them one pillar away from the pillar against which the blast was completed. The pillar immediately adjacent to the blast would have accepted most of the load increase from the removed rock.

Fourth, the time delay between the production blast and the collection of the second set of images was only 16 hours, which allows a short amount of time for displacement of the monitor components to accumulate.

Finally, the rock in the area is known to be quite stable, showing only a one or two thousandths of an inch of vertical convergence per month in isolated areas of the mine. A study concerning the convergence of 8 pillars during pillar extraction showed an average convergence of 0.246 in (6.25 mm) with a minimum of 0.006 in (0.152 mm) and a maximum of 0.955 in (24.2 mm) over the course of the fourteen-month study. On one

hand, these pillars were trapped in cemented rock fill, so the additional confining force would have decreased the overall vertical convergence shown by the pillars. On the other hand, this data is taken from a pillar extraction area which would be expected to show much greater convergence than an area with a single-heading production blast [88, 89].

The vibration test itself was completed using the Nikon D200 with the telephoto lens set to a focal length of 300 mm. The ISO was set to 250 and the shutter speed was $^{1}/_{100}$ of a second. The test was completed on the same day following the mine fog testing at the Fletcher Mine and the incidence lasers were not turned off, thus they warmed up for approximately four to five hours prior to their use with the collection of the first data set. The monitor set-up was as described above and according to Figure 5.20 below, which is a section of the actual mine map of the Fletcher Mine.

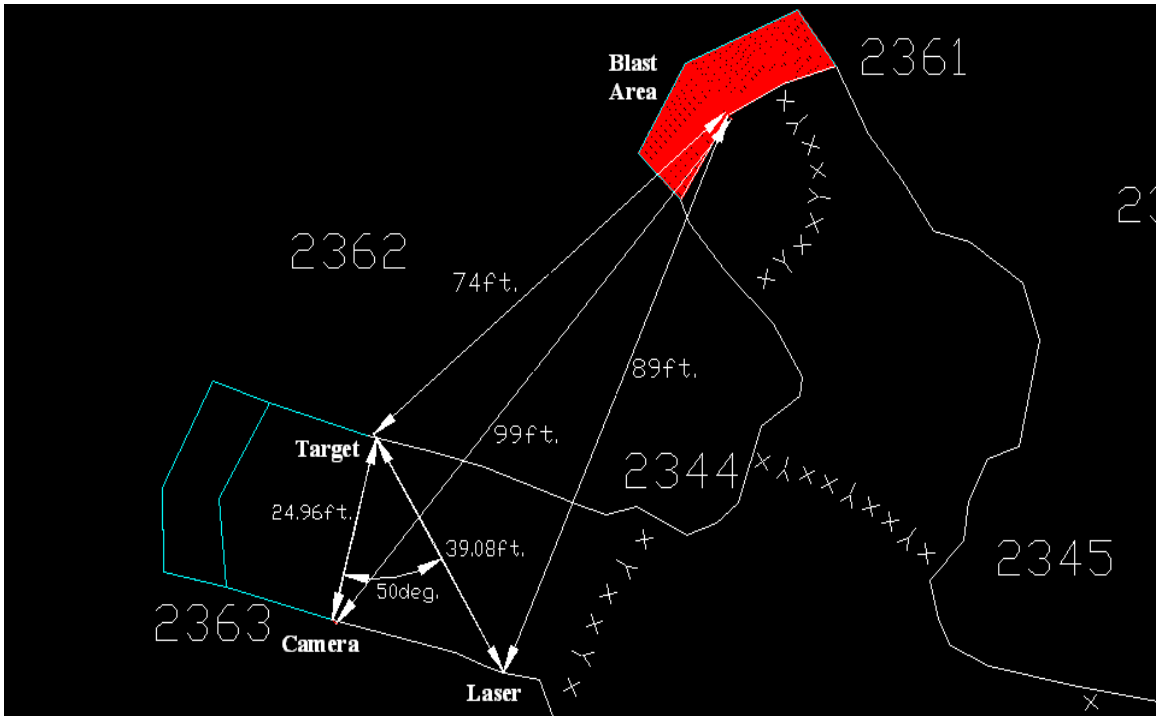

Figure 5.20: The Fletcher Mine Map with the locations and distances of the monitor components superimposed [85].

The blast contained approximately 159 kg (350 lb) of dynamite and 567 kg (1250 lb) of ANFO. Eight delays were used providing for 89.3 kg/delay (197 lb/delay). The blast was underground and highly confined on five sides, though a standard burn cut was used in the center to relieve some of this confinement [87]. This information, along with the distance between the center of the blast and the monitor components, was used to calculate the approximate scaled distance (SD) and peak particle velocity (PPV) found at each of the monitors. This was done in order to allow for future comparison of similar results and followed Equations 36 and 37 [90]. Equation 37 has units of inches per second.

$$SD = \frac{D}{\sqrt{W}}$$

36

$$PPV = 242(SD)^{-1.6}$$

37

The values were calculated for each of the variables and each of the monitor components. They are displayed in Table 5.15: Scaled distance and peak particle velocity values for comparison of future blast tests..

Table 5.15: Scaled distance and peak particle velocity values for comparison of future blast tests.

Component	Peak Particle Velocity (in/s | mm/s)	Scaled Distance
Target	16.9 | 429	5.28
Incidence Lasers	12.6 | 320	6.34
Camera	10.6 | 270	7.05

The two data sets collected were analyzed and compared. It was found that there was indeed significant movement of the centroid between the before and after datasets. The centroid movement was calculated and the direction of centroid movement was determined. The values are shown in Table 5.16, while Figure 5.21 illustrates the centroid movement.

Table 5.16: Centroid movement values due to blast vibration. Imparted error is equal to the false reading of sensitivity that the monitor returned due to the vibration error.

Component	Centroid Movement (pixels)	Centroid Movement Direction (degrees)	Imparted Error (mm)
Laser 1	10.65	62.0	1.382
Laser 2	13.15	48.7	1.706
Laser 3	13.58	90.4	1.762
Average	12.46	67.0	1.616

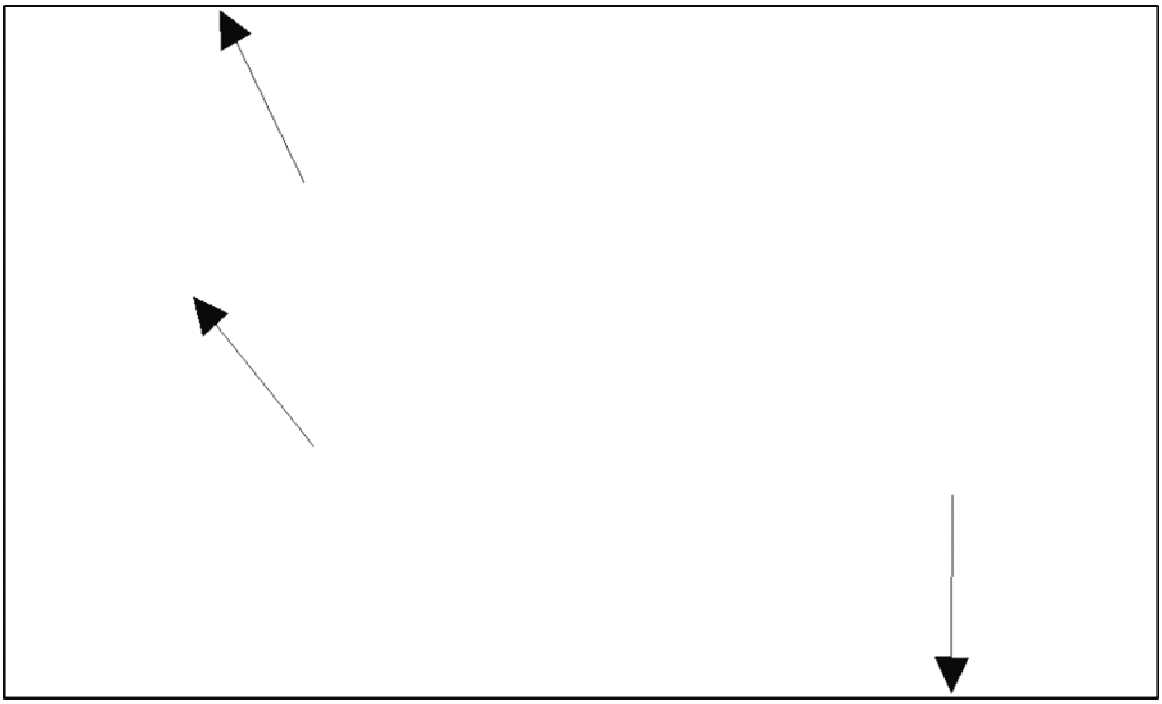

Figure 5.21: Direction and magnitude of the centroid movement for each incidence laser. Magnitudes are to scale, though the distance between the vectors is not.

The cause of the large change in centroid position was undoubtedly due to passive vibration error caused by the main blast vibration. Upon returning to the test site after the air had cleared it was found that the vibrations had been strong enough to shake the

battery pack from the incidence lasers loose and it was hanging from its wires. The two centroid vectors pointing upwards are due to the battery pack pulling on the rear end of the laser, moving the front end upwards. Upon inspecting the rear of the incidence lasers it was found that the wire from the laser that corresponded with the downward-pointing centroid vector had become looped around a part of the bracket that was located above the rear of said laser. When the battery pack fell, the loop over the bracket redirected the downwards pull of the battery packs into an upwards direction, thus moving the rear of the laser upwards and the tip of the laser downwards. Before and after photos of all three components showed no noticeable differences in the positions of any of the other components.

The standard deviations of the before and after datasets represent the random error of the experiment. This is an active vibration error. These were calculated for both the X and Y value of each laser in order to determine if there had been any significant increase in random error caused by the moving heavy machinery nearby. The resulting standard deviations are shown in Table 5.17

Table 5.17: The standard deviations of the data represent the random error - including that due to the vibrations caused by the heavy machinery.

	Laser 1 X	**Laser 1 Y**	**Laser 2 X**	**Laser 2 Y**	**Laser 3 X**	**Laser 3 Y**
Before σ	1.36	2.03	1.39	2.01	1.40	1.97
After σ	1.38	2.63	1.42	2.71	1.47	2.63

Each pair of before and after values were submitted to a two-tailed F-Test in order to determine if the null hypothesis that the standard deviations were equal could be rejected. For all 6 combinations the null hypothesis could not be rejected at the 99%

confidence level. While this doesn't prove that the random error in the before and after datasets was the same, it does considerably favor supporting that conclusion. This would mean that the presence of operating heavy machinery such as loaders and haul trucks within 50 feet of all of the monitor components would not be likely to harm data collected by the monitor.

It is interesting to note that even though the standard deviations are very likely statistically identical, in each case the afterwards dataset had higher values. This could mean that there was error from the machinery vibrations present and that amount of error imparted was too small to be significant, or that another error source had an influence. It is very possible that particulate in the air could have been higher in close proximity to the working machinery, or that dust from the blast had collected on the target or lens of the camera, though this was not noticed.

Given the proximity and strength of the blast the monitor performed rather well. Providing a better method of securing the battery pack for the incidence laser should remove the vast majority of the error from this test. The monitor performed well in response to substantial physical abuse and has shown no loss of functionality since then. Another positive result of the testing at the Fletcher Mine is that the camera and incidence lasers remained active for almost 18.5 hours without any sign of battery decline. The camera's power saving functions automatically put it into a sleep mode, preserving the power for the monitor.

In summary, given that the goal of the experiment was in testing the resilience of the monitor, the results were very positive. The result concerning the close acceptable proximity for working heavy machinery or other similar vibration sources is especially

promising. In order to make a determination concerning the amount of vibration that the monitor could withstand without producing passive vibration error, further research would be necessary.

5.7. PHYSICAL CALIBRATION

Simple installation and calibration of the monitor has already been described under Section 3.3. That section details the procedures for installing the monitor for use and ensuring that the target and the camera line-of-sight are perpendicular. There are two additional methods not previously covered that can be used to calibrate the monitor. These are described below.

The first method involves artificially moving the target towards the camera a known distance. This works under the assumption that the monitor is being utilized with a man-made target installed opposite the camera and is focused directly on an object such as a pillar, back, or slope.

In this method the installed target must have been previously drilled with four holes, one in each corner of the target. A duplicate of the target of known and even thickness has matching holes drilled in each of its corners. Once both targets are thoroughly cleaned to remove all dust and dirt from the surfaces the duplicate target is bolted to the primary target, bringing the monitored surface closer to the camera. A set of 10 or more images taken both before and after installation of the duplicate target will show the average change in position of the incident laser centroid due to the added thickness of the duplicate target. Once the duplicate target has been removed this

movement can be compared to expected movements derived through empirical means in order to better interpret recorded target movements.

This first calibration method allows for calibration due to all measurement variables. It is similar to the method used in laboratory testing, except a duplicate target is being used instead of a micrometer movement stage. The method is limited in its precision to the precision with which the thickness of the duplicate target can be measured. If a high precision micrometer cannot be located, the duplicate target can be made with metal specially ordered to be a known thickness from a metal supplier. With this method all corners, edges, and drill holes on each target must be filed down to eliminate burrs that may prevent the primary and secondary target from pressing perfectly adjacent to one another.

The second calibration method only calibrates for variables relating directly to the camera, the target, and the distance between the two. It is based on the previously reviewed journal article concerning a vision-based approach for monitoring displacements in vibrating systems (Section 2.4).

In the second calibration method two light sources located a precisely known distance apart are placed on or shown onto the target. In the reviewed article two LED lights were placed on the target 10 cm apart. In this method the HRTMM would be able to determine the distance in pixels between the two light sources which would provide the calibration. Once this pixel distance is known it can be used as a calibration factor.

While the method of using two LED lights on the target worked well for monitoring displacements in vibrating systems, it requires that a person must approach the target in order to install the LED lights. If the target is previously installed this may

be unacceptable and time consuming considering the required accuracy of the measurement and installation (this precision would directly affect the precision of the monitor). A method that would still allow for remote use of the monitor would be to install two identical pen lasers in the same fashion as with the targeting laser on the sensor platform. These two lasers could be aligned to have a known offset at any range if they were acceptably parallel. They would project the two light spots onto any target allowing for this calibration method to work without any need to approach the target. They could be turned on and off as needed, or left on indefinitely.

In the second calibration method it must be understood that while variables with respect to the camera, camera sensor, lens, target, and target distance can be calibrated for, variables relating to the incident laser cannot. Also, environmental variables that would cause the incident laser to change propagation direction would also influence the propagation of the two calibration lasers, potentially harming the results. Care should be taken to eliminate as much error due to air velocity, thermal gradients, humidity and particulate matter as possible.

6. ERROR CHARACTERIZATION AND SENSITIVITY ANALYSIS

6.1. SUMMARY OF ERROR

Two types of error are considered in this matter. The first is the difference between the experimental sensitivity value and the modeled ideal sensitivity value. This value represents the accuracy of the monitor and its ability to correctly determine the magnitude of target movement. Expressed as the monitor accuracy, this value is the primary indication of the quality of the monitor results.

The second error is the variation of results caused by random interferences in the data collection. This represents the precision or repeatability of the monitor. Expressed as a plus or minus variable this communicates the degree of certainty about the monitor's results. The precision is given as a plus or minus interval about the accuracy term and is equal to one standard deviation of the data.

A great deal of experimentation during this project has led to results showing the changes in monitor accuracy due to each of the experimental variables and a number of nuisance variables as well. Each variable imparts a different amount of error and the error imparted by each variable is dependent upon the magnitude of that variable. For this reason it is impossible to make a single outright statement concerning the sensitivity, accuracy and precision of the HRTMM. It is therefore more useful to characterize the contributions of each variable to the overall monitor error and provide the means for determining the expected error in a given situation.

6.1.1. Accuracy. It has been shown that monitor sensitivity is modeled by Equation 15 and that it is governed by the interactions of the five fundamental variables. Each variable also contributes to the total accuracy and precision of the monitor.

The accuracy of the monitor is determined by comparing the calculated, expected values to the measured experimental values. As accuracy is dependent upon the systematic errors made during measurement and can be improved if the source of the errors can be determined. This is not always possible as the systematic trend may not be apparent or even understood.

The accuracy is dependent upon the interaction of all five fundamental variables as well as outside interferences acting simultaneously. As such, determination of accuracy was not subdivided into component contributions. The ideal model determined the expected sensitivity of the monitor with all components included, so the experimental value did the same. From these two values the overall monitor accuracy was determined.

Overall determination of the monitor accuracy was completed by calculating the accuracy of each test completed with the monitor and finding the mean of these values. This method allows the influence of a very wide range of monitoring situations and all the internal and external to be expressed within the accuracy value. Results show that the HRTMM has an average accuracy of 7.1×10^{-5} mm with a 95% confidence interval equal to 0.042 mm.

6.1.2. Precision. The five parameters included in the ideal sensitivity model are independent of one another and thus, so are their errors. An overestimation of the target distance provides no basis for an assumption that the incidence angle or any other parameter must also be too large. Each variable contributes to the overall error of the monitor and it is possible that the error of one variable could compensate for the error of another.

Determination of the overall precision of the monitor is accomplished through examination of the propagation of errors. The general form of the equation for determining total error is shown in Equation 38.

$$E_z = \sqrt{\left(\frac{\partial f}{\partial a}E_a\right)^2 + \left(\frac{\partial f}{\partial b}E_b\right)^2 + \left(\frac{\partial f}{\partial c}E_c\right)^2 + \cdots + \left(\frac{\partial f}{\partial n}E_n\right)}$$

38

Where E_z is the total error of formula $f=f(a,b,c\ldots n)$, and E_n is the error of the individual components of function f. In the case of the ideal sensitivity equation, simplification of this function is possible since all mathematical operations within the equation are products or quotients. The actual equation for dealing with the HRTMM is shown below.

$$E_s = |s|\sqrt{\left(\frac{\sigma_w}{w}\right)^2 + \left(\frac{\sigma_{t_d}}{t_d}\right)^2 + \left(\frac{\sigma_{p_w}}{p_w}\right)^2 + \left(\frac{\sigma_f}{f}\right)^2 + \left(\frac{\sigma_\theta}{\theta}\right)^2}$$

39

This equation shows the precision (E_s) of the HRTMM. It depends upon the calculated sensitivity of the monitor, s, the known or measured values for the variables w, t_d, p_w, f and θ, and the calculated uncertainties in the form of standard deviations, δw, δt_d, δp_w, δf, and $\delta\theta$. The standard deviations of the model parameters have been determined experimentally during the course of this research with the exception of δw, which is

considered to have relatively low impact as it is not a variable that is controllable by the monitor user. It is also extremely unlikely that it would change during the course of the monitor's lifetime.

It is not considered necessary to develop an equation to model the precision component of each parameter as graphical estimation methods will suffice. Figures Figure 6.1-Figure 6.5 showing the variation of the precision due to change in each of the four considered fundamental variables are found below.

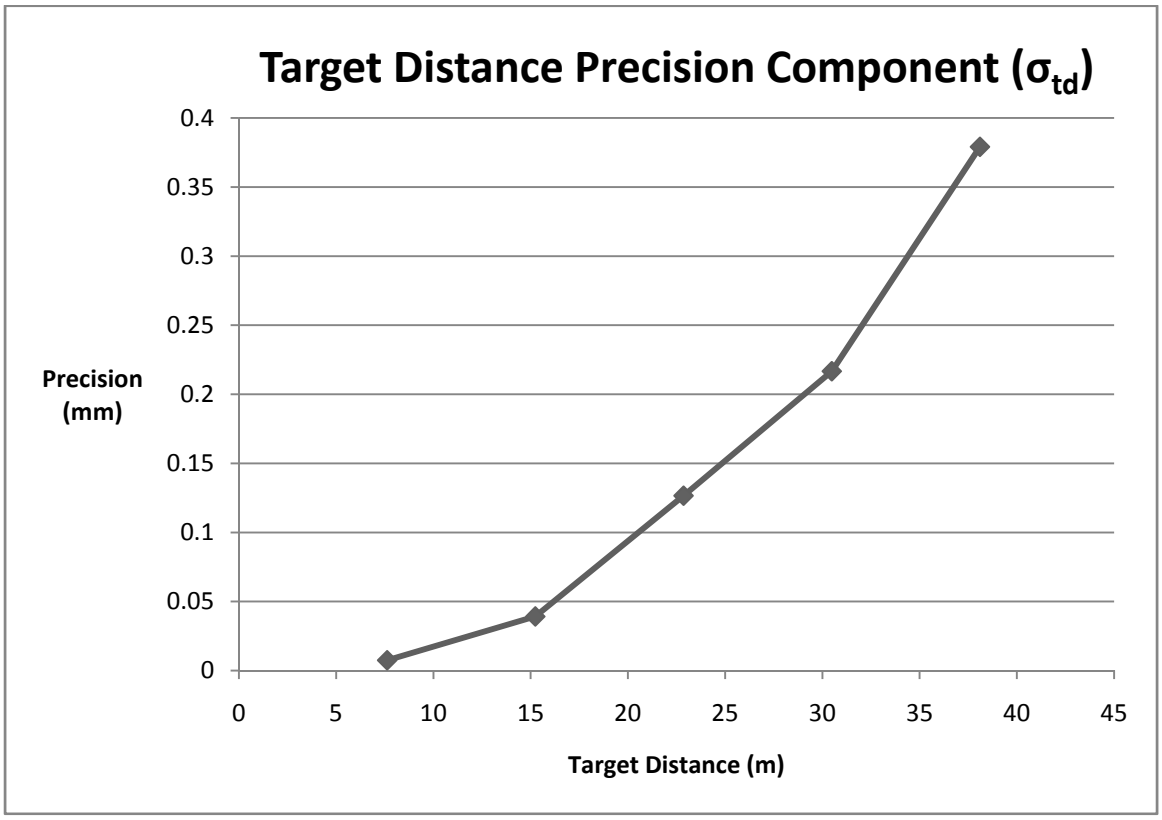

Figure 6.1: Precision component of the variable target distance.

The distance between the camera and the target had the largest component of imprecision. This is not unexpected as increasing the distance provides increasing opportunity for environmental effects to influence the results of the monitor. The extent of this influence is unlimited and will continue to increase as long as the distance continues to increase. This relationship is well known and applies to all optically based monitors that rely upon transmission through the atmosphere.

The changes in precision of the monitor due to changes of incidence angle also match logical arguments. It can be seen from Figure 6.2 that the precision decreases quickly as the magnitude of the incidence angle diminishes. The incidence angle is directly responsible for the rate at which the laser spot moves across the target. As this rate increases a larger centroid movement is calculated for an identical target movement. The movement continues to increase until the incidence angle reaches 90 degrees where the rate becomes infinite. In the other direction the rate of movement will eventually reach zero when the incidence angle equals zero.

The ratio of the target movement to the centroid movement (also known as the experimental monitor sensitivity) becomes smaller as the incidence angles increase. This ratio incorporates two measurement components, a real component caused by the actual movement of the target and an error component caused by random error. The smaller ratios exhibit less random error because the magnitude of their real component is so large in comparison to the error component. This can be best understood with the realization that if the incidence angle were equal to zero then there would be a real component of zero and a random component greater than zero. In effect all that would remain would be the random error regardless of how far the target moved.

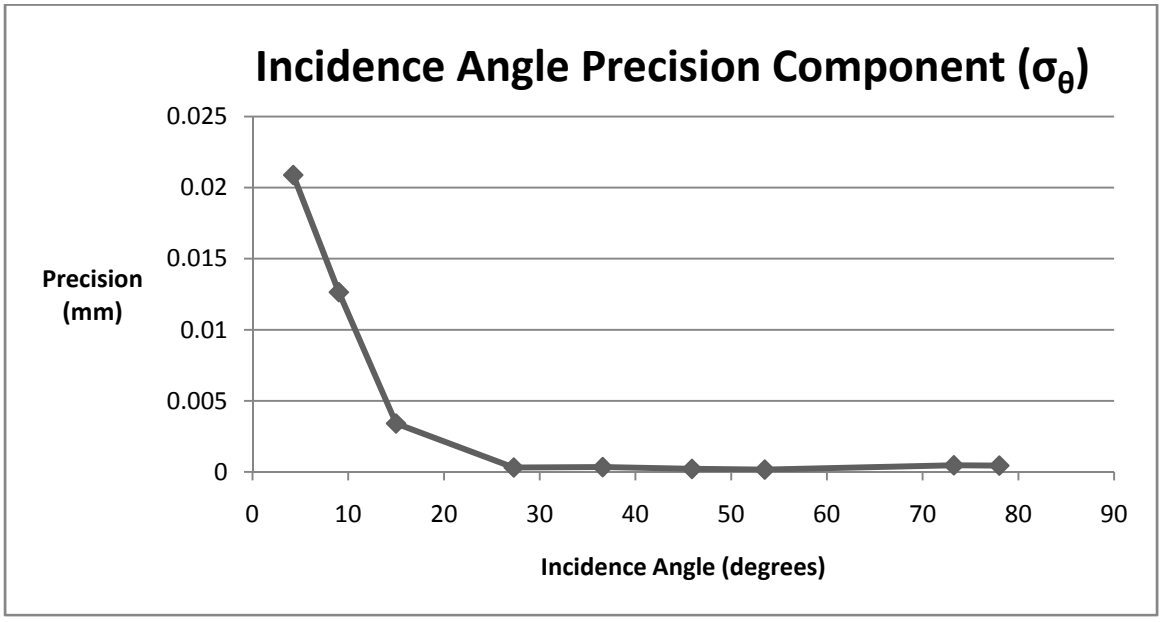

Figure 6.2: Precision determined as a function of laser incidence angle.

In a similar manner to that described for the incidence angle, the focal length of the lens also contains two components, an error component and a real component. In this case the experimental sensitivity is altered by the field-of-view of the lens. It has been described previously that as the focal length increases the field-of-view decreases which in turn decreases the far-field width of a single pixel. This relationship causes an identical target movement to cause a laser spot centroid change that is larger for larger focal lengths. This increases the sensitivity. In the case of focal length, the analogy that best demonstrates the limits of this relationship is that if the focal length could increase indefinitely the sensitivity of the monitor would continue to increase to infinity. Continuously decreasing the focal length to an extreme value would eventually cause the image projected onto the imaging sensor to be small enough to only fill one pixel. At this point monitoring would be impossible as the laser spot centroid could not move to an

adjacent pixel regardless of the magnitude of the target movement. This analogy is invalid in real life as there are limits on how far the focal length can be decreased and still allow the image to be focused enough to complete measurements, but it demonstrates the principle.

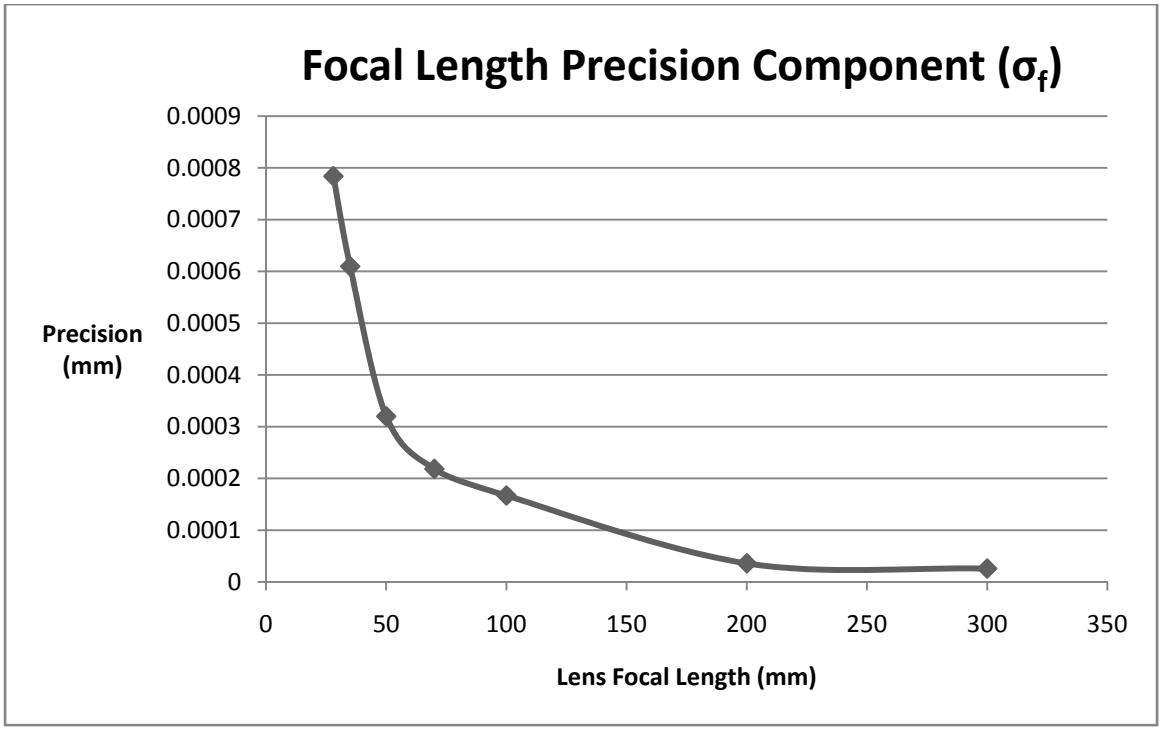

Figure 6.3: The precision due to the magnitude of the focal length variable.

The first three precision components were variables dependent upon the physical set-up of the monitor. The last two are parameters of camera design. The pixel-width of the image is determined by the physical construction of the imaging chip and the image projection of the lens, but the limits of the image are set by the software running on the

camera. This is a value that may be altered through changing the settings on the camera or by using a different camera, but there is actually very little control on the part of the user. Due to this rigidity the function of the camera is identical for all practical intents and purposes no matter what the image pixel-width may be. This claim is based on understanding of the image collection process and data collected with the Nikon D200. Based on this research it is uncertain if there would be differences found between sensitivity values produced with the Nikon D40x, Nikon D60, Nikon D80, and Nikon D200, all of which utilize the same imaging chip in their design.

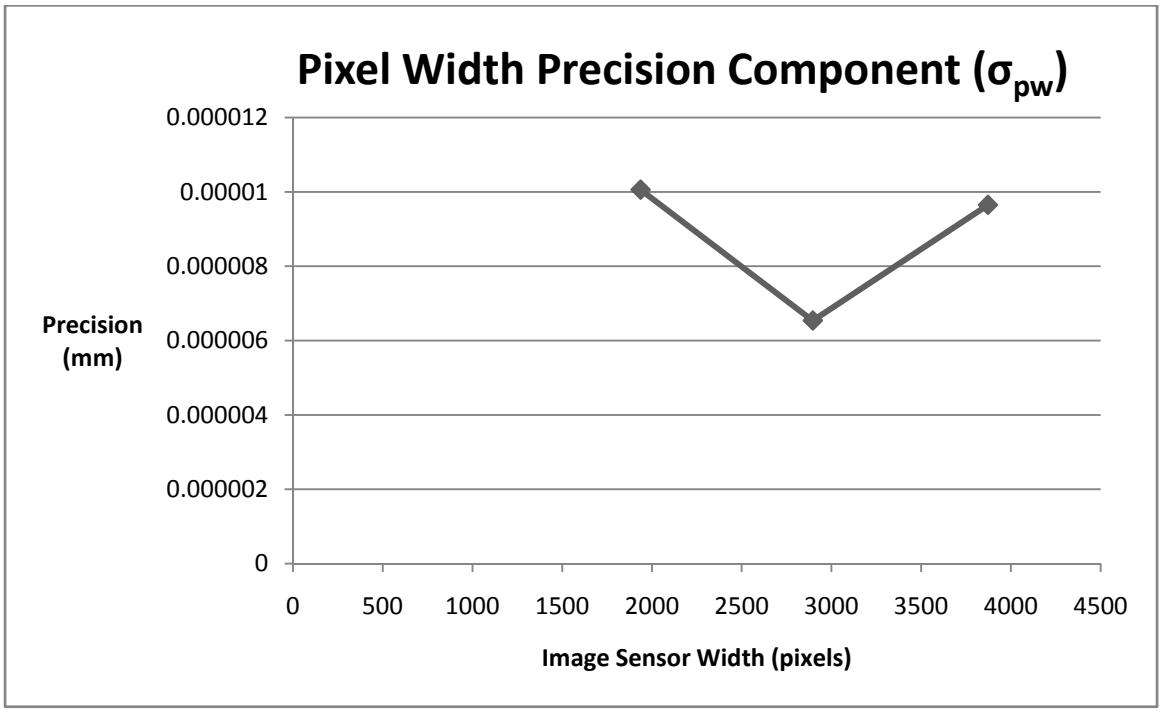

Figure 6.4: Random error due to change in pixel-width.

Based on the sensitivity testing completed, the error component of the monitor with respect to image pixel-width is extremely small. Only three image pixel-width values were available with the D200 so determining a trend is difficult. Based on the results it seems that the error component due to change in pixel-width is so small (all lower than $1x10^{-5}$) that it contributes almost zero error to the overall error of the monitor and could be disregarded. It is expected that the error contribution of the width of a single pixel could also be disregarded for the identical reasons presented in the preceding paragraph, though this has not been experimentally verified.

While the overall precision cannot be exactly stated, some generalizations can be made. It has been determined that the precision components for the image pixel-width and the real width of a pixel are so small they are relatively insignificant. This is especially true when compared to the magnitude of the remaining three components. The lens focal-length precision component is variable but there is little reason to use a lens and setting other than the telephoto lens set to 300 mm focal length. The graph of the incidence angle precision clearly shows that precision worsens as the incidence angle decreases, but that above an angle of approximately 27 degrees the average precision has been determined to be 3.23×10^{-4} mm with a standard deviation of 1.21×10^{-4} mm. Assuming that the incidence angle will remain above this value so as to produce a better sensitivity, this can be used as a general-value incidence-angle error component. The only remaining random error component is that due to distance. This component is the largest by far and increases indefinitely, though it follows a close trend. The trend is best viewed in Figure 4.7. This shows that the error component of the target distance is equal to approximately 0.0077 mm per meter of target distance.

6.2. SENSITIVITY ANALYSIS

Sensitivity analysis is a method of determining how "sensitive" the ideal model is to change in one or more of its variables. Determined graphically, the sensitivity of a model is found by determining the overall change in the output of the model due to a small change in one of the parameters. This can easily be accomplished with a spreadsheet or graphing calculator.

Sensitivity analysis helps to build confidence in a model by helping to understand the uncertainties associated with the parameters in a model. With the HRTMM, it is most useful for determining the accuracy level necessary for measurements of laser incidence angle, target distance and focal length for the model to be sufficiently useful. The results from the sensitivity analysis help to identify the maximum possible sensitivity for the monitor and help to identify which parameters will most easily increase the sensitivity of the monitor for a given condition.

Sensitivity analysis can also be completed mathematically through the use of partial derivatives. When the partial derivative of the model is taken with respect to a particular parameter and all other parameters are held constant the returned value is equivalent to the monitor sensitivity change produced given an increase in the parameter equal to one. The partial derivatives for the five parameters of the ideal model equation (Equation 15) are outlined below.

The first partial derivative defines the sensitivity of the model due to an increase in the width of the camera imaging sensor expressed in millimeters. A change in width of 1 mm is a very large change so the equation has been adjusted to show sensitivity due to

change in width of 0.1 mm (Equation 40). Sensitivity over an entire range of potential image chip widths is shown in Figure 6.5.

$$\frac{\partial s}{\partial w} = \frac{t_d}{10 f p_w \tan\theta} \quad (40)$$

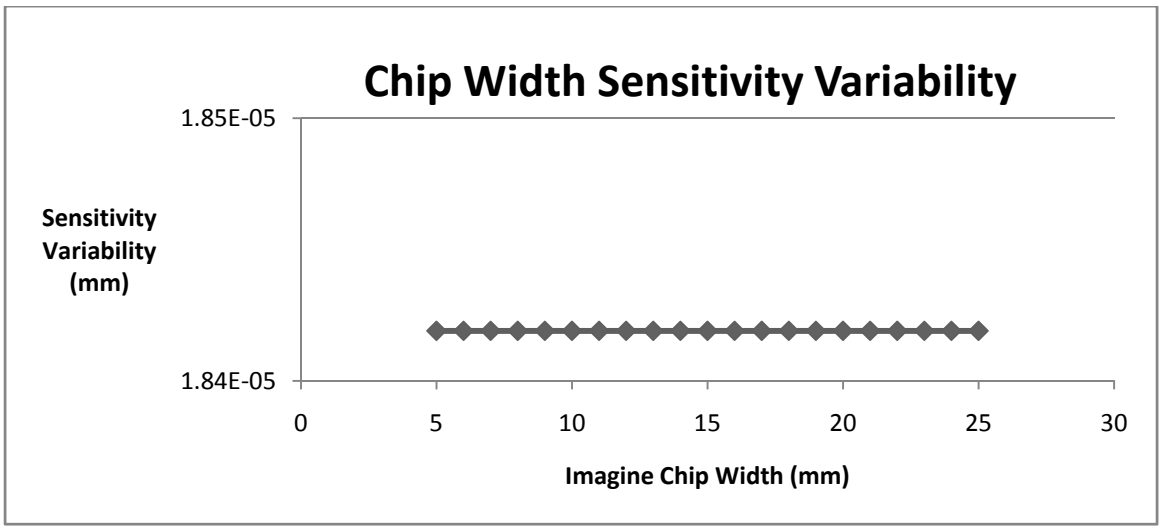

Figure 6.5: The sensitivity of the monitor varies depending on the width of the imaging chip. This graph shows the increase in monitor sensitivity due to a decrease of chip width of 0.1 mm.

The second partial derivative outlines the sensitivity of the model due to an increase in the target distance of 1 mm (Equation 41). The results of this analysis are especially important as they help to define the accuracy that is necessary when measuring the distance between the target and sensor. It has been found that a measurement

inaccuracy of only 1 mm will produce a sensitivity error of 0.000019 mm. This is insignificant and shows that a target distance measurement inaccuracy of 10 cm would produce a sensitivity error of only 0.0019 mm. This may be acceptable but given available measurement technology there is no reason to accept a target distance measurement with less than 1.0 cm accuracy. Figure 6.6 shows the monitor sensitivity variability due to a change in target distance equal to 1 mm.

$$\frac{\partial s}{\partial t_d} = \frac{w}{f p_w \tan\theta}$$

41

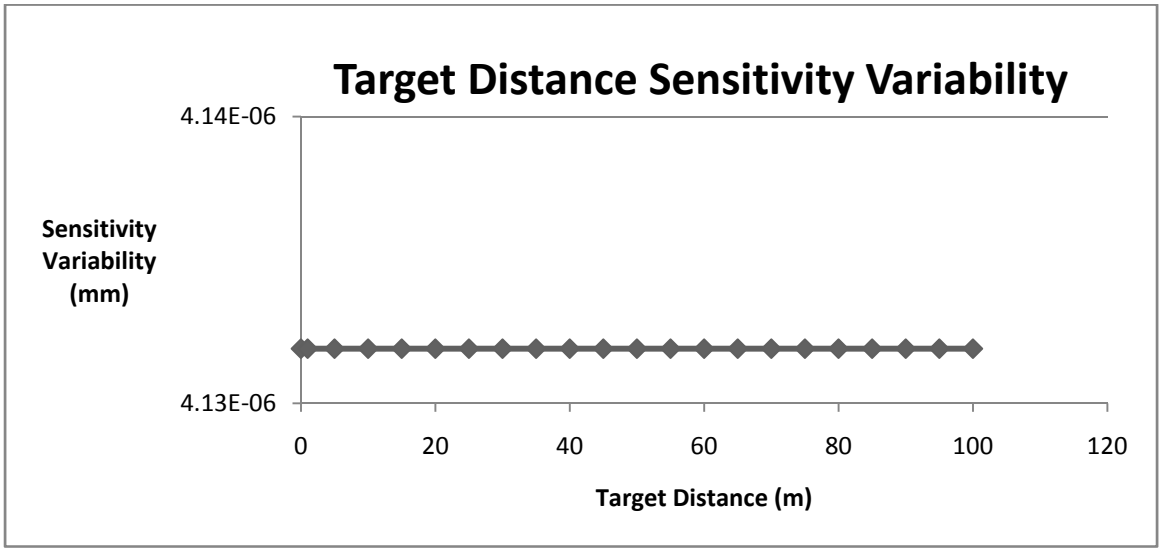

Figure 6.6: This shows the change in monitor sensitivity that can be expected if the target distance increases by 1 mm at the plotted target distance.

Sensitivity analysis for the remaining parameters shows a different pattern than with the first two. In Equation 42 the partial derivative determining the sensitivity of the model to changes of 1 mm of focal length is shown. Sensitivity over an entire range of likely focal length values is shown if Figure 6.7. It can be seen that this variable suffers from the law of diminishing returns.

$$\frac{\partial s}{\partial f} = -\frac{wt_d}{f^2 p_w \tan\theta} \tag{42}$$

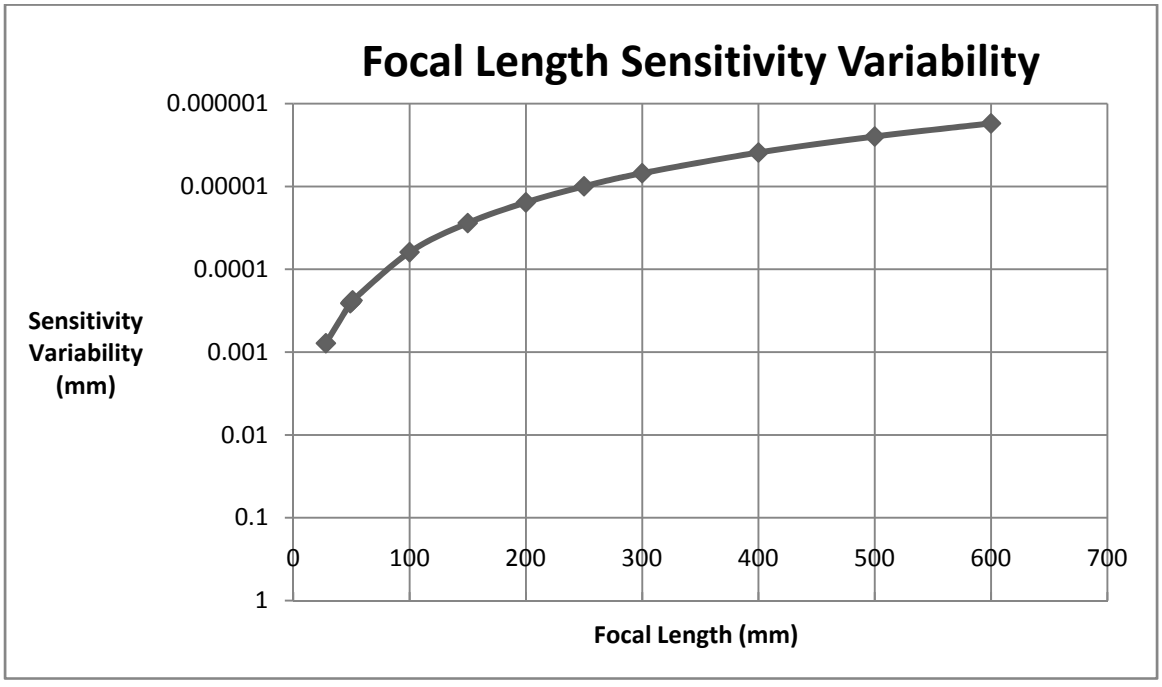

Figure 6.7: Sensitivity changes according to a nonlinear pattern and is shown here on a semi-logarithmic plot.

The second to last partial derivative determines the sensitivity of the ideal model to changes in the width of the image expressed in pixels (Equation 43). As before, a chart is included that shows the expected change in monitor sensitivity due to a change in width of one pixel over a range of potential pixel-width values (Figure 6.8). This variable also suffers from the law of diminishing returns.

$$\frac{\partial s}{\partial p_w} = -\frac{wt_d}{fp_w^2 \tan\theta} \qquad 43$$

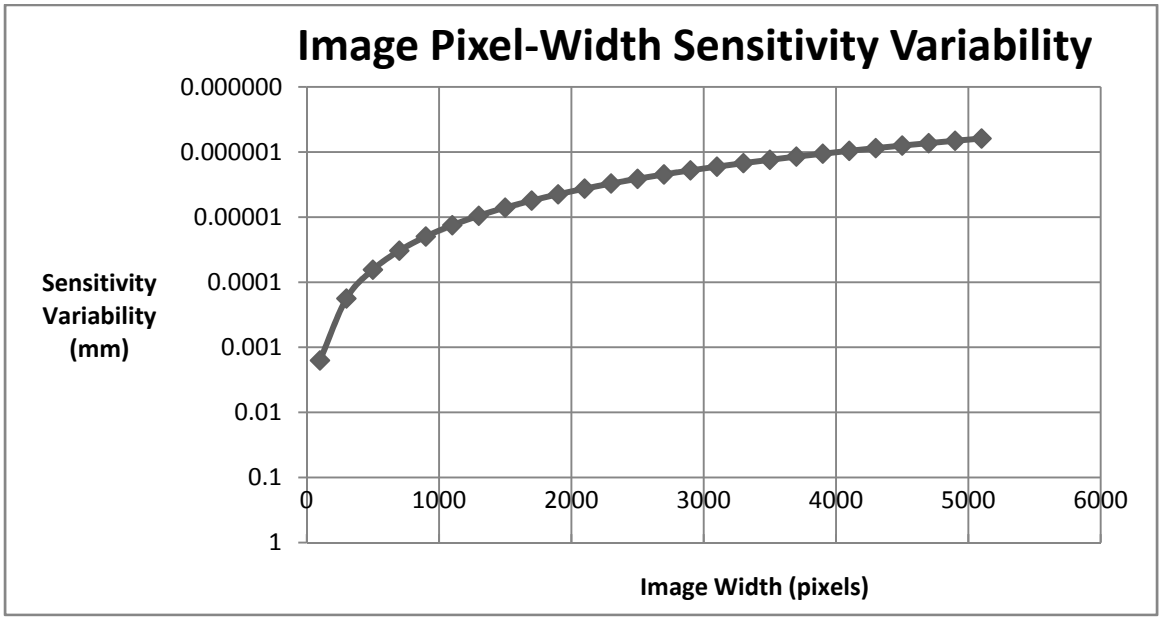

Figure 6.8: An increase in image pixel-width will create a sensitivity change according to this graph.

The final partial derivative expresses the model sensitivity to changes of incidence angle of one degree (Equation 44). Judging from Figure 6.9 showing the sensitivity depending on the incidence angle, this parameter seems to be the most likely to bring error to the model. This brings about the understanding that incidence angle measurement is the parameter requiring the most accurate measurement of all five parameters. For this reason it is recommended that the incidence angle be determined by trigonometric calculation whenever possible as this will provide a much more precise and accurate incidence angle determination. As with each of the other variables found in the denominator of the ideal sensitivity model the law of diminishing returns applies here as well.

$$\frac{\partial s}{\partial \theta} = -\frac{wt_d}{fp_w \sec^2 \theta}$$

44

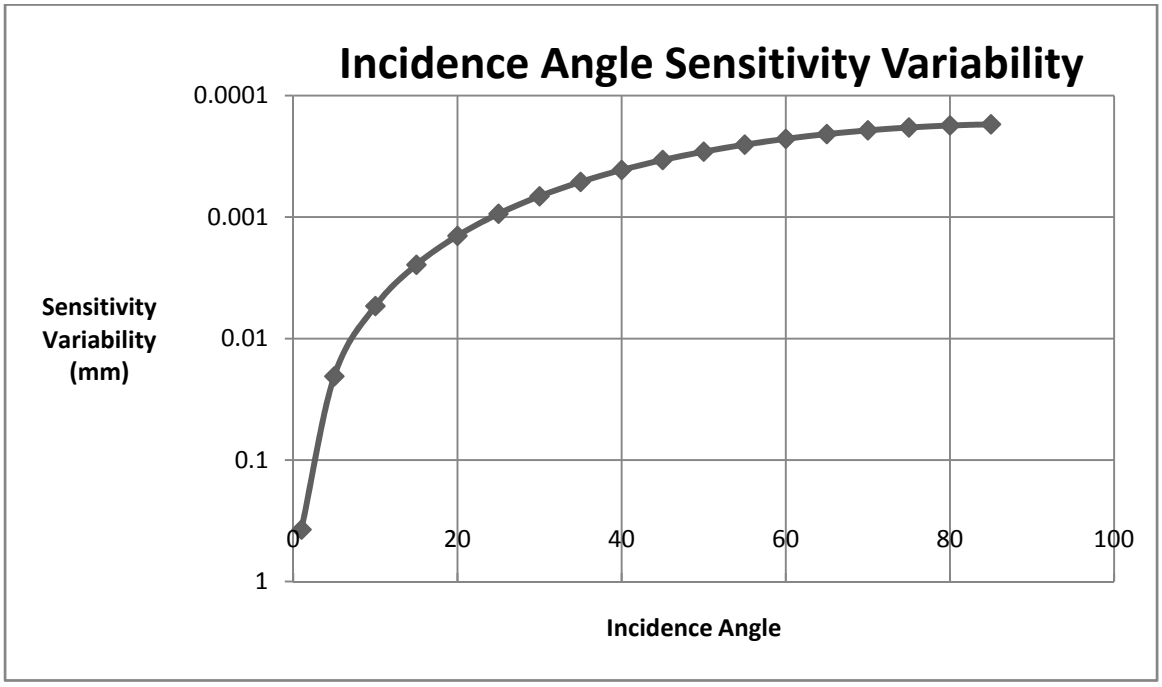

Figure 6.9: A change of incidence angle equal to one produces a greater change in monitor sensitivity than with any other parameter.

7. RESULTS AND DISCUSSIONS

7.1. MONITOR SENSITIVITY

The sensitivity of the HRTMM is highly dependent upon the physical set-up of the monitor and can be modeled according to Equation 15. The results given by the monitor are accurate relative to the ideal model to within 0.042 mm 95 percent of the time. The precision of the monitor is highly variable but can be calculated based on Equation 39. An estimate of the precision of the monitor can be determined based on the assumptions made at the conclusion of Section 6.1.2.

Due to the large magnitude of the target distance error relative to all other errors this value should be included separately. A more fitting statement of monitor sensitivity would be that it is sensitive according to Equation 15 with an accuracy of 0.042 mm ±0.008 mm/m of target distance (0.0016 in ±0.000091in/ft).

7.2. OPPORTUNITIES FOR AUTOMATION

In its current form the HRTMM is not an automatic ground movement monitor though it has potential to be so. An automatic ground monitoring system must incorporate four features in order to be truly automatic: data collection, analysis, reporting, and the ability to alert if further attention may be necessary. Perhaps the best example of this sort of automatic monitoring system for ground movement monitoring is the automated slope monitoring system. Other excellent examples can be found in some of the mine atmospheric monitoring systems used for tracking methane and other gas levels in coal mines.

7.2.1. Software Automation. The HRTMM currently has the ability to perform some functions automatically. The Nikon Capture version 4.4 used in conjunction with the monitor is responsible for the largest share of the current automatic capabilities. This program provides the monitor with the ability to capture images at preset time intervals and in preset quantities. The program also allows images to be automatically downloaded to a computer and stored in a specified location with a very flexible file naming system, eliminating the need to change or download camera memory cards. One feature that is missing that would be very beneficial for the HRTMM would be the ability to take a specified number of images at periodic times (i.e. the camera takes 30 images spaced 5 seconds apart and repeats this action every 2 hours). Currently the program can perform either function, but not both.

Improvements are also necessary to the HRTMM software itself as extensive testing has shown that the current HRTMM software requires much too much manual operation. In its current form the only automatic action that the software provides is the ability to automatically locate laser spots and calculate the centroids of these spots. While this is necessary, the entire process should be automated. In its current form each image is individually and manually loaded into the program through command line operation, the processing parameters of the program are set, and the centroids of each laser spot are located. The centroid data remains on the command line and must be manually copied into a spreadsheet for analysis. This data output should be automated as well to create a spreadsheet or database that stores all data gathered from the images.

It is necessary that the program be capable of automatically running the centroid locating procedure with any number of images instead of one at a time. It would be best if

it could locate the centroids immediately whenever a new image was captured by the camera, but at the very least it would be necessary for the HRTMM software to process every image in a specified location.

The software should be able to automatically determine the ideal threshold to use for data processing. This is a feature that would need to be enabled the first time the monitor was used in a given location and then disabled in order to force the program into using the same threshold parameters thereafter. This is because changing thresholds does change the centroid of the laser spot. It is possible that this sort of automation could be accomplished with the quality ratio mentioned in Section 5.3.3.

Currently the HRTMM does not have an alert capability if a predetermined ground movement threshold is reached. In order to achieve this system upgrade, the automation recommendations listed above must first be completed. The system would then need to incorporate a simple procedure for comparing the movement between measurements. As the system is a relative movement monitoring system it is incapable of determining movement from only one data point. Two points are required and three or more data points are necessary in order to determine any sort of movement trend. The alert notification could be based on the magnitude of movement between two data points or could be based on the rate of movement. The later of the two would be more likely useful.

7.2.2. Targeting Automation. Robotic total stations have the ability to measure many different target points with a single instrument. The greatest benefit of this is the reduced number of monitoring instruments that are necessary. If the same capability

could be developed for HRTMM it would be very beneficial. This is an extremely difficult task though, considering the off-the-shelf limitations of the project.

One potential off-the-shelf option for robotically aiming the monitor at a target is with a consumer-grade telescope and this method of target acquisition was tested with the HRTMM. A Meade EXT-70 AT telescope was utilized. This scope includes a servo controlled base that moves the telescope to focus on stars and other celestial objects. The base also has the ability to be programmed in order to allow for terrestrial viewing. For the trial the telescope was used as the lens while the Philips ToUCam Pro II webcam was fitted into the aperture of the telescope and used to record data. Considering the extreme distance and small size of celestial objects and the long focal length of a telescope it was thought that this servo controlled base might be sufficiently accurate to allow the HRTMM to be automatically focused on various targets.

The goal of this trial was to examine the ability of the servo-controlled base to make the same motions repetitively. Given the extremely high sensitivity of the HRTMM method the servo motions needed to be extremely precise to prevent introducing error. If the telescope did not return to the same position accurate to within just a fraction of a pixel to a few pixels (depending on the distance to the target) the change in telescope position would eliminate the servo-controlled scope as a potential automatic sensor.

It was necessary to calibrate the servo motors with terrestrial objects in order to "train" them to successfully repeat the same motions. This was accomplished by erecting the telescope outside and using the strobe light on top of two radio towers, each over 5 miles away, as targets. The distance, small size, and focal length of the telescope provided the best potential calibration for the servo motors.

Following the calibration procedure the telescope was brought into the laboratory and erected on its servo-controlled base. The incidence laser on the target was the focus of the telescope. The distance to the target was approximately 2.00 meters. The short target distance was used because failure of the servo motors to properly locate and aim the telescope at the short distance would ensure failure at a longer distance. The target was held stationary so that any change in laser spot centroid would be due to the movement of the servo motors.

Data collection followed a pattern where one image was captured, a command was given to move the telescope to an alternate target and then return to the original (laser spot) target where another image was captured. This process was repeated ten times. Unfortunately it was found that the laser spot centroid was never located in the same position twice and had centroid displacements between five and 17 pixels. At a target distance of 2.00 m and an incidence angle of 45 degrees this symbolizes a movement error of between 0.2 and 0.7 mm. This is unacceptable for an automatically aimed ground movement monitor.

From the results of this simple experiment it was determined that an inexpensive, off-the-shelf system for controlling the movements of the sensor would not provide acceptable data quality. While servo motors are available that could reach the desired positional precision, their cost is prohibitive. Unless this hurdle is overcome, the HRTMM will remain a monitor only capable of measuring one point at a time.

However, the HRTMM program was initially designed to allow it to determine the centroids of any number of laser spots within an image as long as the spots did not overlap and the computing power was available to handle the processing. Given this

attribute it is still possible to monitor more than one location at once with a single sensor. This claim is made with the understanding that all laser spots must be held within the field of view of the sensor throughout the monitoring process, and that the highest sensitivity of the monitor is found when the sensor is utilizing the highest possible focal length. If it were determined that sensitivity could be sacrificed, the focal length could be reduced in order to increase the field of view and the number of incidence lasers could be increased.

The fact remains that the sensor must remain stationary. Error from sensor movement (i.e. if the camera battery needed to be changed) could be eliminated if at least two light sources such as bright red light emitting diodes were affixed to the target. These light sources could be used as points for registering the images before and after sensor movement. They would act very similarly to a calibration frame used with a tape extensometer by providing points of reference within the image.

7.3. UNDERGROUND USE AND PERMISSIBILITY

The HRTMM was primarily designed as an underground movement monitor. Its precision is at its maximum in that environment where ambient light is typically at a minimum. It has been shown that whether the Nikon D200 is configured to automatically determine exposure or is manually set, it has the ability to successfully track the movement of a laser spot across a digital image even in the presence of ambient light or intense light such as headlights or cap lamps.

The sensitivity of the HRTMM is partially dependent on the distance between the camera sensor and the target. In the underground environment these distances are

typically limited by the span and height of the excavation. Measurements in excess of 100 m are considered unlikely. As a potential replacement for the tape extensometer these distances are unnecessary as even the longest tape extensometers rarely extend beyond 35 m.

The current version of the HRTMM utilizes a water resistant camera and unprotected lasers. This has been sufficient for laboratory and field evaluation purposes. It is possible that the components would be perfectly suitable in some mines and monitoring situations and very likely that they would be quickly destroyed in others. For this reason, unless the potential installation area for the monitor is expected to be safe it would be prudent to include a waterproof housing for the camera and lasers. The additional protection would also help protect the monitor components from dust and humidity.

One option for waterproof housings would be the underwater housings specially designed to offer waterproof operation of the camera and lens. Prices for these housings can be as low as $1,500, though with a 300-mm telephoto lens prices around $4,000 would be more likely. Construction of a housing is not out of the question and could be considered an inexpensive option to the alternative expensive purchase. One additional advantage to installing a waterproof housing would be dust protection. While the clear UV filter has been used during testing as a dust protector a more robust method of dust protection would be prudent. Dust is prevalent underground, especially in underground coal mines so periodic cleaning would definitely be necessary.

The dark underground reduces the requirements on the incidence laser as the contrast between the background and the laser spot is much higher. Low power lasers

also require less energy, are less likely to cause damage from an accidental gaze, and given the diameter of the laser beam, ignition of coal dust or an explosive atmosphere by the laser beam is extremely unlikely. These factors help to make the HRTMM a practical choice for underground use.

Unfortunately, the HRTMM is not permissible in the form recommended in this project. This does not, however, totally preclude the use of the technology in the segment of the industry most in need of assistance in reducing rock fall injuries. Given larger capital expenditures it would be possible to substitute the components of the monitor with permissible components. The (currently) ideal substitution for the incidence laser would be the L202 Single Beam Laser manufactured by Hilti. This laser costs approximately $700 compared to the $50-$200 for the non-permissible version.

Permissible cameras are also available though these would be used with a severe loss of monitor sensitivity. Most of them come in the form of industrial surveillance cameras. At short distances such as those that might be found in low-coal applications the small target distance would compensate for some of the loss of focal length and camera resolution. Unfortunately these surveillance-style cameras also have smaller imaging which that will decrease the sensitivity of the monitor further. Increasing the laser incidence angle is an obvious method of increasing monitor sensitivity to combat these losses. The smaller imaging chip will also change the field-of-view of the camera which will influence the maximum number of laser spots potentially seen in a single image and the total range of movement through which the monitor is capable of measuring a single spot.

Underground use has one potential major shortfall. The HRTMM is a relative movement monitor. It relies upon the convergence of two points in order to sense a change. This fact itself is not a problem as the camera and target can freely move closer and further apart. However, unless the incidence laser is fixed directly to the camera platform there is potential that the incidence lasers could move separately from the other two installed monitor components. This could potentially be a serious problem in a highly active mine with overall movement. In more stable mines this may not be as much of a concern and the problem may be limited if the monitor is installed in a stable area in order to monitor an unstable area.

Unfortunately, there is currently no method of determining if the incidence lasers are remaining in a fixed position without measuring the distance between the lasers, the camera, and the target with a secondary technology such as a tape extensometer. This may seem to defeat one of the purposes of installing the HRTMM to begin with, however this is untrue. These calibration measurements would only be necessary periodically in order to determine movement of the incidence lasers. If movement is discovered or suspected, then additional action may be taken.

One potential but untested method of ensuring alignment would be to install an adjustable mirror on the camera platform that could be adjusted to point its normal directly at the incidence laser. A secondary laser could be installed on the top of the incidence laser. Once the incidence laser was aimed at its target the secondary laser could be aligned so that the mirror on the camera returned the laser beam of the secondary laser back to its source. This would be a visible method of determining if relative movement had occurred between the camera and the incidence laser.

In an active mine it would be very possible that all three components would move relative to one another so much that the incidence laser would be required to be fixed directly to the target. This would guarantee that the incidence laser and the camera remained in fixed relative positions simplifying the data capture process. The lasers would still need to be held away from the camera some distance in order to provide an acceptable incidence angle. The larger the incidence angle the more sensitive the monitor would be. However, the longer the metal arms supporting the lasers the more vibration-induced error there would be.

7.4. SURFACE USE

Use of the HRTMM on the surface follows the same principles and guidelines as when used underground with a few exceptions. Most notably, it is likely that the monitor would not be subject to the problem of incurring relative movement between all three components. Ground movement monitoring completed on the surface generally has the components located away from the active area being monitored far enough so that a stable platform can be erected. Construction of monuments such as those used in permanent surveying positions would help to stabilize the monitor beyond anything that could be accomplished underground.

Another major difference would be the introduction of full sunlight to the target. The monitor has not yet been tested under this level of ambient lighting and while it is likely that the monitor would work, higher error would be probable. The error would come in the form of reflections from surfaces having the full intensity of the sun. This type of reflection would appear almost identically to the monitor as the incidence laser

would. The other error would be caused by reduction in the contrast between the background and the laser spot. This would cause the image of the spot to be reduced in size which would make it more sensitive to small movements. The precision of the monitor would decline. Lower contrast could be combated with installation of a more powerful incidence laser though this does come with safety concerns that would need to be attended to.

Surface ground monitoring would most likely take place at a greater target distance than underground. For high precision work, longer focal length lenses could always be substituted for the 300 mm telephoto lens used in this research. Alternately, the greater field-of-view provides the potential of utilizing more than one incidence laser per monitor. The open areas and clean lines of sight would also simplify location of the incidence laser making large incidence angles easier to achieve.

It would be recommended that a housing of some sort be constructed around the camera and incidence laser. This could be something as simple as a small sealed box with a clear front side. Dust contamination on the surface could still be a problem and periodic cleaning of the camera lenses or the clear side of the housing may still be necessary. Experience would best determine this for each situation.

7.5. NON MINING-SPECIFIC USE

The HRTMM has been developed with ground movement monitoring in mining as the intended use. The technology though, is rather robust and has many potential uses outside of the mining industry. Certainly it has potential for monitoring purposes other than ground convergence as well.

7.5.1. Tunnel Monitoring. The most closely related non-mining activity is tunneling. Tunneling engineers routinely utilize tape and borehole extensometers and total stations for monitoring the stability of the tunnel during the construction phase. The environment during tunneling is very similar to that found in an underground mine and all of the recommendations presented here would apply fully in the case of tunneling. Following completion of the tunnel the environment typically becomes more conducive to monitoring with the HRTMM as dust levels decrease and moisture is controlled. Air velocity within a tunnel is generally steady, but moving vehicles cause turbulence. It is uncertain if this would simply add error to the data or if it would actually remove error by continuously mixing the air to prevent thermal gradients from forming.

The remote nature of the HRTMM is an advantage for monitoring within a tunnel. Tunnels are constructed for the purpose of transporting people or other material down the length of the tunnel. This is just as true during construction as upon completion. The HRTMM could be utilized as a convergence monitor within a tunnel without interrupting the flow of the tunnel at any time.

A tunnel is also quite confined compared to many underground mining spaces and so would have shorter target distances, increasing the sensitivity of the monitor. Access is generally good for installation of the target (if necessary), camera and incidence laser.

7.5.2. Civil Projects. Civil engineers are often tasked with monitoring the stability of large public works. This typically falls under the purview of the Army Corps of Engineers or private contractors. Constructions such as dams, levees, bridges and some road embankments are monitored on a continual basis. Surveying targets are permanently

installed on reservoir dams and bridges and procedures call for routine monitoring of displacement across the structures. Here there is potential for the HRTMM.

Dams are especially well monitored. Displacement is monitored at the toe, heel, foundation, crest and face of large dams. Movement can signal instability and require action to be taken.

Typically inclinometers are also used as a method of monitoring a dam. These instruments measure the tilt of the structure. The HRTMM could be utilized to sense tilt if two or more light sources were permanently fixed to the dam. These would most likely be standard light bulbs. If viewed from a distance the HRTMM could track the position of the lights and calculations could reveal if tilt was occurring by comparing the vertical position of the lights, assuming they were installed along a level line. The incidence laser would not be necessary.

A similar technique could be utilized to monitor crack width. If the camera platform were positioned opposite a forming crack, then a LED light could be permanently fixed to each side of the crack. The telephoto lens could be used to narrow the field-of-view to its minimum and images could be periodically taken of the two lights. If the centroids of the lights were found to be moving apart, then this would correspond directly to a widening crack.

In both cases where lights would be permanently fixed to the target to track movement the incidence laser would not be necessary. In these cases, the principles governing the sensitivity of the monitor would be slightly different. Sensitivity would still vary according to target distance, sensor width, pixel-width, and focal length, but not according to incidence angle. The best method of determining sensitivity and calibrating

the system at the same time would be installation of two LED lights on each side of the crack for a total of four lights. If the four lights were installed as a square with a given distance separating each light the distance between the vertical sides of the square (in pixels) could be used to determine the far-field pixel-width. The far-field pixel-width could then be used to calculate movement between the two horizontal sets of lights (assuming a vertically oriented crack).

8. CONCLUSIONS

8.1. LITERATURE REVIEW

An extensive literature review was conducted in order to explore all of the many components of this research project. As the principles of the research are so far ranging and varied, the existing literature was relied upon greatly for determining the proper method of conducting the research with regards to the most applicable field of study.

The HRTMM uses strain rate as a key indicator that would warn of impending failure of a rock mass. This topic was reviewed in the literature in order to examine the fundamentals behind the strain-rate theory and apply the same concepts to this monitor.

The literature was also used as justification for undertaking this research. It was discovered that while ground movement monitoring is widely used for structural stability analysis purposes, the technology is not universally used in all mines. While some mines use multiple methods of monitoring, some mines only use one or none.

Additional justification came in the form of the fatality figures provided by the Mine Safety and Health Administration. It was shown that fatalities from rock mass movement in the form of falls and slides is higher than it has been in five years. Danger of being killed or injured by falling ground was especially high in the underground coal sector of the mining industry within the United States.

The literature search was also used to great effect for gathering information concerning other monitoring technologies currently available. This was necessary in order to determine where improvements needed to be made and what others had already accomplished.

8.2. MONITOR CONSTRUCTION

One of the goals of the project was to construct the monitor for lowest cost using off-the-shelf components. This was accomplished along with a little metalworking. The monitor was constructed in three main parts, one for the sensor, one for the incidence lasers, and a fabricated target, each of which could be installed in an underground or surface mine using brackets that attach to rock bolts or anchors. Other installation methods were discussed though not actually attempted.

The sensor unit consisted of a Nikon D200 camera with a 300-mm telephoto lens. This was mounted on an aluminum platform that was attached to a high-quality camera tripod head. Aluminum was used in an attempt to use a light-weight material that would not rust in a wet environment. The tripod head attached directly to the wall bracket. The unit included a laser for aiming the monitor and for determining that the camera was perpendicular to the face of the target.

The target was constructed out of a ¼ inch sheet of stainless steel. Stainless steel was used in order to help make the target more rigid and the heavier mass would help to stabilize the target given the presence of vibrations. This was attached using a right-angle bracket to a micrometer movement stage for calibration and testing purposes. The stage was attached to a high-quality tripod head attached to the wall bracket.

The incidence lasers(s) were housed in aluminum holders that attached directly to a rotational movement stage. This was used for aiming and occasionally measuring the incidence laser angle. The movement stage attached directly to a bracket in the rock.

8.3. FUNDAMENTAL VARIABLES

The fundamental variables are those that can be refined to improve the sensitivity of the monitor. It is no surprise that they are also the only variables included directly in the ideal sensitivity model. This model includes five variables and can be used to predict the sensitivity of the monitor, which can be compared to a measurement to back-calculate the expected target movement. The fundamental variables are the width of a single pixel in the imaging chip of the sensor, w, distance between the target and the sensor, t_d, the focal length of the sensor, f, the cross sectional pixel-width of the imaging chip, p_w, and the angle of incidence of the incidence laser relative to the target normal, θ. All variables are measured in millimeters with the exception of the pixel-width, which is a count of the number of pixels across the imaging chip along a cross sectional line that corresponds with the direction of movement of the laser spot centroid. The ideal equation is found in Equation 15.

Each of the fundamental variables was evaluated to determine its influence on the sensitivity of the monitor and the contribution that it made to the overall precision of the monitor. A sensitivity analysis was completed on the fundamental variables and it was determined that of the fundamental variables easily set by the user, the incidence angle was found to be the most sensitive variable, though it and the other variables in the denominator of the ideal model suffer from the law of diminishing returns. At some point the returns achieved from increasing the incidence angle will be less than those gained by decreasing one of the other variables instead.

As the incidence angle and target distance are the two variables most influential on the monitor sensitivity, much experimentation was conducted focusing on them. A

number of comprehensive tests were completed, the results of which were used to form a model based solely on the experimental data. It was found that this model very closely approximated the ideal model and served as a good verification that the formation of the ideal model was correct.

8.4. NUISANCE VARIABLES

A large number of nuisance variables exist for the purposes of determining the sensitivity of the monitor. Within this research nuisance variables are considered and recommendations are made on how to best limit their influence on the monitor's performance. Nuisance variables include such things as ambient light levels, particulate matter or water vapor in the air, vibrations, temperature, humidity, barometric pressure, air movement, target texture, target reflectivity, and laser thermal drift.

Two different classes of nuisance variables can be developed with respect to the HRTMM. The first class contains variables that can be minimized to the point of insignificance through the use of updated monitoring procedures. Ambient lighting is included in this class, as installation of proper optical filters removed a vast majority of erroneous readings from the monitor data output. This also allows the user to make use of a camera's automatic exposure feature instead of necessitating manual feature setting.

Target texture can be included in the first class as well. Installation of a flat target certainly removes the error imparted from a rough rock surface. For applications where target installation is not possible, it is recommended that rock surfaces be relatively flat and perpendicular to the camera (use the mirror reflection method with the sensor aiming laser to ensure perpendicularity). Flatness should correspond with a JRC value of 0-2.

This should be done in combination with an incident laser with a diameter large enough to limit error. It has been shown that increasing the diameter of the incidence laser reduces the amount of erroneous centroid movement, though the diameter of typical lasers would not be large enough for a JRC of greater than 2.

Also in the first class, target reflectivity has been shown to have an impact on the results of the HRTMM. A color study was completed that showed that lighter colors and surfaces with a higher reflectivity are preferable for optimum monitor performance. It was also shown through literature review that a wet target, which would appear darker, would reduce the reflectivity and the light returned to the monitor. Wetness will not have as great an impact on a light-colored target, though, as it will on a dark-colored target. If a light, constant-colored target cannot be found at the monitoring site, installation of a target can be used as a substitute. Light coats of white spray paint applied without leaving drips will also help to reduce error due to poor reflectivity.

Laser thermal drift is the final variable found in the first class. Thermal drifting is a change in the aim of the incidence laser over time as it heats up or cools down due to operation or environmental effects. This error can be eliminated by allowing the laser to warm up sufficiently before monitoring begins. A 90-minute warm-up period was found to be sufficient for the lasers used within this study. This value would most likely be acceptable for similar low-power lasers.

The second class of nuisance variables includes humidity and particulate matter or water vapor in the air. These variables are present at all times to some extent. Their influence on monitor performance comes in the form of random error that degrades the

precision of the monitor. They cannot be realistically removed from the monitoring environment and compensation is extremely difficult.

Temperature is similar to the first three variables described in the preceding paragraph in that compensation is nearly impossible. However, for temperature some influence can be limited based on the care taken in installing the monitor. Error due to temperature comes in the form of an alteration of the path of light between the incidence laser, target and sensor. This refraction is caused by a change in the refractive index as the light moves through air of different temperatures. This often happens along extended measurements made near to rock or tunnel walls or warm objects such as machinery.

Air velocity is the final variable found in this class. Air velocity is caused as air travels from an area of high pressure to low pressure. In effect, a location with moving air is located at some point along a barometric pressure gradient. This gradient, whether naturally or artificially created through the use of fans, has the ability to alter the refractive index of air which in turn alters the propagation direction of the monitor's laser and reflected signal. In addition, air movement has been known to cause a scintillation effect in optical measuring devices. These errors can be limited by installing the monitor to take measurements in a direction perpendicular to the normal air movement direction. This has the effect of limiting the influence of the gradient as the propagating light takes the most direct route across the airflow. The errors introduced into the measurements due to air velocity could be great enough that all measurements should be taken under the same air velocity conditions if possible.

8.5. OTHER CONCLUSIONS

During the course of the research, attention was given to the potential automation of the monitor. It was decided that automation could occur in two ways, software automation that would streamline the monitoring process and reduce the manual steps in data processing, and targeting automation that would eliminate the manual aiming and aligning of the sensor as well as allow for movement from one target to another. The current monitoring capabilities of the monitor give it an advantage over most other ground movement monitors that would serve the identical purpose as the HRTMM. The HRTMM is capable of being automatically set to record data at any given time intervals from one hour to six hours or any other time period desired between data collections. This would greatly decrease the personnel hours required for data collection as compared to a tape extensometer.

Though testing showed that using off-the-shelf components to deal with automation in an inexpensive manner was unfeasible, there is room for a lot of improvement in the capabilities of the HRTMM software. Data output should be streamlined so that all results automatically go to a spreadsheet instead of being manually entered from the command line. Image processing should at least be automated so that a single command will process a whole group of images automatically, though the best solution would be to automatically process an image whenever it is downloaded from the computer. Image thresholding should be automated and a method of determining the quality of the resulting thresholded image and laser spot centroid data should be integrated. Also, the program could use updating so that the user interaction was through

a graphic user interface instead of through the command line. This would simplify use, speed training, and create a more attractive monitoring program.

The overall accuracy for the monitor was determined be 0.042 mm ±0.008 mm/m. The precision is dependent upon a combination of the error components from each fundamental variable. This increases the difficulty of reporting the precision of the monitor as the fundamental variables have varying precisions depending upon their magnitude. While a single precision value cannot be determined for the monitor an equation was presented that would enable simple determination of the precision in a given circumstance.

While each variable has a precision that changes depending upon its magnitude, some basic assumptions can be made that simplify the matter. Both the pixel-width and image-width are determined by the manufacturer of the sensor. While each does have some variation in its precision, the values are so low and similar that they can be considered insignificant and ignored for the purposes of determining composite precision. The laser incidence angle was found to have greatly varying precision, but above about 27 degrees the precision remains approximately the same and can be estimated to be 0.000323 mm. The precision of the focal length is also highly variable but there is little reason to ever use a focal length lower than 300 mm. In this case the focal length precision component could just be considered to be equal to the 300-mm value.

Discussion showed how the monitor can be employed in both surface and underground mines. Attention was also given to the use of the monitor in fields outside the mining sector. Civil engineers would have great use for the monitor, especially in bridge and dam monitoring uses. Tunneling engineers would also be interested in what

the monitor has to offer for tunnel convergence measurements. Finally, thought was given to the potential for using the monitor as a crack width monitor instead of as a relative convergence meter. This would be easily attainable and would require less equipment and less expensive equipment. It is likely though, that it would still be more expensive than a normal crack meter.

8.6. FINAL RECOMMENDATIONS

The HRTMM has potential for use in underground and surface mines as a convergence meter for ground control monitoring. The HRTMM also has potential to function with a wide variety of components. Table 8.1 lists the recommended parameters for the HRTMM during optimum normal usage. These parameters should be considered when selecting components for the monitor.

Table 8.1: Recommended parameters for optimal use of the HRTMM.

Parameter	Recommendation
Target Distance	Dependent upon sensitivity requirement, generally below 50 m
Laser Incidence Angle	$30 \leq \theta \geq 80$
Pixel-Width	As high as possible
Image Sensor-Width	As high as possible
Lens Focal Length	$f \geq 300$ mm
Incidence Laser Output Power	5 mW
Target	Fabricated or flat surface

In addition, the recommended method for collecting data for strain-rate analysis would be to have the computer automatically capture at least 10 or more images spaced between two and five seconds apart (when using .jpg files and the setup described within

this document) and to repeat this capture periodically at a time interval deemed appropriate for the monitoring condition.

8.7. EVALUATION OF PROJECT OBJECTIVES

Table 8.2: Evaluation of project objectives. Achieved = goal was attained, Partially Achieved = goal was attained under some circumstances, Unachieved = goal was unachieved.

Goal	Achieved	Partially Achieved	Unachieved
Monitor sensitivity ≤ 0.1 mm		**X**	
Monitor cost ≤ $1500	**X**		
Monitor capable of remote operation		**X**	
Develop method of aiming sensor without viewport	**X**		
Incorporate calibration methods into design	**X**		
Develop method of securing monitor in the field	**X**		
Develop a model for the sensitivity of the monitor	**X**		
Evaluate the major errors influencing the monitor	**X**		

9. FUTURE RESEARCH AND DEVELOPMENT

The broad nature of this project has precluded investigating every potential avenue concerning the HRTMM, its justification, its usage, and the errors that affect it. Additionally, as with every research project striving to complete the work to answer the questions concerning the subject has only managed to produce more questions. It is at this point that some of these questions and recommendations will be addressed.

During the course of the original literature review a paper was located that detailed the use of roof monitoring as a means to decrease the injury rate in stone mines. One particular section of that paper pointed out that pursuant to a survey of underground limestone mines ground movement monitoring was not a constant factor in every mine. Some mines were found to use multiple different monitoring technologies, while other mines were found to use none. Given the previously mentioned data concerning the recent increase in fatalities due to falling and sliding material, especially in underground coal mines, this is actually a much more important observation than was explained in the article [3].

The observation begs the question why? Why is it that some mines should be very proactive in their approach to ground movement monitoring while others are yet to use the technology? Only four potential reasons can really exist; the mine is either Unaware of the potential benefits of a comprehensive monitoring program, it is Unwilling to install a system for some reason, or the mine is Unable to install the system potentially due to monetary concerns or site condition constraints. The use of a monitoring system may also be Unnecessary for some mines.

The impetus of this research project has been on development of a new, more easily accessible and affordable ground convergence monitor that would have many of the same capabilities as other types of similar monitors. However, if the reason that these mines were not taking advantage of the technology was because they were unwilling to, or unaware of the benefits, the introduction of a more accessible and affordable monitor would have little effect on the overall use of monitoring. It is necessary, therefore, to determine exactly why these mines are not using monitoring technology so as to approach the problem of fatalities due to rock mass movement from a more appropriate direction. It would also be useful to conduct the same sort of survey found in the initial article along with the questions posed here with groups of mines from other segments of the industry – especially the underground coal industry.

The research undertaken has been completed with a very limited range of components. The Nikon D200 has been the primary sensor for almost the entire project. The sensitivity equations developed as a consequence of this research should theoretically be applicable to any image sensor and lens, but this should be tested in order to have a more complete knowledge about the relationships involved. In particular, testing could be completed with one or more of the Nikon Brand cameras, that each utilize the same 23.6 mm wide DX format imaging sensor chip. The imaging sensor chip width was one of the most difficult parameters to examine due to the inability to vary it without changing cameras.

There have been many improvements suggested for the HRTMM program throughout this research such as the development of a Quality Ratio algorithm that would allow for automatic selection of all true laser spots in an image as opposed to false,

erroneous laser spots. Other program-based improvements include the development of an automatic image thresholding algorithm, automatic analysis of images either in real time as they are downloaded from the camera, or automatically analyzing all images in a given folder. The results from these images should also be stored directly in a spreadsheet instead of being manually copied from the command line.

Additional research should be conducted into some of the nuisance variables evaluated during this project. It was found that vibration from heavy machinery plays very little part in the total random error of the monitor even in close proximity. This is a helpful guide for understanding potential sensor locations in a mine setting, but what is needed is an understanding of what vibrations *do* negatively impact the monitor. It is only by determining this and other boundaries that outline the nuisance variable values that should be avoided that a true understanding of the variable is formed. Due to the sheer number and complexity of these problems this was impossible for this research to accomplish this. Another nuisance variable that would follow this same reasoning is ambient light. It should be determined how much ambient light is too much for the monitor to successfully operate.

Research should also be completed dealing with the surface roughness. A trend has been suggested from the results of this project that suggests that increasing the diameter of the incident laser would allow for monitoring of a rougher target. It should be determined exactly what the relationship is between laser diameter and Joint Roughness Coefficient. This would allow determination of an acceptable diameter before implementation of the monitor in a given situation.

Throughout the project other uses were discussed for the HRTMM. One potential future use of the technology would be as a method of monitoring changes in orientation of a surface instead of only convergence. If multiple incidence lasers were shone on a surface from multiple directions it should be possible to use the collected centroid movement data in order to calculate the three dimensional deformation of a surface. This may be a worthy goal suitable for future research.

The answers to these questions and the ones that will surely come up in the future will help to better define the robustness and sensitivity of the HRTMM. They should help to improve the HRTMM components and software, making it a better and more useful monitor. They should help to bring a better understanding of why a proven technology such as ground movement monitoring is not being used universally. Finally, they could help to determine a better approach to the question of “how do we stop the increase in rock-mass movement related fatalities”.

10. SUMMARY

This research has been completed with the goal of developing an alternative ground convergence meter for use in underground mines. The monitor is capable of remotely operating across a room or a roadway. It has been found to be capable of achieving accuracies of 0.042 mm ±0.008mm/m with a sensitivity that varies according to the ideal equation developed within.

The ideal sensitivity equation has been shown to correspond with experimentally collected values and is suitable for determining an expected sensitivity dependent upon five fundamental variables including the distance between the sensor and the target, the width of the sensor's imaging chip, the cross sectional pixel-width of the image, the incidence angle of the incidence laser, and the focal length of the sensor's lens.

Literature review demonstrates a wide range of monitors currently available and shows that an opportunity is still available for a monitor of this type. It clearly shows the need for additional ground movement monitoring technology in the fight to eliminate injury and fatality due to falling and sliding rock material.

External error sources were evaluated with the goal of determining how they affect the monitor. Recommendations have been made for how to best eliminate or reduce the effects of these error sources.

Future research should focus on firmly setting the boundary conditions of the nuisance variables, on updating the speed, efficiency and accuracy of the monitor's centroid detection program, and on determination of why ground movement technology is not universally used with the goal of better understanding the needs of the industry.

APPENDIX A

SENSOR SPECIFICATIONS

This appendix contains the most pertinent specifications of the sensors used in this research, as far as they could be determined. Not all information is available for each sensor. More detailed information concerning the capabilities of each sensor can be found on the internet, as the full users manuals can typically be downloaded from the manufacturer for no cost.

NIKON D200

Camera Specifications	Details
Pixels	10.92 million total pixels
	10.2 million effective pixels
Sensor	23.6 x 15.8 mm CCD sensor
	DX format
	RGB Color Filter Array
	Built-in fixed low-pass filter
	3:2 aspect ratio
Image Sizes	3872 x 2592
	2896 x 1944
	1936 x 1296
Available file formats	NEF
	NEF and JPG
	JPG
Crop Factor	1.5
Lens Type	Nikon F type
Lenses	AF Nikkor (including AF-S, DX, VR and D-/G-type) : All functions possible
	D-type Manual-Focus Nikkor: All functions except autofocus and some exposure modes available
	AF Nikkor other than D-/G-type: All functions except 3D Color Matrix Metering and 3D Multi-Sensor Balanced Fill-Flash possible
	AI-P Nikkor: All functions except 3D Color Matrix Metering, 3D Multi-Sensor Balanced Fill-Flash and AF possible
	Non-CPU AI Nikkor : Usable in [A] or [M] mode with Matrix-Metering,

	Center-Weighted and Spot metering available. Indication of aperture No., after user inputs the aperture f/No. and focal length f=mm by multi-selector operation. Electronic Rangefinder usable with maximum aperture of f/5.6 or faster.
Sensitivity	ISO 100-3200
Shutter	30 to 1/8000 seconds
LCD Viewscreen	2.5” LCD
Shooting Modes	Single frame
	Continuous High [CH] - 5 fps
	Continuous Low [CL] - 1 to 4 fps (custom)
	Self-Timer (programmable)
	Mirror-up mode
	Interval timer (Time-lapse)
Video Out	NTSC
	PAL
Storage	Compact Flash Type I or II
	Microdrive supported
Connections	USB 2.0
	Video out
	Remote control
	External Flash
Communications	802.11 b/g wireless file transfer with optional WT-3 transmitter
GPS	Yes, with optional accessory NMEA 0183 Interface
Power	Lithium-Ion EN-EL3e (7.4 V, 1500 mAh)
	Included battery charger MH-18a
	Optional AC adapter EH-6
	Optional MB-D200 battery pack / vertical grip
Body material	Magnesium alloy
Dimensions	147 x 113 x 74 mm (5.8 x 4.4 x 2.9 in)
Weight (no batt)	830 g (1.8 lb)
Weight (inc. batt)	920 g (2.0 lb)

KONICA MINOLTA DIMAGE A2

Camera Specifications	Details
Pixels	8.3 megapixel (total) CCD
	8.0 million effective pixels
Sensor	2/3" Type
	RGB Color Filter Array
Image Sizes	3264 x 2448
	3264 x 2176 (3:2)
	2560 x 1920
	2080 x 1560
	1600 x 1200
	640 x 480
Available file formats	RAW
	RAW and JPG
	JPG
	TIFF
	MOV
Integrated Lens	7x optical zoom
	28 - 200 mm equiv.
	F2.8 - F3.5
	16 elements in 13 groups (including 2 AD glass, 2 aspherical elements)
	Manual mechanically linked zoom ring
	Filter thread 49 mm
Sensitivity	ISO 64-800
Shutter	30 to 1/4000 seconds
LCD Viewscreen	1.8” LCD
Video Out	NTSC
	PAL
Storage	Compact Flash Type I/II
	Microdrive supported
Connections	USB 2.0
	A/V out
	DC-IN
	PC Sync flash terminal
Communications	802.11 b/g wireless file transfer with optional WT-3 transmitter
GPS	No
Power	NP-400 Lithium-Ion rechargeable battery
	Battery charger

Body material	Metal Alloy and Plastic
Dimensions	117 x 85 x 114 mm (4.6 x 3.4 x 4.5 in)
Weight (no batt)	565 g (1.2 lb)
Weight (inc. batt)	654 g (1.4 lb)

PHILIPS TOUCAM PRO II

Specification	**Details**
Sensor	VGA CCD
Resolution	Max. (Interpolated) photo resolution 1280 x 960 (1.2 MP)
	Max. (real) photo resolution VGA 640 x 480
	Max. video resolution VGA 640 x 480
	Max. framerate 60 fps
Lens	6 mm
	f/2.0
Connections	USB 1.1
Power	Via USB connection
Dimensions	Standing: 85 mm x 47 mm x 80 mm
	Folded: 88 mm x 47 mm x 36 mm
Weight	100 g

APPENDIX B

MONITOR COST BREAKDOWN

The cost of the monitor is here broken down into two different sets. The first price column contains the costs of the components purchased new from stores or the manufacturer and represents the normal suggested retail price. The second price column contains the lowest price found new from any source, including internet auction sites. In most cases the items are the same, but substitutions have been allowed for similar products of the same quality in the case of micrometer movement stages and rotational stages. While all prices are, of course, subject to change, the second set of prices is certainly more likely to fluctuate than the first. The prices are all determined as of March, 2008.

The purchasing locations of the components are identified by number according to the table below.

Component Number	Manufacturer Price	Lowest Price
1	www.nikon.com	www.shoppingcartusa.com
2	www.sigmaphoto.com	www.ebay.com
3	www.edmundsoptics.com	www.edmundsoptics.com
4	www.edmundsoptics.com	www.edmundsoptics.com
5	www.thinkgeek.com	www.ebay.com
6	www.metalsdepot.com	www.metaldepot.com
7	www.bhphotovideo.com	www.amazon.com
8	www.bealasers.com	www.bealasers.com
9	www.siskiyou.com	www.ebay.com
10	www.radioshack.com	www.radioshack.com
11	www.newport.com	www.ebay.com
12	www.siskiyou.com	www.ebay.com
13	Local dealer	Local dealer
14	Local dealer	Local dealer
15	http://nikoneurope-en.custhelp.com	http://nikoneurope-en.custhelp.com

Monitor Section	Component Description	Typical Price	Lowest Price	Quantity	Typical Total	Lowest Total
Sensor	Nikon D200[1]	$1,399.95	$699.00	1	$1,399.95	$699.00
	Sigma 70-300 mm lens[2]	$200.00	$79.95	1	$1,599.95	$778.95
	R-60 filter[3]	$29.50	$29.50	1	$1,629.45	$808.45
	58mm UV filter[4]	$29.50	$29.50	1	$1,658.95	$837.95
	Class III Red Laser Pointer[5]	$9.99	$1.00	1	$1,668.94	$838.95
	Aluminum Stock[6]	$115.00 (estimate)	$115.00 (estimate)	1 x 2 ft.	$1,783.94	$953.95
	Giottos MH-5000 Tripod Head[7]	$54.95	$49.95	1	$1,838.89	$1,003.90
Incidence Lasers	650 nm Class IIIA laser[8]	$55.00	$55.00	1	$1,893.89	$1,058.90
	Rotation stage[9]	$215.00	$115.00	1	$2,108.89	$1,173.90
	AA battery holder[10]	$1.69	$1.69	1	$2,110.58	$1,175.59
	Mounting materials	Metal scrap	Metal scrap	n/a	$2,110.58	$1,175.59
Target	Stainless steel plate[10]	$150.00 (estimate)	$150.00 (estimate)	1	$2,260.58	$1,325.59
	Right angle bracket[11]	$69.00	$24.99	1	$2,329.58	$1,350.58
	Manual micrometer Stage[12]	$219.00	$40.00	1	$2,548.58	$1,390.58
	Giottos MH-5000 Tripod Head[7]	$54.95	$49.95	1	$2,603.53	$1,440.53
	Calibration mirror[13]	$5.00	$5.00	1	$2,608.53	$1,445.53
Other	Miscellaneous nuts/bolts[14]	$5.00	$5.00	n/a	$2,613.53	$1,450.53
	Nikon Capture 4.4.0[15]	Free Download	Free download	1	$2,613.53	$1,450.53
				TOTAL	**$2,613.53**	**$1,450.53**

It can be seen that the monitor can be built for under $1,500.00, thus meeting the goal of the project. The price could be lowered even more if a rotational stage was substituted for simply measuring the sides of the right triangle and an alternate method of mounting the incidence laser were developed. Further deductions could be made if the aluminum and stainless steel stock were to come from a mine scrap pile. This is,

however, unrecommended as no assurances can be made for the flatness and suitability of the metal. If these three reductions were made the estimated monitor cost would be $1,070.53 for using the lowest price suppliers. Prices for the D200 will likely continue to fall also.

A note must be made to point out that these estimates are made assuming that a laptop computer is already available.

BIBLIOGRAPHY

1. Mine Safety and Health Administration, 2007, "MSHA Fatality Statistics", *www.msha.gov*, accessed Oct. 26, 2007.

2. Marshall, T.E., et al., 2000, "Roof monitoring in limestone mines; experience with the roof monitoring safety system (RMSS)," *Proceedings of the 19th International Conference on Ground Control in Mining*, S.S. Peng and C. Mark, eds., pp. 185-191, Aug 8-10, 2000, Morgantown, WV.

3. Iannacchione, A.T., et al., 2000, "Roof monitoring helps prevent injuries in stone mines," *Mining Engineering*, Vol. 52, No. 11, pp. 32.

4. Iannacchione, A.T. and L.J. Prosser, 1998, "Roof and rib hazard assessment for underground stone mines," *Mining Engineering*, Vol. 50, No. 2, pp. 76.

5. Szwedzicki, T., 2003, "Rock mass behavior prior to failure," *International Journal of Rock Mechanics & Mining Sciences*, Vol. 40, No. 4, pp. 573-584.

6. Gray, B.R., 2006, "High Resolution Distance Monitoring System Using Laser Light," M.S. Thesis, University of Missouri-Rolla, Rolla, MO, 80 pp.

7. Szwedzicki, T., 2004, "Warning Signs to Geotechnical Failure of Mining Structures," *International Journal of Surface Mining, Reclamation and Environment*," Vol. 18, No. 2, pp. 150-163.

8. Kennedy, B.A. and Niermeyer, K.E., 1970, "Slope Monitoring Systems used in the Prediction of a Major Slope Failure at the Chuquicamata Mine, Chile," *Symposium on the Theoretical Background to the Planning of Open Pit Mines with Special Reference to Slope Stability*, Van Rensburg, P.W.J., ed., pp. 215-225, Johannesburg, South Africa, The South African Institute of Mining and Metallurgy.

9. Malan, D.F., et al., 2003, "Experimental validation of a mine-wide continuous closure monitoring system as a decision making tool for gold mines," Safety in Mines Research Advisory Committee: CSIR division of Mine Technology, GAP 852, Johannesburg, South Africa, pp. 1-66.

10. Drescher, K. and Handley, M.F., 2003, "Aspects of time-dependent deformation in hard rock at great depth," *Journal of the South African Institute of Mining and Metallurgy*, Vol. 103, No. 5, pp. 325-335.

11. Hoek, E. and Bray, J. 1981, *Rock Slope Engineering,* 3rd edition, Taylor & Francis, 360 pp.

12. Kennedy, B.A., 1978, "Slope failure of 1967-1969, Chuquicamata Mine, Chile," *Rockslides and Avalanches - Engineering Sites*, B. Voight, ed., Elsevier. pp. 595-632.

13. Kennedy, B.A., et al., 1971, "A case study of slope stability at the Chuquicamata Mine, Chile," *Transactions of the American Institute of Mining, Metallurgical and Petroleum Engineers*, Vol. 250, No. 1, pp. 55-61.

14. Malan, D.F., 1999, "Time-dependent Behavior of Deep Level Tabular Excavations in Hard Rock," *Rock Mechanics and Rock Engineering*, Vol. 32 No. 2, pp. 123-15.

15. Kavanagh, B.F. and Bird, G.J., 2000, *Surveying: Principles and Applications*, 7th edition, Prentice Hall, 801 pp.

16. Wolf, P.R. and Ghilani, C.D., 2002, *Elementary Surveying: An Introduction to Geomatics*, 10th edition, Prentice-Hall, 900 pp.

17. Schmitt Measurement Systems, Inc., 2007, "AR4000 Laser Rangefinder Users Manual," *www.acuityresearch.com*, accessed Dec. 16, 2007.

18. Schmitt Measurement Systems, Inc., 2005, "Manual for Acuity Laser Measurement systems," www.acuityresearch.com, accessed Dec. 16, 2007.

19. Palojärvi, P., 2003, "Integrated electronic and optoelectronic circuits and devices for pulsed time-of-flight laser rangefinding," Ph.D. Dissertation, University of Oulu, Oulu, Finland, 56 pp.

20. Kilpelä, A., 2004, "Pulsed time-of-flight laser rangefinder techniques for fast, high precision measurement applications," Ph.D. Dissertation, University of Oulu, Oulu, Finland, 98 pp.

21. Snow, M., 2002, "Laser Triangulation Sensors in the Tire Industry," *Sensor Magazine*, Vol. 19, No. 3.

22. Kennedy, W.P., 1998, "The Basics of Triangulation Sensors," *Sensors Magazine*, Vol. 16, No. 5.

23. Waycon Inc., 2007, "Users Manual for Analogue Laser Displacement Transducer," *http://wegaufnehmer.de/e_laser.html*, accessed Dec. 16, 2007.

24. Dumberger, M., "Taking the Pain out of Laser Triangulation," *Sensor Magazine*, Vol. 19, No. 7.

25. Moduloc Control Systems, 2008, "ODS Type C Laser Triangulation Meters," *www.moduloc-usa.com/PDF/Brochures/MC-ODS-LTM-005.pdf*, accessed Jan. 30, 2008.

26. Brady, B.H.G. and Brown, E.T., 2004, Rock Mechanics for Underground Mining, 3rd edition, Kluwer Academic Publishers, 626 pp.

27. Harris, R.K., Jewsbury, W., and Shoup, D.W., 1978, "Vibratory-Wire Strain Gage," Slope Indicator Company.

28. Eibeck, P.A. and Muramatsu, B., 2000, "Theory of Operation," http://bits.me.berkeley.edu/beam/lvdt_2.html, accessed Nov. 11, 2007.

29. Yow, J.L. and Wilder, D.G., 1981, "Tape extensometer sensitivity and reliability," *24th Annual Meeting of the Association of Engineering Geologists*, Sep. 27-Oct. 2, 1981, Portland, OR, Association of Engineering Geologists.

30. RST Instruments, 2006, Convergence Monitor, *www.rstinstruments.com*, accessed Jan. 10, 2006.

31. Haas, C.J., 1982, "Basic tools for deformation measurements in mines," *Underground Mining Methods Handbook*, W.A. Hustrulid, ed., Society of Mining Engineers of the American Institute of Mining, Metallurgical, and Petroleum Engineers, pp. 1506-1512.

32. Stacey, T.R. and Wrench, B.P., 1985, "The convergence meter," *Canadian Geotechnical Journal*, Vol. 22, No. 4, pp. 604-607.

33. Girard, J.M., 2001, "Assessing and Monitoring Open Pit Mine Highwalls," *Proceedings of the 32nd Annual Institute on Mining Health, Safety and Research*, F.M. Jenkins, J. Langton, M.K. McCarter and B. Rowe, eds., August 5-7, 2001, Salt Lake City, UT, University of Utah.

34. Boisen, B.P., 1982, "Borehole Extensometers," *Underground Mining Methods Handbook,* Hustrulid, W.A., editor, Society of Mining Engineers of the American Institute of Mining, Metallurgical, and Petroleum Engineers, pp. 1512-1519.

35. Hebblewhite, B.K. and Lu, T., 2004, "Geomechanical behavior of laminated, weak coal mine roof strata and thee implications for a ground reinforcement strategy," *International Journal of Rock Mechanics and Mining Sciences*, Vol. 41, No. 1, pp. 147-157.

36. International Society for Rock Mechanics Commission on Standardization of Laboratory and Field Tests, 1977, "Suggested methods for the quantitative description of discontinuities in rock masses," *International Journal of Rock Mechanics and Mining Sciences and Geomechanical Abstracts*, Vol. 15, No. 6, pp. 319-368.

37. Leica Geosystems, 2005, *www.leica-geosystems.com*, accessed Aug. 8, 2005.

38. Trimble, 2005, *www.trimble.com*, accessed Aug. 8, 2005.

39. Crouse, R.L., 2003, "Practical Geotechnical Engineering for Geologists and Engineers at Open-Pit Mines," Call & Nicholas Incorporated.

40. Newmont Gold, 2002, "Automated Slope Monitoring System AFE," Funding Request, Newmont Mining Corporation, Nov. 2, 2002, 7 pp.

41. Kavanagh, B.F., 2003, *Surveying: Principles and Applications*, 6th edition, Prentice Hall, 756 pp.

42. United States Corps of Engineers, 2003, "Engineering and Design: NAVSTAR Global Positioning System Surveying," Department of the Army, Jul. 1, 2003, Publication EM 1110-1-1003.

43. United States Corps of Engineers, 2002, "Engineering and Design: Structural Deformation Surveying," Department of the Army, Jun. 1, 2002, Publication EM 1110-2-1009.

44. Wahbeh, A., et al., 2003, "A vision-based approach for the direct measurement of displacements in vibrating systems," *Smart Materials and Structures*, Vol. 12, No. 5 pp. 785-794.

45. Iannacchione, A.T., et al., 1999, "Preventing injuries caused by unrecognized stone mine roof beam failure with a pro-active roof control plan, Society for Mining, Metallurgy and Exploration Annual Meeting, Preprint 99-87, 9 pp.

46. Konica Minolta, 2003, "DiMAGE A2 Users Manual," 2003, 179 pp.

47. Rigel Laser Measurement Systems, 2008, "High Accuracy, High Resolution 3D Terrestrial Laser Scanner System LMS-Z390i," *Datasheet for the LMS-Z390i*, *www.riegl.com*, accessed Jan. 28, 2008.

48. Rigel Laser Measurement Systems, 2008, "Long Range 3D Terrestrial Laser Scanner System LMS-Z210ii," *Datasheet for the LMS-Z210ii*," *www.riegl.com* accessed Jan. 28, 2008.

49. Rigel Laser Measurement Systems, 2008, " Long Range and High Accuracy 3D Terrestrial Laser Scanner System LMS-Z420i," *Datasheet for the LMS-Z420i*," *www.riegl.com* accessed Jan. 28, 2008.

50. Nikon Corporation, 2005, "D200 Digital Camera," *Users Manual for the Nikon D200*, Nikon Corporation, Tokyo, Japan.

51. Peppers, P., Jones, T.H., 2007, Personal communication, Feb 2007, Denver, CO.

52. American National Standards Institute, 1993, "American National Standard for the Use of Safe Lasers," *ANSI Z136.1,* American National Standards Institute.

53. Dubaniewicz, T.H., 2006, "Methane-air mixtures ignited by CW laser-heated targets on optical fiber tips: comparison of targets, optical fibers, and ignition delays," *Journal of Loss Prevention in the Process Industries*, Vol. 19, No. 5, pp. 425-432.

54. Dubaniewicz, T.H., Cashdollar, K.L and Green, G.M., 2003, "Continuous Wave Laser Ignition Threshold of Coal Dust Clouds," *Journal of Laser Applications*, Vol. 15, No. 3 pp. 184-191.

55. Dubaniewicz, T.H., et al., 2000, "Ignition of methane-air mixtures by laser heated small particles," *Journal of Loss Prevention in the Process Industries*, Vol. 13, No. 3-5 pp. 349-359.

56. Dubaniewicz, T.H., Cashdollar, K.L., and Monaghan, W.D., 1999, "Laser Ignition of Flammable Gas," *Proceedings of the International Laser Safety Conference*, March 7-11, 1999, Orlando, FL, Laser Institute of America.

57. McHugh, S., 2008, "Tutorials: Digital Camera Sensors," *www.cambridgeincolour.com/tutorials/sensors.htm*, accessed Jan 30, 2008.

58. Gray, B.R., et al., 2007, "Optical projection and image processing approach for mine wall monitoring," *Optical Engineering*, Vol. 46, No. 1 pp. 013601.

59. Gonzalez, R.C. and Woods, R.E., 2002, *Digital Image Processing*, 2nd edition, Prentice Hall, 793 pp.

60. McCollough, E., 1893, "Photographic Topography," *Industry: A Monthly Magazine Devoted to Science, Engineering and Mechanic Arts*, Industrial Publishing Company, San Francisco, CA, pp. 399-406.

61. Apel, D.B., et al., 2007, "Development and Laboratory Trials of the Light-Based High-Resolution Target Movement Monitor for Monitoring Convergence at Underground Mines," *Journal of Geotechnical and Geoenvironmental Engineering*, Vol. 133, No. 9 pp. 1167-1171.

62. Slope Indicator, "Digital Tape Extensometer Datasheet," *www.slopeindicator.com*, accessed Jan 15, 2008.

64. Martikainen, A.L. and Marks, J., 2007, "Fogging in mines: The role of visibility, unfamiliar fog removal methods, and future research ideas," *Journal of the Mine Ventilation Society of South America*, Q2, 7 pp.

65. Yoder, D., 1986, "Introduction to the Optical Transfer Function," *Opto-Mechanical System Design*, 2nd edition, Wiley-Interscience, 464 pp.

66. Saleh, B.E.A. and Teich, M.C., 1991, "Postulates of ray optics," *Fundamentals of Photonics*, Wiley-Interscience, pp. 1-39.

67. Tatarski, V.I., 1959, *The Effects of the Turbulent Atmosphere on Wave Propagation*. 1959, Moscow.

68. Marchello, J.M., 1976, *Control of Air Pollution Sources*, Marcel Dekker, 630 pp.

69. American Meteorological Society, 2006, "Glossary of Meteorology," *http://amsglossary.allenpress.com/glossary*, accessed Mar. 14, 2006.

70. Brown, M.B. and Forsythe, A.B., 1974, "Robust test for the equality of variances," *Journal of the American Statistical Association*, Vol. 69, Jun. 1974, pp. 364-367.

71. Levene, H., 1960, "Robust tests for equality of variances," *Contributions to Probability and Statistics*, I. Olkin, et. al., eds., Stanford University Press, pp. 278-292.

72. Eadie, W.T., et al., 1971, *Statistical Methods in Experimental Physics*, North-Holland, pp. 269-271.

73. Askey, P., 2007, "Nikon D200 Review," *www.dpreview.com/reviews/nikond200*, accessed Apr. 10, 2007.

74. Strahler, A.N. and Strahler, A.H., 1989, *Elements of Physical Geography*, 4th Edition, John Wiley & Sons, 562 pp.

75. Edmunds Optics, 2007, "*Transmission Curves*," Transmission curve for a Hoya R-60 filter, http://www.edmundoptics.com/images/catalog/4726.gif, accessed Apr. 12, 2006.

76. Edmunds Optics, 2007, "*Transmission Curves*," Transmission curve for a UV filter, http://www.edmundoptics.com/images/catalog/3802.gif, accessed Apr. 12, 2006.

77. Ångstrom, A., 1925, "The Albedo of Various Surfaces of Ground," *Geographic Annals*, Vol. 7, 323 pp..

78. Leckner, J. and Dorf, M.C., 1988 "Why some things are darker when wet," *Applied Optics*, Vol. 27 No. 7 pp. 1278-1280.

79. Twomey, S.A., Bohren, C.F., and Mergenthaler, J.L., 1986, "Reflectance and albedo differences between wet and dry surfaces," *Applied Optics*, Vol. 25, No. 3, pp. 431-437.

80. Barton, N. and Choubey, V., 1977, "The shear strength of rock joints in theory and practice," *Rock Mechanics and Rock Engineering*, Vol. 10, No. 1, pp. 1-54.

81. Scesi, L. and Gattinoni, P., 2007, "Roughness control on hydraulic conductivity in fractured rocks,". *Hydrogeology Journal*, Vol. 15, No. 2 pp. 201-211.

82. Hu, Y., 1996, "The dependence of cloud optical properties on equivalent radius," http://asd-www.larc.nasa.gov/~yhu/paper/thesisall/thesisall.html, accessed Mar. 7, 2008.

83. Schimmelpfennig, M.A., 1982, "Fogging in Underground Mine Atmospheres," M.S. Thesis, University of Missouri-Rolla, Rolla, MO, 89 pp.

84. Deirmendjian, D., 1969, *Electromagnetic Scattering on Spherical Polydispersions*, Elisevier, 312 pp.

85. Technical Services Department, 2007, "Fletcher Underground Mine Map," Doe run Company, Unpublished.

86. Lane, W.L., et al., 2001, "Pillar extraction and rock mechanics at the Doe Run Company in Missouri 1991 to 2000," *Underground Mining Methods: Engineering Fundamentals and International Case Studies*, W.A. Hustrulid and R.L. Bullock, eds., Society for Mining, Metallurgy, and Exploration, pp. 95-101.

87. Carmack, J., et al., "The Viburnum Trend underground - An overview," *Underground Mining Methods: Engineering Fundamentals and International Case Studies*, W.A. Hustrulid and R.L. Bullock, eds., Society for Mining, Metallurgy, and Exploration, pp. 89-93.

88. Yanske, T.R., Jones, T.H., 2007, Personal Communication, Jul. 2007, Bunker, MO.

89. Zur, K.J. and Apel, D.B., 2004, "Use of cemented rock fill for enhanced pillar recovery in area 1 of the Doe Run Company," *Proceedings of the Fifth International Conference on Case Histories in Geotechnical Engineering*, S. Prakash, ed., Apr. 13-17, 2004, New York, NY, University of Missouri-Rolla.

90. International Society of Explosives Engineers, 1998, "Vibration and airblast," *Blaster's Handbook*, R.B. Hopler, ed., International Society of Explosives Engineers, pp. 591-644.

VITA

Tristan Harrison Jones was born in Saginaw, Michigan, in the United States of America on August 25, 1981. In May of 2005 he graduated from the Central Michigan University Honors Program with dual degrees; a B.S. in Geology and a B.A. in Geographic Information Sciences, with an emphasis on geographic information systems, remote sensing, and cartography.

Before his final year of his undergraduate education he received a grant from the United States Geological Survey to pursue a research project creating a quaternary geologic map of Beaver Island, Michigan. Field mapping of the area was carried out alone.

Tristan attended the Missouri University of Science and Technology in Rolla, Missouri, United States, to pursue his Ph.D. During study he spent semesters working as a graduate assistant with time spent preparing for and helping to teach various rock mechanics laboratory courses. He also spent time doing rock testing for various mining companies in the surrounding area. He also completed a summer internship working for the Doe Run Company at the Fletcher mine, an underground lead mine in southeast Missouri.

During his undergraduate and graduate education he has published numerous conference and journal papers, some of which are listed in the references of this document. He has twice presented at the annual meeting of the Society for Mining, Metallurgy, and Exploration, once as a lead author. He has been a member since 2004.

He was also a member of the American Institute of Professional Geologists and the Geological Society of America. He was inducted into the Golden Key international honor society in 2003. He received his Eagle Scout award from the Boy Scouts of America in 1996 and is a Vigil Honor member of the Order of the Arrow.